SYNTHESIS AND APPLICATIONS OF ANISOTROPIC COLLOIDAL DIMERS

by

Sijia Wang

A thesis submitted to the Faculty and the Board of Trustee of the Colorado School of Mines in partial fulfillment of the requirements for the degree of Doctor of Philosophy (Chemical Engineering).

Golden, Colorado

Date: _____

Signed: _____
Sijia Wang

Signed: _____
Dr. Ning Wu
Thesis Advisor

Golden, Colorado

Date: _____

Signed: _____
Dr. David W.M. Marr
Professor and Head
Department of Chemical and Biological Engineering

ABSTRACT

Nowadays, anisotropic particles have attracted a lot of attention due to their wide applications in optical display, emulsion stabilization, biomedical imaging, and active materials, and drug delivery. However, methods to produce anisotropic particles with precise tunability, large quantity, high monodispersity, and low cost are still elusive. This challenge also limits the scope of studies of those particles in both scientific research and practical applications. This thesis focuses on a special class of anisotropic particles - colloidal dimers. We have successfully developed a series of bulk synthetic strategies for dimers with geometric, interfacial, compositional, and combined anisotropies based on the modification of seeded emulsion polymerization.

Dimers with geometric anisotropy show new and rich assembly structures such as Ising-like lattice and chiral clusters under AC electric fields. While dimers with interfacial anisotropy, e.g., platinum-polystyrene dimers, could be used as self-propelling motors in both AC electric fields and hydrogen peroxide solution. We discover a new type of electric-field driven propulsion mechanism based on broken symmetry in electrohydrodynamic flow. Interestingly, our dimers swim in hydrogen peroxide based on bubble propulsion, which is different from the conventional self-diffusiophoresis. With additional studies, we reveal the interconnection between these two mechanisms, which depends on the surface coating of platinum. Moreover, the geometric anisotropy of colloidal dimers are crucial to generate circular motion. We also demonstrate a new concept in making colloidal emulsifiers and phase-transfer vehicles that are important for encapsulation and sequential release of small molecules across two different phases. Finally, we explore the possibility to use non-polymerizable swelling agents such as toluene and tetraethyl orthosilicate, and investigate their impacts on making dimers with combined geometric, interfacial,

or compositional anisotropies. Our method not only simplifies the procedure for synthesizing dimers, but also can be potentially extended to other types of non-polymerizable swelling agents for expanding the existing catalogue of anisotropic particles.

TABLE OF CONTENTS

ABSTRACT iii

LIST OF FIGURES vi

LIST OF PUBLICATIONS ix

ACKNOWLEDGEMENTS ix

CHAPTER 1 INTRODUCTION 1

1.1 Motivation and Significance 1

1.2 Literature Review 4

1.2.1 Synthesis of Anisotropic Particles 4

1.2.2 Applications of Anisotropic Particles 10

1.3 Summary 24

CHAPTER 2 BULK SYNTHESIS OF METAL-ORGANIC HYBRID DIMERS AND THEIR PROPULSION UNDER ELECTRIC FIELDS 35

2.1 Abstract 35

2.2 Introduction 36

2.3 Experimental Methods 38

2.3.1 Materials 39

2.3.2 The synthesis of polystyrene (PS) dimers 39

2.3.3 Selective coating of gold nanoparticles on the crosslinked lobe 40

2.3.4 Gold/silver and platinum shell growth on gold-coated dimers 40

2.3.5 Characterization of the hybrid dimers 41

2.3.6 Propulsion Pt-PS dimers under electric fields 41

2.4 Results and Discussion 42

2.4.1 Synthesis of the metal-organic hybrid dimer 43

2.4.2 Propulsion of hybrid dimers under electric fields 49

2.5 Conclusions 53

2.6 Acknowledgement 55

CHAPTER 3 SELECTING THE SWIMMING MECHANISMS OF COLLOIDAL PARTICLES: BUBBLE PROPULSION VS. SELF-DIFFUSIOPHORESIS 61

3.1 Abstract 61

3.2 Introduction 62

3.3 Experimental Methods 64

3.3.1 Materials 64

3.3.2 Selective coating of gold nanoparticles on the crosslinked lobe 64

3.3.3 Deposition of the platinum (Pt) shell on gold-coated dimers 65

3.3.4 Synthesis of polystyrene particles with rough surfaces 65

3.3.5 E-beam evaporation of platinum on polystyrene spheres 65

3.3.6 Characterization of the platinum-polystyrene (Pt-PS) particles 65

3.3.7 Propulsion of Pt-PS dimers in hydrogen peroxide 66

3.3.8 Measurement of the oxygen production rate 66

3.4 Results and Discussion 66

3.4.1 Synthesis of the platinum-polystyrene hybrid dimers. 67

3.4.2 Bubble-propulsion vs. self-diffusiophoresis of Pt-PS particles.....68

3.4.3 The motion of Pt-PS dimers driven by periodic bubble growth and collapse 77

3.5 Conclusions 86

3.6 Acknowledgement 87

CHAPTER 4 BICOMPARTMENTAL PHASE TRANSFER VEHICLES BASED ON COLLOIDAL DIMERS 93

4.1 Abstract 93

4.2 Introduction 94

4.3 Experimental Methods 96

4.3.1 Chemicals 97

4.3.2 Synthesis of polystyrene dimers 97

4.3.3 Dye/catalyst encapsulation 98

4.4 Results and Discussion 100

4.4.1 Dimer synthesis and active-agent encapsulation 100

4.4.2 Structural emulsifier 102

4.4.3 Oil phase delivery and hydrogenation 105

4.4.4 Dimer surface modification 109

4.5 Conclusions 111

4.6 Acknowledgement 111

CHAPTER 5 THE IMPACT OF SWELLING AGENT ON THE SYNTHESIS OF ANISOTROPIC PARTICLES AND THEIR APPLICATIONS 117

5.1 Introduction 117

5.2 Materials and Experimental Methods..... 119

5.3 Results and Discussion 122

5.3.1 Using toluene as a swelling agent for making dimers 122

5.3.2 Synthesis of polystyrene-silica hybrid particles 136

5.3.3 Propulsion and assembly of PS-silica hybrid particles under AC electric fields 140

5.4 Conclusions 146

CHAPTER 6 SUMMARY AND OUTLOOK 153

6.1 Summary 153

6.2 Outlook 154

6.2.1 Synthesis of anisotropic particles 154

6.2.2 Applications of anisotropic particles 156

LIST OF FIGURES

Figure 1.1 Schematic of anisotropic particles with different types of anisotropic dimensions... 1

Figure 1.2 Strategies to selectively modify the surface of particles. 5

Figure 1.3 The effect of wetting degree between monomer and the crosslinked seed on the particle morphology. 8

Figure 1.4 Various types of dimers that have been synthesized so far. 9

Figure 1.5 Assembled structures via hydrophobic interactions. 11

Figure 1.6 Assembled structures under electric fields from anisotropic particles. 14

Figure 1.7 Different propulsion mechanisms for micro/nanomotors. 15

Figure 1.8 Different parameters that affect the motion of Pt-insulator Janus particles in hydrogen peroxide solutions. 17

Figure 1.9 Bubble-propelled micromotors with different geometries. 19

Figure 1.10 Stimuli responsive anisotropic colloidal surfactants. 23

Figure 2.1 Two methods for calculation the speed of dimers. 41

Figure 2.2 The chemical route to synthesizing metal-organic hybrid dimers with independently tunable (a) geometric and (b) interfacial anisotropy. 43

Figure 2.3 Geometric anisotropy of the dimers. 44

Figure 2.4 Interfacial anisotropy of the dimers. 45

Figure 2.5 Gold coating on dimers. 46

Figure 2.6 Silver coating on dimer. 47

Figure 2.7 Platinum coating on dimers. 48

Figure 2.8 Propulsion of Pt-PS dimers under AC electric field. 51

Figure 2.9 Propulsion speed as a function of electric field strength and frequency. 52

Figure 3.1 Synthesis of platinum-polystyrene dimers. 67

Figure 3.2 A summary of particles that have been tested in hydrogen peroxide solution and their corresponding swimming mechanisms. 69

Figure 3.3 Snapshots of a dimer with two bubble nucleation sites. 70

Figure 3.4 Trajectories and velocities of Pt-PS Janus spheres and Pt-PS hybrid dimers in hydrogen peroxide solutions. 70

Figure 3.5 The amount of oxygen produced by two types of Pt-PS Janus spheres in separate vials of 10 ml 5% hydrogen peroxide solution. 72

Figure 3.6 Platinum coated polystyrene spheres with different surface roughness. 75

Figure 3.7 Three types of motion of the Pt-PS hybrid dimers 78

Figure 3.8 Change of the angle (triangle) between the dimer's long axis and the horizontal reference line as a function time. 79

Figure 3.9 The time dependence of the bubble radius during both linear and circular motions. 79

Figure 3.10 The plot of the bubbles radius (circle) and the particle's instantaneous displacement (triangle) versus time 82

Figure 3.11 The accumulative displacement of dimers (triangle) and the bubble radius (square) versus time 83

Figure 3.12 A schematics showing the solvent flow during the moment of the bubble collapse. 84

Figure 3.13 Bubble collapse moments captured by an ultra-high speed camera in linear and circular motions. 85

Figure 4.1 A schematic of the bi-compartmental vehicle (colloidal dimer) targeted for delivering catalysts to oil phase underground. 96

Figure 4.2 The synthetic route of polystyrene dimers encapsulating different molecules. .. 102

Figure 4.3 Conventional polystyrene dimers in oil-water biphasic mixture. 103

Figure 4.4 Oil phase delivery by dye encapsulated dimers. 106

Figure 4.5 Oil-Phase delivery of the Wilkinson's catalyst and hydrogenation reaction. 107

Figure 4.6 Adding amphiphilicity to polystyrene dimers to shorten the release time. 109

Figure 5.1 Dimers formed by swelling CPS with toluene. 124

Figure 5.2 The impact of CPS compositions on dimer morphologies. 127

Figure 5.3 Stabilization of dimers. 128

Figure 5.4 Surface charge characterization on dimers. 130

Figure 5.5 Metallic nanoparticles coating on dimers. 131

Figure 5.6 Functionalization of the second lobe. 133

Figure 5.7 Synthesis and interfacial activity of pH responsive dimers. 135

Figure 5.8 PS-silica dimer synthesis and characterization. 137

Figure 5.9 Morphology study of PS-silica dimers. 139

Figure 5.10 Propulsion of PS-silica dimers under AC electric field. 142

Figure 5.11 A simple dumbbell model to explain the propulsion of polystyrene-silica dimer 142

Figure 5.12 Assembly of PS-silica hybrid dimers under low frequency. 144

Figure 5.13 Assembly of PS-silica dimers under high frequency. 146

LIST OF PUBLICATIONS

1. Wang, S.; Wu, N. Bicompartmental Phase Transfer Vehicles Based on Colloidal Dimers. *ACS Appl. Mater. Interfaces* **2014**, *6*, 20164–20170 (based on Chapter 4).

2. Wang, S.; Wu, N. Selecting the Swimming Mechanisms of Colloidal Particles: Bubble Propulsion versus Self-Diffusiophoresis. *Langmuir* **2014**, *30*, 3477–3486 (based on Chapter 3).

3. Wang, S.; Ma, F.; Zhao, H.; Wu, N. Bulk Synthesis of Metal–Organic Hybrid Dimers and Their Propulsion under Electric Fields. *ACS Appl. Mater. Interfaces* **2014**, *6*, 4560–4569 (based on Chapter 2).

4. Wang, S.; Wu, N., "Swelling Agents Effect during Anisotropic Particle Preparations and Their Diverse Applications", in preparation (based on Chapter 5).

Other publications based on the whole thesis:

5. Ma, F.; Wang, S.; Zhao, H.; Wu, D. T.; Wu, N. Colloidal Structures of Asymmetric Dimers via Orientation-Dependent Interactions. *Soft Matter* **2014**, *10*, 8349–8357.

6. Ma, F.; Wang, S.; Smith, L.; Wu, N. Two-Dimensional Assembly of Symmetric Colloidal Dimers under Electric Fields. *Adv. Funct. Mater.* **2012**, *22*, 4334–4343.

7. Ma, F.; Wang, S.; Wu, D. T.; Wu, N. Electric-Field Induced Assembly and Propulsion of Chiral Colloidal Clusters. *Proceedings of the National Academy of Sciences*, 2015, under review.

8. Senyuk, B.; Varney, M. C. M.; Lopez, J. a; Wang, S.; Wu, N.; Smalyukh, I. I. Magnetically Responsive Gourd-Shaped Colloidal Particles in Cholesteric Liquid Crystals. *Soft Matter* **2014**, *10*, 6014–6023.

ACKNOWLEDGEMENTS

First of all, the biggest “thank you” is addressed to my advisor Dr. Ning Wu, who is the most patient, inspiring, and understanding person I have ever met, probably the best advisor one can ever wish to have. His enthusiasm and curiosity about science influences every member in our group. Meanwhile he is always so thoughtful and cares deeply about our daily life. I would also like to thank my committee comprised of Dr. Hongjun Liang, Dr. Stephen G. Boyes, Dr. John R. Dorgan, and Dr. Keith Neeves, for all of their help and guidance from my proposal defense through my dissertation defense. Thanks also go to our collaborators, Dr. David T. Wu, and Dr. Hui Zhao, for all the support and professional advices in simulation work.

Special thanks go to Mr. John Chandler. His profound knowledge in SEM benefits my research a lot, and makes the characterization process much more efficient. Many thanks go to the staff from Colorado Nanofabrication Lab, who assisted me with various deposition techniques, such as thermal evaporation and e-beam evaporation. I am also deeply grateful for the help from Dr. Ryan M. Richards and Dr. Jeremy G. Leong, who generously allow me use their equipments and help me perform the hydrogenation experiments. Many thanks go to Mr. Gary Zito and Mr. Edward Dempsey as well, for their special proficiency, precious time and kindness. I would like to thank Dr. James F Ranvillehelp for ICP-AES characterization and Dr. Thomas Wildeman for valuable discussion about the sample preparation. I appreciate the help from Dr. Hongjun Liang, and Dr. Liangju Kuang as well, for the fabrication of magnetic nanoparticles. I want to thank Dr. David W.M. Marr’s group as well, for the aid in spinning coating and Dr. Colin Wolden’s group for the assistance in silica coating. I would also like to thank Dr. Anderson Ho Cheung, Shum’s group from the University of Hong Kong, for hosting me and teaching me building glass capillary microfluidic devices.

In the meantime, I really enjoyed the time I spent with my lab mates, Chixia Tian, Fuduo Ma, Xingfu Yang, Jingjing Gong, Kelly Heatley, Guo Yang, and Tao Yang, who create the most comfortable and enjoyable work environment. I really appreciate the insightful discussions we have, and also the assistance for my experiments. Special thanks go to Fuduo Ma. His enormous knowledge in electric field assembly facilitates my research progress to a large extent. I cannot thank Chixia Tian enough, for being like my sister, who always looks after me and shares everything with me.

Many thanks go to undergraduate students who have helped me in the lab, for example, the REU students, Lois Smith, Adam Gage, Jason Trevithick, and Frank Youmbi. Their passion for knowledge also deepens my understanding about the scientific fields. Without their help, I could not achieve the progress I currently have. Meanwhile working with them provides me lots of valuable teaching experience. Special thanks go to Taylor Peters, who is an undergraduate student in CSM. I cannot thank him enough about the amount of time he devoted to the work and the tremendous assistance in the lab.

Moreover, I want to thank my beloved family members for being so supportive during these years, sharing my excitements and disappointments in life. Special thanks go to mom, who takes a good care of me during the last five months. I would like thank my friends in CSM as well. They make CSM feel like home to me now.

Finally, I would like to thank my Funding agencies, start-up funds from Colorado School of Mines, National Science Foundation, and American Chemical Society Petroleum Research Fund for their financial support.

CHAPTER 1

INTRODUCTION

This chapter describes our motivation for studying anisotropic particles, and also presents literature review of current progress on anisotropic particles synthesis and applications.

1.1 Motivation and Significance

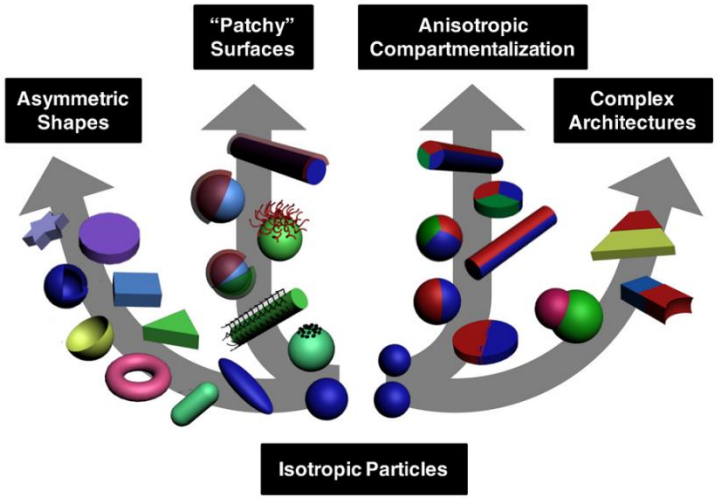

Figure 1.1 Schematic of anisotropic particles with different types of anisotropic dimensions.[1] Reprinted with permission from ref [1]. Copyright 2011 Elsevier.

Due to surface energy minimization, particles synthesized on the micron scale are usually in spherical shapes with homogeneous surface chemistry. The simplicity of this kind of particles limits their assembly behavior and applications. Therefore, particles with different anisotropic dimensions (Figure 1.1)[1] have drawn extensive attention recently because of their potential to form complex assembly structures and diverse engineered properties.

The most well studied application of anisotropic particles is to use them as building blocks for self-assembly, with the hope of fabricating complex structures with tailored properties. The assembly of isotropic particles has been studied for a long time which significantly expands our knowledge in many aspects of material science, such as crystal nucleation and glass transition. Anisotropic particles, in principle, can exhibit a multitude of additional properties due to their

complexity in shape, composition, or architecture. For example, an array of anisotropic particles can interact with light collectively and exhibit exotic photonic properties when the size of colloids is comparable to or smaller than the wavelength of visible light. Electric field-driven bicolored display has also be successfully demonstrated.[2] Metamaterials that can eventually lead to a revolution of optical microscopes can also be assembled by anisotropic colloids.[3] Considering our preliminary results in the electric field-induced assembly of dimers, it is highly possible for our system to be used for optical applications.

From the scientific point of view, anisotropic particles can provide a powerful tool to help gain deeper understanding of molecular interactions. For example, anisotropic particles have been used as model systems to predict the interaction between proteins.[4,5] They can also mimic the polymerization process by treating each particle as a monomer.[6,7] However, there is a knowledge gap in the relationship between different properties of the anisotropic particles and their assembly behavior. A systematic study about the specific impacts of each parameter is important for designing particles rationally for targeted assembly into specific structures.

Another research area for anisotropic particles is developing artificial self-propelling micro/nanomotors. Nanomotors are ubiquitous in biology in the form of F1-ATPase, myosin, kinesin, bacterial flagellar, etc. Most of them rely on the effective conversion of chemical fuels (such as ATP) into mechanical motion, but the complexity in structures and sensitivity to environment in biomotors severely hinder their applications. Besides, the propulsion mechanisms for many motors are not fully understood. Moreover, they typically have a narrow operating range in temperature. They must be preserved in an aqueous medium with proper pH and salt concentration. As a result, the lifetime of these nanomotors is typically short.[8]

Artificial motors, in general, can be divided into three categories, depending on actuating mechanisms: (1) motors actuated by deformation;[9,10] (2) motors actuated by external fields, such as the magnetic and electric fields;[10,11] and (3) motors actuated by asymmetric chemical reactions.[12]

Among different types of artificial motors, the chemically powered motors have been extensively studied. The most commonly used chemical fuel is hydrogen peroxide (H_2O_2). However, even for those motors, the governing propulsion mechanism can be quite different depending on the constituting materials or the fabrication process. Anisotropic particles are excellent candidates for propelling motors because multiple compartments in them can perform different tasks simultaneously.

Studies of synthetic nanomotors are still at the beginning stage; therefore, synthetic nanomotors are less competitive to natural motors in terms of efficiency. However, considering the large effort people have already made, they could reach a stage of real applications in near future, such as active drug delivery, environment sensing, waste water remediation, minimally invasive surgery (MIS), and so on.[13,14]

The third type of applications for anisotropic particles is to stabilize the oil-water interfaces, as they can be good mimics of molecular surfactants. Particles such as silica and clay serve as natural surfactants to stabilize crude oil emulsions. The stability of those emulsions is usually higher than molecular surfactants due to a high energy barrier of desorption.[15] It is, however, hard to understand the actual function of those particles at interfaces since their surface properties are inherently inhomogeneous. This is why there is an arising interest to use anisotropic particles as colloidal surfactants. One example is the so-called Janus particles (named after the Roman god Janus) in which two hemispheres possess different surface properties. Recent literature has shown

the advantages of using Janus particles as colloidal surfactants both theoretically and experimentally.[16–18].

Most Janus particles studied in literature are, however, spherical. We propose that the colloidal dimers have several advantages: (1) they can provide more degrees of anisotropic dimension in geometry, such as the aspect ratio and bond length; (2) they can naturally mimic the structure of molecular surfactants more faithfully by combining both geometric and interfacial heterogeneities; and (3) compared with the common two-dimensional template method to make Janus particles, dimers can be bulk-synthesized with good monodispersity.

In addition to the amphiphilic dimers, colloidal dimers that are stimuli-responsive also attract lots of attention. Colloidal emulsifiers that can change both geometry and hydrophilicity by varying pH from 2 to 12 have been reported recently.[19] The advantage of such a kind of system is that we can study the geometry and hydrophobic contrast effects simultaneously. On-demand stabilization or destabilization of the emulsions can also be conveniently achieved.

1.2 Literature Review

In this section, we reviewed different types of synthetic methods for anisotropic particles, and their applications in self-/directed-assembly, micro/nanomotors, and colloidal surfactants.

1.2.1 Synthesis of Anisotropic Particles

In the past decade, we have witnessed a rapid growth of synthetic methods for anisotropic particles. Different types of anisotropic particles have been fabricated, such as particles with asymmetric shapes,[20,21] patchy surfaces,[22] different compositions,[23,24] or combined types of anisotropy.[25] In general, the synthetic methods can be characterized by two-dimensional templating methods and three-dimensional processes. Below we briefly review different synthetic strategies that have been commonly adopted and are relevant to our work.

Templating method

The most intuitive way to break the symmetry of spheres is to selectively mask one part of the particle while modifying the rest (Figure 1.2). For example, one can prepare a monolayer of isotropic spheres on substrate and then apply a directional flux of atoms of metal or metal oxide. Other strategies include masking the hemispheres by temporary trapping them in a PDMS gel[26] or melted Parafilm[27] and microcontact-printing[28] (Figure 1.2). The most practical strategy is to trap particles at the interface between two media. Then the particle surfaces can be partially modified if the reactive agents are present in one medium only.[29] In addition to planar interfaces, the curved interface provides opportunities to overcome the intrinsic limitation of the two-dimensional templating method, i.e., low throughput. Granick's group utilized silica particles to prepare Pickering emulsions, where melted paraffin wax was the oil phase.[30] Once oil-in-water emulsions are formed, the oil phase can be solidified. Then the exposed surfaces of silica particles can be modified in the aqueous phase. Although this method has high throughput, it is challenging to provide Janus particles with a uniform degree of surface modification because it requires that all particles go to the interface and maintain the same contact angle.

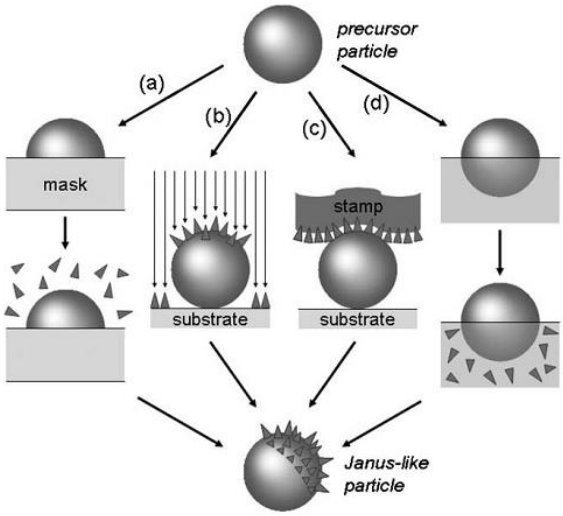

Figure 1.2 Strategies to selectively modify the surface of particles.[31] Reprinted with permission from ref [31]. Copyright 2005 Royal Society of Chemistry.

Controlled surface nucleation and growth

Different crystalline planes on an inorganic particle have different interfacial energies, which can be exploited to nucleate and grow materials selectively at certain locations. However, most work done in this area focused on particles of ~10nm, which makes *in-situ* observation of the assembly process formidable at the current stage. A more feasible approach for making larger anisotropic particles is to pre-modify micronsized particles. A few examples have been reported. For example, calcination of silica particles with hydrophobic siloxane on their surfaces can induce the asymmetric growth of silver patches.[32] Organic-inorganic hybrid particles are of particular interest because of their large contrast in dielectric constants which could have potential application in self-assembly. The difference in refractive indices can also help build optical devices. Silica-polystyrene particles can be made by coating methacryloxy-alkyltrimethoxysilane on silica spheres, which can promote the growth of individual polystyrene lobes on them.[33] By changing the concentration or size of the silica particles, hybrid colloidal clusters with different morphologies, such as dumbbells, tripods and tetrapods, can all be produced. The bottleneck of this method is that the final product is always a mixture of clusters, with the best yield around 70% for dumbbells.

As we mentioned above, templating methods can help make Janus particles. As seeds, they can provide selective nucleation sites, so that the growth of secondary particles can be achieved on one part of the Janus particle surface. For example, Yang's group first treated silica particles with 3-acryloxypropyl trimethoxysilane, and then etched the particles at the Pickering emulsion interface.[24] The protected parts were used to grow polystyrene with various morphologies (e.g., caps, spheres, or nanoflowers) because of the vinyl groups.

Controlled phase separation

The incompatibility of two different materials usually results in phase separation. Sundberg et al built a mathematical model to show that different morphologies of particles consisting of two polymers can be obtained by changing the interfacial tension between two polymers and between the polymers and solvent.[34] This model can be used for predicting the morphology of composite particles that are controlled by thermodynamic equilibrium. For example, Okubo et al prepared a mixture of polystyrene (PS) and poly(methyl methacrylate) (PMMA) in toluene and then emulsified them in water with nonionic surfactant.[35,36] By evaporating toluene slowly, PS and PMMA will phase separate. The poor compatibility between two polymers and low interfacial tension of the polymer/water interface help segregate PS and PMMA into two compartments (i.e., snowman-like particles) rather than forming a core-shell structure. Varying the type or concentration of surfactants will change the particle morphologies. The same principle can be applied to produce magnetic Janus particles, too.[37] Hydrophobic iron oxide nanoparticles and poly (styrene-b-allyl alcohol) were first dispersed in chloroform and emulsified in polyvinyl alcohol solution. During the slow evaporation of the chloroform, the iron oxide nanoparticles precipitated out at the early stage due to its much lower solubility than that of polymer. The magnetic nanoparticles then aggregated further because of the van der Waals interaction, leading to the formation of magneto-biphasic nanocomposites.

Besides solvent evaporation, several other methods have been invented to trigger the phase separation between polymers, such as seeded dispersion polymerization[38,39] and *in situ* polymerization.[40,41] Making anisotropic particles using the seeded emulsion polymerization was first discovered by Sheu et al, [42,43] and then improved by Weitz's group.[44] Crosslinked polystyrene seeds (CPS) were swollen by styrene. The phase separation between the monomer and polymer

occurs after swelling. A thermodynamic model to explain this phenomenon has been proposed by Sheu et al[42,43] The chemical potential of the monomer in the particle $\Delta\bar{G}_{m,p}$ is expressed as the following:

$$\Delta\bar{G}_{m,p} = \Delta\bar{G}_m + \Delta\bar{G}_{el} + \Delta\bar{G}_t \quad (1.1)$$

Where $\Delta\bar{G}_m$ is the free energy of mixing between the monomer and the polymer; $\Delta\bar{G}_{el}$ is the elastic energy of the cross-linked polymer network; and $\Delta\bar{G}_t$ is the interfacial tension between the particle and continuous phase. Substituting the Flory-Huggins expression[45,46] for $\Delta\bar{G}_m$, the Flory-Rehner equation[47] for $\Delta\bar{G}_{el}$, and the Morton equation[48] for $\Delta\bar{G}_t$, one can obtain the following expression:

$$\Delta\bar{G}_{m,p} = \mathrm{RT}[\ln(1 - v_p) + v_p + \times_{m,p} v_p^2] + RTNV_m\left(v_p^{\frac{1}{3}} - \frac{1}{2}v_p\right) + 2V_m\gamma_{p,w}/r \quad (1.2)$$

where v_p is the volume fraction of polymer in the swollen seed; $\times_{m,p}$ is the monomer-polymer interaction parameter; N is effective number of chains in the network per unit volume; V_m is monomer molar volume; $\gamma_{p,w}$ is interfacial tension between particle and water; and r is radius of the swollen seed.

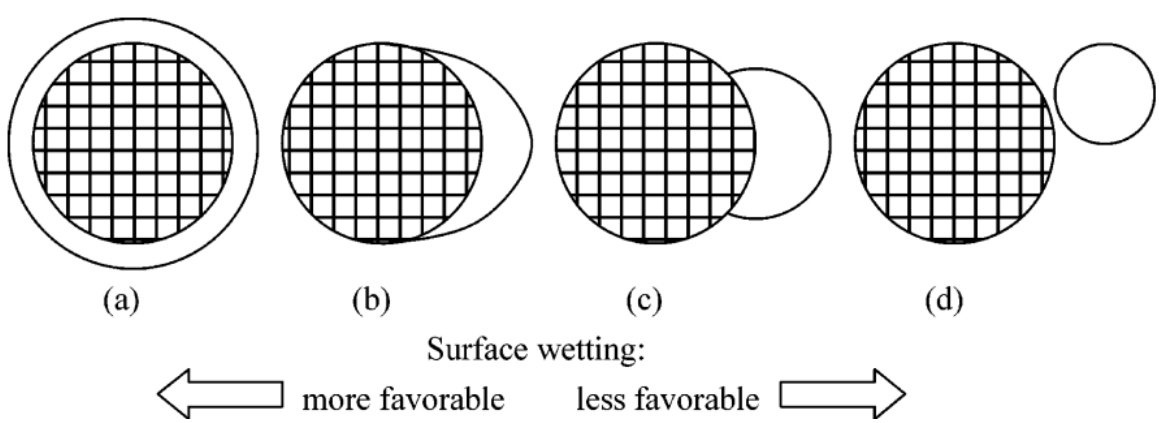

Figure 1.3 The effect of wetting degree between monomer and the crosslinked seed on the particle morphology.[49] Reprinted with permission from ref [49]. Copyright 2006 American Chemical Society.

From the above equation, we can conclude that temperature, monomer/polymer swelling ratio, affinity of monomer to polymer, crosslinking density, interfacial tension, and the size of

seeds, can all affect final particle morphology. For instance, Figure 1.3 illustrates the effect of surface properties of CPS.[49] When $\gamma_{p,w}$ is large or $\gamma_{p,m}$ (the interfacial tension between particle and monomer) is small, the expelled monomer will tend to cover the whole surface of the CPS uniformly (forming a core-shell structure), which is similar to the case of making composite PS-PMMA particles.[35,36] Hence, surface modifcation of the seed is necessary to obtain a desired particle morphology.

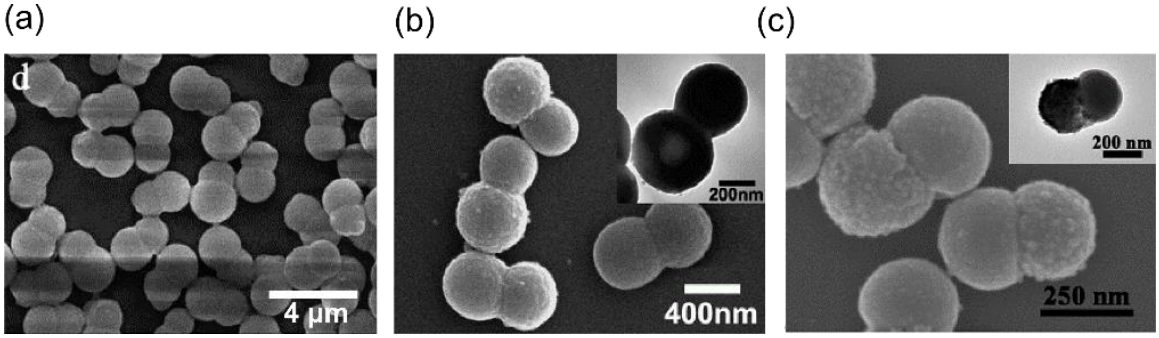

Figure 1.4 Various types of dimers that have been synthesized so far. (a) PMMA dimers.[50] (b) PAN-PS dimers.[52] (c) TiO_2 coated PS dimers.[53] Reprinted with permissions from ref [50], ref [52], and ref [53]. Copyright 2012 Royal Society of Chemistry, 2010 American Chemical Society, 2012 American Chemical Society.

So far, seeded emulsion polymerization is the only method that can be potentially scaled up for industrial applications. In addition to high throughput, this method also offers other advantages, such as high monodispersity, low cost, and versatility. For instance, diverse types of anisotropic polymer particles, such as PMMA dimers (Figure 1.4a),[50] and PMMA-PS dimers[51] have been synthesized. Tang et al made polyacrylonitrile-polystyrene (PAN-PS) dimers out of a crosslinked polyacrylonitrile shell (Figure 1.4b).[52] This work largely expands the dimer species hypothetically, as long as the seed particles can be coated with a crosslinked polymeric shell. However, most dimer particles are polymeric. As we mentioned previously, synthesizing organic-inorganic hybrid particles is within our best interest. One strategy is to directly coat a functional layer, such as TiO_2 on the seed before swelling (Figure 1.4c).[53] However, this method requires that

the thickness of the TiO_2 coating is thin enough so that the monomer can diffuse through to swell the polymeric core and the protrusion can also come out of the shell. Moreover, the morphology of the protrusion was not in high quality due to non-uniform coating of TiO_2.

In summary, there are several challenges in terms of synthesizing anisotropic particles with good monodispersity, high throughput, and great versatility. For example, the seeded emulsion polymerization involves multiple steps that are both tedious and hard to control, especially for people who have little particle synthesis expertise. Even for dimers, we still lack a method that can achieve surface modification on both lobes of dimers independently. Although organic-inorganic hybrid particles are highly desirable, current approaches have shown limited success.

1.2.2 Applications of Anisotropic Particles

Self- and directed-assembly

Anisotropic particles are unique building blocks due to their directional interactions, which have been adopted to self-assemble into complex structures. Relying on depletion interaction, particles with geometric anisotropies can be assembled into a variety of different structures. For example, Scanna et al mixed spherical particles with a dimple as locks and spheres that match the dimple size as keys. With the help of depletant, the reversible lock-and-key attraction can be used to produce dimers, trimers, tetramers, and even polymers.[54] Kraft et al also investigated the assembly behavior of dimers on which one lobe is rough while the other is smooth.[55] They found that, when the depletant size is much smaller than lobe roughness, the smooth lobes can attract each other due to a larger excluded volume compared with the rough lobes. The dimers behave like molecular surfactants that can assemble into clusters above a critical concentration. The "CMC" is affected by the size ratio between smooth and rough lobes. The advantage of exploiting the depletion force is to make reversible superstructures without delicate surface modification.

However, similar to the clustering of isotropic particles via depletion interactions, the monodispersity of the assembled structures is low especially for large clusters.

More specific interactions can also be utilized to assemble particles, especially when the targeted clusters are less than 100 nm. Thiol-metal complexation,[56] streptavidin-biotin interaction,[57] and peptide hybridization[58] have been adopted to make dumbbells or chains based on surface modified metallic nanoparticles. Albeit the assembled clusters via chemical bonding are very stable, it is still difficult to control the monodispersity when the clusters are made up of more than three units. It is also crucial to carefully manipulate other non-covalent forces which can play important roles during the clustering process.

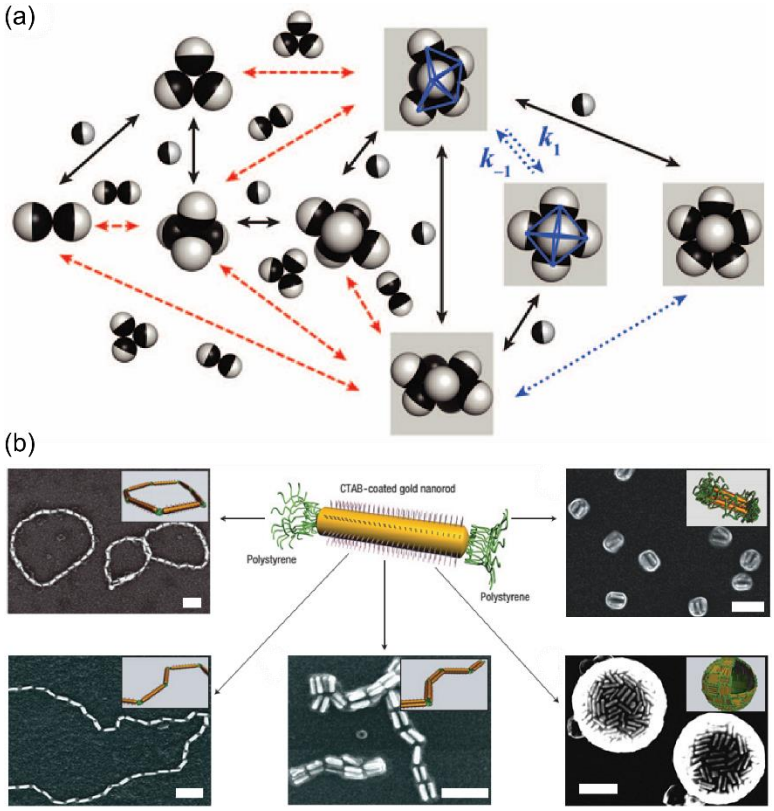

Figure 1.5 Assembled structures via hydrophobic interactions.(a) Networks of reaction pathways, all of the clusters have been observed in 3.8 mM NaCl.[59] (b) SEM images of the self-assembled structures in different solvents mixture.[60] The insets are corresponding schematic graphs. Scale bars: 100 nm. Reprinted with permissions from ref [59], and ref [60]. Copyright 2011 the American Association for the Advancement of Science, 2007 Nature Publishing Group.

By coating hydrophobic molecules on the patches of Janus spheres, one can assemble them into dimers, trimers, and tetramers[59] via directed hydrophobic interactions in low salt concentration (Figure 1.5a). The clusters are formed via three pathways: monomer addition (black arrows), cluster fusion (red arrows), and isomerization (blue arrows). With increasing salt concentration, the small clusters can further aggregate into chainlike structures because of screened electrostatic repulsion between the hydrophilic hemispheres. In addition, solvent also plays an important role in controlling the final configuration (Figure 1.5b).[60] Nie et al prepared cetrimonium bromide (CTAB) coated gold nanorods with two tips attached by thiol-ended PS to generate superstructures, such as rings, chains, and bundle of chains, which can be conveniently controlled by the volume ratio of good versus poor solvent for PS or CTAB.

Directed-assembly using external fields is within our interest too. The strength, effective range, and even sign of field-induced interactions can be easily manipulated over a much wider range than intrinsic particular interactions. Rich assembly phenomena of Janus spheres (hemispheres deposited with a thin magnetic layer) have been observed under magnetic fields. The most intuitive configuration is a linear chain, which can be either "staggered" or "parallel" depending on the thickness of the magnetic layer.[61,62] Granick's group fabricated Janus rods (one hemicylinder of the micron sized silica rod was coated with ~10 nm nickel layer) and discovered different ribbon configurations.[63] The extra dimension of geometric anisotropy clearly adds complexity to the assembled structures. Zerrouki et al adopted the solvent evaporation method to create magnetic patches on silica spheres and studied their assembly behavior under magnetic fields.[64] Because of the steric hindrance between silica spheres, the assembled configurations can be tuned simply by adjusting the size ratio between silica spheres and magnetic patches. Similar structures were also observed in polymer dimers which have magnetic cores encapsulated in the

neck .[65] Pine's group highlighted the significance of the diamagnetic parts. They first partially encapsulated micron-sized hematite cubes in polymerized silicone oil (3-methacryloxypropyl trimethoxysilane).[66] By increasing the size of the diamagnetic parts, the favorable cluster configuration can change from trimers to dimers.

All of the above examples utilized water as the surrounding medium, while particles are somehow paramagnetic. If the water is mixed with ferrofluids, diamagnetic materials can have negative dipoles and paramagnetic materials have positive dipoles. Such kind of dipolar particles can be used for making more complex structures, when combined with geometric anisotropy. As long as the magnetic materials are not superparamagnetic, the assembled structures can be fixed because of the residual magnetism. In comparison, electric fields typically induce structures that will disassembly when the field is turned off. But self-assembly under AC magnetic fields is less interesting because neither ions nor particles respond to uniform AC fields.

Electric-field induced assembly of anisotropic particles is one of the major research areas in our group. We have studied the behavior of both symmetric and asymmetric polystyrene dimers under perpendicularly applied AC electric fields. Symmetric dimers show rich phase phenomena by varying the field strength and frequency.[67] As shown in Figure 1.6a, in lower field strength, the dimers within the aggregate change their orientation from "S" (standing) to "L" (lying) along path 1 and "L" to "S" along path 2. The hydrodynamic, electric, and Brownian torques are all considered to influence the complex phase transition behavior. When the size ratio between two lobes is not equal to one, i.e., for asymmetric dimers, an attractive interaction can be induced between oppositely oriented dimers (Figure 1.6b), which leads to ordered assemblies including square or triangular "Ising-like" lattices at high particle concentrations (~30%).[68] Those interesting phenomena can never be expected in isotropic particle systems.

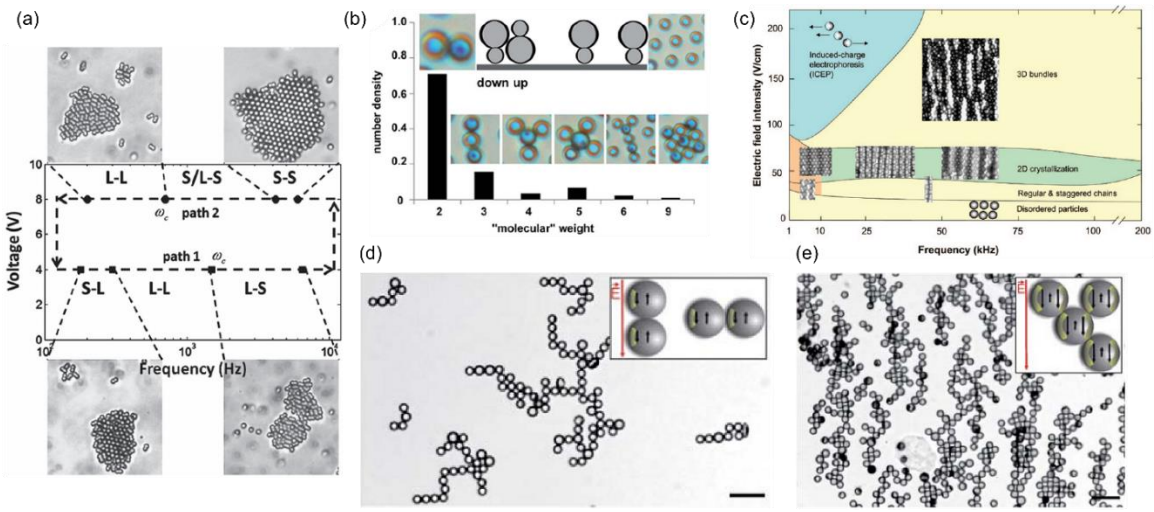

Figure 1.6 Assembled structures under electric fields from anisotropic particles.(a) The phase diagram of symmetric polystyrene dimers under AC electric fields in 10^{-3} M KCl. The squares and circles represent the boundaries between different phases. The phases are marked by "S" (standing up) and "L" (lying down) two letters. The first letter depicts the orientation of the dimers in aggregates while the letter after the hyphen depicts the orientation of the dimers away from the aggregates.[67] (b) Small clusters with different "molecular weight" formed by asymmetric dimers when they are oppositely oriented.[68] (c) Phase diagram of gold-polystyrene Janus spheres in AC electric fields.[69] From (a) to (c), the electric field direction is between the top and bottom of the optical images. (d) Both parallel and perpendicular chains within electric fields are formed by Janus particles with individual 11% gold patches.[70] (e) The Janus particles with two 25% gold patches form diagonal chains.[70] Scale bars: 20 µm. Reprinted with permissions from ref [67], ref [68], ref [69], and ref [70]. Copyright 2012 John Wiley and Sons, 2014 Royal Society of Chemistry, 2008 American Chemical Society, 2010 Royal Society of Chemistry.

The above two examples highlight the important role of geometric anisotropy during assembly. Comprehensive studies about the effect of surface anisotropy were performed by Velev's group.[61,69,70] They applied a perpendicular AC electric field to gold-polystyrene Janus spheres (with a 50% gold patch) solutions (Figure 1.6c).[69] Particles aligned into either regular or staggered chains. By increasing the field intensity, the attraction between chains became stronger and two-dimensional crystals formed. At even higher field strengths, three-dimensional bundles appeared. Moreover, they studied the effect of size and number of gold patches on polystyrene spheres.[70] For particles with 11% gold patches, parallel, perpendicular, and staggered chains are observed (Figure 1.6d), which indicates that the induced dipoles between gold patches and that

between polymer cores are of the similar magnitude. Therefore there is no preferential chain orientation. However, when the polymer particles were coated with two 25% gold patches, they preferred to form diagonal chains as shown in Figure 1.6e, and the possible orientations and magnitude of the induced dipoles are depicted in the inset.

There are still many unexplored questions in the electric-field directed assembly. For example, particles with combined geometric and surface anisotropy are worthwhile to investigate considering the synergistic impacts. The improved understanding of the fundamental interactions involved in the electric-field assembly requires closer collaboration between experimentalists and theoreticians. Such understanding is crucial in order to synthesize particles with tailored anisotropy, before we can build any desired structures.

Propelling Micro/nano-motors

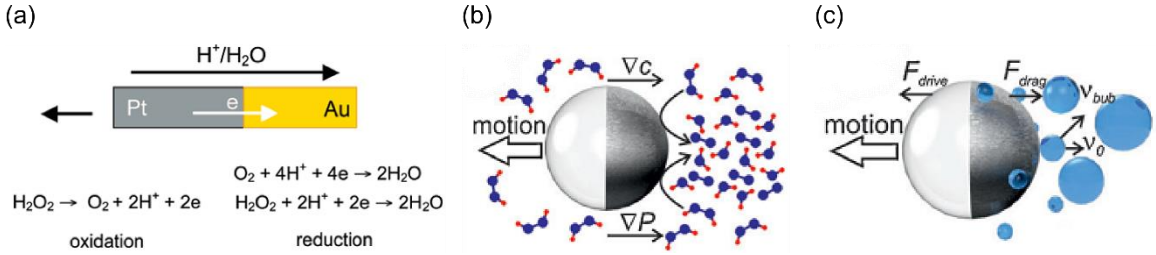

Figure 1.7 Different propulsion mechanisms for micro/nanomotors. (a) self-electrophoresis.[71] (b) self-diffusiophoresis.[75] (c) bubble propulsion.[76] The schemes of (b) and (c) are adopted from Ref. [14], the grey sides are catalytic sides. Reprinted with permissions from ref [71], and ref [14]. Copyright 2006 American Chemical Society, 2014 John Wiley and Sons.

Making self-propelling motors that can move in low Reynolds number (where inertia is negligible) is an extremely difficult task. One approach is to build either a concentration or interfacial tension gradient intrinsically along an anisotropic particle, which can propel in the μm/sec or even mm/sec range (Figure 1.7). Several mechanisms have been explored, which include self-electrophoresis,[71] self-diffusiophoresis,[72] bubble propulsion,[73] self-thermophoresis,[74] etc.

Sen et al pioneered in this field by discovering the autonomous movement of platinum-gold (Pt-Au) hybrid nanorods in an aqueous solution of hydrogen peroxide.[77] Although they first attributed this phenomenon to the interfacial stress gradient caused by different hydrophobicity between two metals,[77] they finally concluded that the self-electrophoretic mechanism is responsible for the motion.[71] Self-electrophoresis is a process when oxidation and reduction take place simultaneously at two ends of the rod. The electron flow within the rod leads to proton migration in the aqueous phase, resulting in an electroosmotic flow (Figure 1.7a). Lots of experimental evidence strongly support this theory. First, by comparing 15 nanorods with different metallic combinations, Sen's group found that the larger the electrochemical potential difference between two metals, the faster the rods move.[71] The propulsion speed can be as high as 30 μm/s (15 body length/s) in 5% H_2O_2. If the surface area is increased (e.g., making rods more rough), the propelling speed can be even faster.[78] Second, by the addition of carbon nanotubes in Pt-Au nanorods, an enhanced speed (~50 μm/s) was observed which can be contributed to the enhanced electron transfer rate.[79] Third, the speed of hybrid nanorod motors can reach 150 μm/s by substituting the gold segments for Ag/Au alloys,[80] because of the enhanced electron transfer reaction of H_2O_2. The same group also found that the speed of bimetallic motors increased five times when 0.1 mM silver salt was added in the solution.[81] Since silver can deposit on the more active Pt end in the hydrogen peroxide solution, it generates the similar Ag/Au alloy effect.

Of course, a rod is not necessarily the best geometry for propulsion.[82] Wheat et al reported a comparable propelling ability using a 5 μm spherical Janus motor with a similar composition.[83] Both the bimetallic rods and Janus spheres were prepared by a template-assisted method. This two-dimensional strategy leads to an extremely low throughput. Moreover, bimetallic rods cannot

move in salt solutions (other than silver nitrate) which severely limit their applications in biologically relevant fluid.

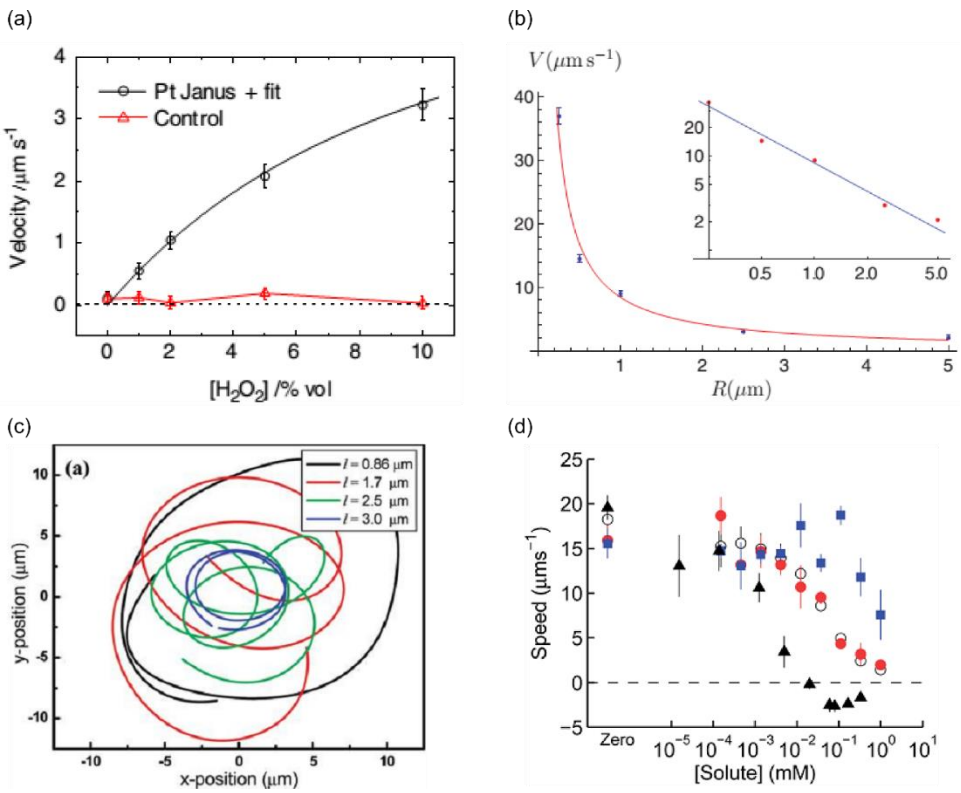

Figure 1.8 Different parameters that affect the motion of Pt-insulator Janus particles in hydrogen peroxide solutions.(a) Comparison of the velocities of Pt-PS Janus spheres and control PS spheres (~1.6 μm) in hydrogen peroxide solutions with different concentrations.[72] (b) Speed of Pt-PS Janus spheres as a function of the particle size in 10% H_2O_2 solution. Inset is the same results shown in log-log form.[85] (c) The trajectories of Pt-SiO_2 Janus particles with TiO_2 arms at four different lengths.[86] (d) Speed of Pt-PS Janus spheres (2 μm) as a function of concentration of CTAB (▲), KBr (●), NaCl (○), and NaOH (■). Positive speed means propulsion towards PS.[87] Reprinted with permissions from ref [72], ref [85], ref [86], and ref [87]. Copyright 2007, 2012 American Physical Society, 2011 American Chemical Society, 2014 Royal Society of Chemistry.

The working principle for self-electrophoresis requires that the motors must be made of electron-conductive materials. To make self-propelling motors out of dielectric materials, different propulsion mechanisms need to be exploited. The self-diffusiophoresis takes advantage of a self-generated concentration gradient by selective reactions (e.g. H_2O_2 decomposition) on one side of the motor, which generates a pressure gradient along the surface of the particle and creates solvent

flow (Figure 1.7b). The most common system in this category is Pt-coated Janus particles.[72,76,84] The motor speed is usually three body length per second, which is weaker than those based on self-electrophoresis. Although the propulsion speed increases with increasing fuel concentration (Figure 1.8a) for a given particle size,[72] Ebbens et al showed an inverse correlation between the particle size and velocity in the range of 100 nm to 5 μm (Figure 1.8b).[85] More interesting moving behavior has been observed when a TiO_2 arm is purposely grown on the Pt side.[86] As the arm length increases, the curvature of the moving trajectory increases (Figure 1.8c).

Although the above experiments largely supported the self-diffusiophoresis mechanism, a recent study on the effect of several ionic species on the motion challenges the above understanding.[87] It is known that the propulsion of Janus particles slows down when pH neutral salt concentration increases. But Brown et al found that the concentration of sodium hydroxide (NaOH) has little effect (Figure 1.8d). When changing the salt from potassium bromide (KBr) or sodium chloride (NaCl) to CTAB, or varying the Pt film thickness from 5 nm to 10 nm, the propulsion direction can even be reversed. The authors attributed the propulsion mechanism to self-electrophoresis, which is induced from an ionic current passing between the pole and equator of the coated Pt film. The exact mechanism behind the propulsion of metallic-dielectric Janus particles is still under debate. More careful studies are necessary to provide further insights into the governing mechanism.

In 2002, the Whitesides group made millimeter sized thin PDMS plates mounted with Pt covered glass filters and observed the motion of plates at the liquid (H_2O_2 solution)/air interface.[88] They attributed the motion to the impulse of bubbles generated due to the decomposition of H_2O_2 catalyzed by the Pt. Ever since this study, micro/nanomotors based on bubble propulsion have

gained tremendous progress, albeit the majority of the motors used in this category is in a tubular structure, the so-called "microjets".[89–91]

The tubular structures favor the formation of bubbles, because the diffusion of oxygen molecules generated from catalytic surface is confined. Subsequently the oxygen molecules accumulate inside the tube to form bubbles. They then escape from the larger opening, as shown in Figure 1.9a. Menjare et al performed a comprehensive theoretical work, which showed that the length, the radius of the microjet, and the H_2O_2 concentration are all important factors for propulsion.[92]

Kuhn et al developed a facile method to fabricate bubble-propelled microengines by electrodepositing Pt clusters on one end of the carbon microtubes (Figure 1.9b).[93] The relative position of the Pt cluster on the carbon tube determines whether it will have linear or circular motion. Another strategy to promote bubble generation is coating pre-synthesized Pt nanoparticles on a thin polymer single crystal film with thiol groups on the surface.[94] Multiple functions can be integrated into the films by the coating of additional nanoparticles (e.g., Fe_3O_4).

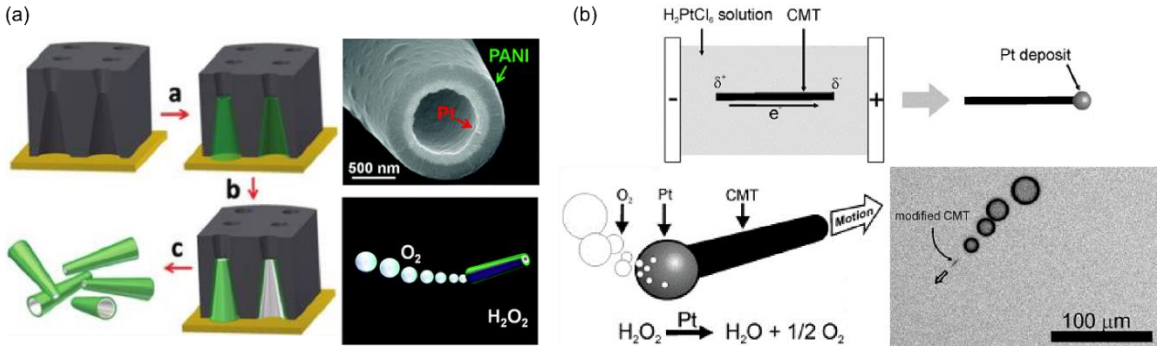

Figure 1.9 Bubble-propelled micromotors with different geometries.(a) Tubular PANI/Pt microengines prepared by cyclopore polycarbonate membranes.[73] (b) Carbon tubes with platinum spheres at one end by the electrodeposition process.[93] Reprinted with permissions from ref [73], ref [93]. Copyright 2011 American Chemical Society, 2011 Elsevier.

In fact, the energy required for bubble formation is the highest on convex surfaces and higher on flat surfaces than on concave surfaces.[95] Only one example of silica-Pt Janus spheres

shows bubble propulsion behavior when the particle size is larger than 10 μm. When the particle size is smaller, the motion is found to be controlled by self-diffusiophoresis.[95] Therefore, there should be some interconnections between the bubble propulsion and the self-diffusiophoresis mechanisms. Meanwhile, the strategy to generate bubbles on a convex surface of a small size particle is missing.

Overall, bubble propulsion can overcome the limitation of low ionic strength required in both self-electrophoresis and self-diffusiophoresis, making motion in biological fluids possible.[73,96] Furthermore, the velocity of bubble-propelled motors can be controlled by ultrasound. Because bubbles can be disrupted by an ultrasonic field, the motors can be turned "on" and "off" within 0.1 second by using an external transducer.[97] Nevertheless, the swimmers that developed, based on the above mechanisms, cannot accomplish directional motions. Utilization of the magnetic field[98] or concentration gradient of the fuel, directional motions can be possibly achieved. The exclusive use of H_2O_2 as a fuel hinders the application of synthetic motors in the biomedical field. Another bottleneck is that the synthesis of micro/nanomotors typically involves costly and inefficient two-dimensional templating methods.

Colloidal Surfactants

People have realized the special activity of colloids at interfaces for a long time. Since then, small particles have been used for different applications, such as the enhanced oil recovery, additives in food industry, and emulsifiers in cosmetics.[99–102] A great deal of work has been devoted to obtaining a deeper understanding in the stabilization mechanisms for better control of emulsions/foams. [16,18]

It is known that molecular surfactants adsorb onto interfaces preferentially because of their amphiphilic properties. It is, however, not necessary for colloids to be amphiphilic in order to

adsorb at an interface. For example, when a particle moves from water to a water/air interface, the original water/air interface will be replaced by two new interfaces: the particle/water and particle/air interfaces. The difference between the original and new interfacial energies can be expressed[15]

$$\Delta G = \pi r^2 \gamma_{\alpha\beta} (1 \pm cos\theta)^2 \quad (1.3)$$

where θ is the contact angle of the particle at the interface, r is particle radius, and $\gamma_{\alpha\beta}$ is interfacial tension between water and air. For a 1 μm particle adsorbed at the water-air interface ($\gamma_{\alpha\beta}$ = 72 mN/m), the energy required for removing it can be as high as 10^7 kT if θ= 90°. But one should notice that ΔG decreases quickly when θ deviates from 90°: It is ~kT when θ is smaller than 20° or higher than 160°. Therefore, the wettability of particles is still important to determine their stability at an interface. This is why commonly used colloidal particles, such as silica or polystyrene, are always pretreated to tune their contact angles close to 90º before using them as emulsifiers.[103,104]

Recently, studies using Janus spheres as colloidal surfactants have shown clear advantages over isotropic particles due to the distinct wettability on two sides of the Janus particles.[16,105–110] The interfacial property of a Janus sphere can be more flexibly tuned by changing the relative hydrophobicity and surface area between two hemispheres. In considering the inherent anisotropic properties of natural particles (such as geometrical or chemical defects), Janus spheres provide a faithful and more controllable model. Meanwhile, unlike homogeneous particles which only show high desorption energy when the contact angle is around 90°, the desorption energy of Janus spheres can still be ~1000 kT even when the average contact angles (θ_{avg}=(θ_{apolar}+θ_{polar})/2) approach to 0° or 180°.[111]

However, Janus spheres are still of spherical shapes, which are very different from their molecular analogues. The geometric anisotropy is very limited in Janus spheres.[112] Kim et al employed amphiphilic colloidal dimers to emulsify hexadecane in water and observed Pickering emulsions in spherical, ellipsoidal, and cylindrical shapes.[113] They contribute the richness of the emulsion shapes to the geometry of the dimers considering Janus particles only produce spherical emulsions. Theoretically, Park et al performed a comprehensive simulation on the equilibrium orientation of Janus ellipsoids and dumbbells at oil-water interface.[114] They showed that both interfacial and geometric anisotropies have profound impacts on the equilibrium orientation and effectiveness for interface stabilization.[115–117]

Aside from simple consideration of the stabilization efficiency of colloidal surfactants at interface, the response of particles toward external stimuli represents another appealing feature. Sun's group fabricated Fe_3O_4-SiO_2 nanorods (Fe_3O_4 nanospheres coated with silica arms) to emulsify water in toluene, and they found that the optimum particle aspect ratio to form stable emulsions is between 2:1 and 4:1.[115] The magnetic colloidosomes showed strong magnetic response and they can even aligned into chains.

Other commonly studied stimuli within the context of biological applications include pH and temperature. As shown in Figure 1.10a, Okubo's group developed mushroom-like Janus particles via the combination of solvent evaporation and atom transfer radical polymerization (ATRP).[17] The polymer particles have a grafted poly (2-(dimethylamino) ethyl methacrylate) (PDM) cap which can reversibly change between amphiphilic and hydrophobic states in response to both pH and temperature. They compared the stabilization efficiency of Janus particles with core-shell particles of similar compositions at 25°C and 60°C as a function of pH. The Janus particles demonstrated much enhanced interfacial activity over a wide pH range at room

temperature. In 2014, Lee et al showed a fascinating example of pH responsive colloidal surfactants composed of polystyrene and poly (acrylic acid) which is capable of emulsifying oil-in-water and water-in-oil droplets by changing the pH in the aqueous phase (Figure 1.10b).[19] This is because the poly (acrylic acid) incorporated compartment can transform into different shapes in response to pH, which is equivalent to changing the contact angle of isotropic particles. The aggregation and dispersion behavior of Janus particles in the range of pH 2.2-7 can also be potentially applied to generate attractive and repulsive emulsions which can lead to complex fluids with pH responsive rheological properties.

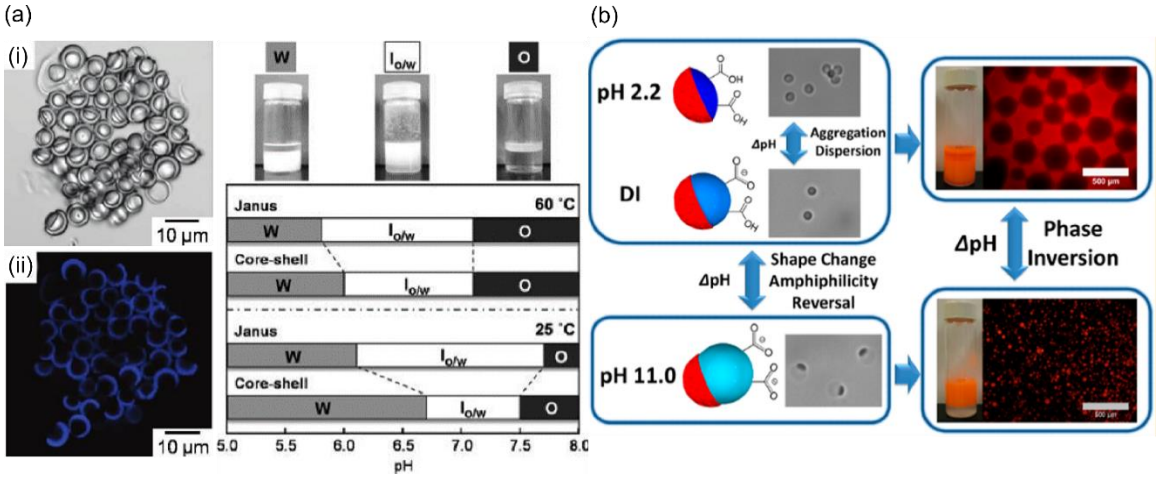

Figure 1.10 Stimuli responsive anisotropic colloidal surfactants.(a) Optical and corresponding fluorescent image of PMMA/P(S-BIEM)-graft-PDMAEMA Janus particles with a pH and thermo-responsive PDMAEMA cap. The scheme shows locations of Janus and core-shell particles at different pH and temperature. "W", "$I_{o/w}$", and "O" denote "in water", "at o/w interface", and "in oil" respectively.[17] (b) Morphology and surface property change of polystyrene and poly (tert-butyl acrylate) Janus particles in response to solution pH and triggered phase inversion emulsion.[19] Reprinted with permissions from ref [17], ref [19]. Copyright 2010, 2014 American Chemical Society.

In principle, parameters such as particle shape, concentration, surface functionality, and contact angle, can all impact the interactions between particles at interfaces. To predict the combined effects of those parameters on both interfacial behavior and interactions of particles is very challenging, which deserves more experimental and theoretical work.

1.3 Summary

As we have mentioned in the above sections, several challenges exist in the synthesis and applications of anisotropic particles. For instance, tedious procedures involve in the seeded emulsion polymerization which makes the synthesis time consuming; methods for generating organic-inorganic hybrid with good monodispersity and high throughput remain elusive; understanding the swimming mechanisms of micro/nanomotors is in slow progress; the combined impacts of geometric and interfacial anisotropy on self-propelling motors are unknown; and the preparation of colloidal surfactants needs elaborate surface modification. Moreover, developing anisotropic particles that can perform multiple tasks as intelligent engines is still at its preliminary stage. This thesis is devoted to address some of the above challenges.

In chapter 2, we combined seeded emulsion polymerization and heterogeneous nucleation to make metal-organic colloidal dimers and demonstrated their novel propulsion behavior under AC electric fields. This bulk synthetic strategy makes a family of hybrid dimers with different metallic compartments. Moreover, it allows us to tune the geometric and interfacial anisotropy of dimers independently. Because of the competition between the electrohydrodynamic flow along the substrate and the induced-charge electroosmotic flow along the metallic lobe, the propelling direction of the hybrid dimer can be controlled under electric fields. The same dimers can also be adopted as chemically powered motors. In chapter 3, we studied the swimming mechanism of platinum-polystyrene (Pt-PS) dimers in hydrogen peroxide solution. We found that both high catalytic activities and surface roughness are essential to induce bubble formation on convex Pt surface. The particle geometry also affects the motion behavior. For example, Pt-PS dimers exhibit both linear and circular motion depending on the position of bubble formation on dimers, while uniformly coated Pt-PS spheres only show linear motion. Our work is the first to uncover the link

between two different propulsion mechanisms, i.e., the self-diffusiophoresis and bubble propulsion. The propulsion behavior of the hybrid dimers under AC electric fields and hydrogen peroxide both emphasizes the importance of combined geometric and interfacial anisotropy on particles. In chapter 4, we developed a new type of colloidal surfactants, which can be utilized to encapsulate active molecules, e.g., organometallic catalysts, to deliver them from water phase to oil phase, and to perform catalytic reaction in the oil phase. This work presents the first demonstration of using bi-compartmental particles for both emulsifier and phase transfer vehicles. It expands the category of colloidal surfactants, simplifies the fabrication process, and can be used as a method for *in situ* cracking of the heavy oil underground. In chapter 5, we investigated the impact of different swelling agents for making anisotropic particles with new types of interfacial and compositional anisotropies. The facile synthetic approach we have developed can fabricate composite particles with high throughput, good monodispersity, and versatility to incorporate different functionalities. Those particles exhibit novel properties such as pH responsive and automotive in electric fields. In chapter 6, we summarize all key conclusions and provide a personal perspective on future directions.

References

(1) Lee, K. J.; Yoon, J.; Lahann, J. Recent Advances with Anisotropic Particles. *Curr. Opin. Colloid Interface Sci.* **2011**, *16*, 195–202.

(2) Nisisako, T.; Torii, T.; Takahashi, T.; Takizawa, Y. Synthesis of Monodisperse Bicolored Janus Particles with Electrical Anisotropy Using a Microfluidic Co-Flow System. *Adv. Mater.* **2006**, *18*, 1152–1156.

(3) Engheta, N. Circuits with Light at Nanoscales: Optical Nanocircuits Inspired by Metamaterials. *Science* **2007**, *317*, 1698–1702.

(4) Chen, T.; Zhang, Z.; Glotzer, S. C. A Precise Packing Sequence for Self-Assembled Convex Structures. *Proc. Natl. Acad. Sci. U. S. A.* **2007**, *104*, 717–722.

(5) Villar, G.; Wilber, A. W.; Williamson, A. J.; Thiara, P.; Doye, J. P. K.; Louis, A. A.; Jochum, M. N.; Lewis, A. C. F.; Levy, E. D. Self-Assembly and Evolution of Homomeric Protein Complexes. *Phys. Rev. Lett.* **2009**, *102*, 118106.

(6) Aranovich, G. L.; Donohue, M. D. Modeling Self-Assembly in Molecular Fluids. *J. Chem. Phys.* **2002**, *116*, 7255–7268.

(7) Pawar, A. B.; Kretzschmar, I.; Aranovich, G.; Donohue, M. D. Self-Assembly of T-Structures in Molecular Fluids. *J. Phys. Chem. B* **2007**, *111*, 2081–2089.

(8) Schmidt, J. J.; Montemagno, C. D. Bionanomechanical Systems. *Annu. Rev. Mater. Res.* **2004**, *34*, 315–337.

(9) Leoni, M.; Kotar, J.; Bassetti, B.; Cicuta, P.; Lagomarsino, M. C. A Basic Swimmer at Low Reynolds Number. *Soft Matter* **2009**, *5*, 472–476.

(10) Dreyfus, R.; Baudry, J.; Roper, M. L.; Fermigier, M.; Stone, H. A.; Bibette, J. Microscopic Artificial Swimmers. *Nature* **2005**, *437*, 862–865.

(11) Loget, G.; Kuhn, A. Electric Field-Induced Chemical Locomotion of Conducting Objects. *Nat. Commun.* **2011**, *2*, 535.

(12) Mano, N.; Heller, A. Bioelectrochemical Propulsion. *J. Am. Chem. Soc.* **2005**, *127*, 11574–11575.

(13) Fernandes, R.; Gracias, D. H. Toward a Miniaturized Mechanical Surgeon. *Mater. Today* **2009**, *12*, 14–20.

(14) Sánchez, S.; Soler, L.; Katuri, J. Chemically Powered Micro- and Nanomotors. *Angew. Chem., Int. Ed.* **2015**, *54*, 1414–1444.

(15) Binks, B. P. Particles as Surfactants—similarities and Differences. *Curr. Opin. Colloid Interface Sci.* **2002**, *7*, 21–41.

(16) Binks, B. P.; Fletcher, P. D. I. Particles Adsorbed at the Oil-Water Interface : A Theroretical Comparision between Spheres of Uniform Wettability and " Janus " Particles. *Langmuir* **2001**, *17*, 4708–4710.

(17) Tanaka, T.; Okayama, M.; Minami, H.; Okubo, M. Dual Stimuli-Responsive "Mushroom-like" Janus Polymer Particles as Surfactants Particulate. *Langmuir* **2010**, *26*, 11732–11736.

(18) Park, B. J.; Brugarolas, T.; Lee, D. Janus Particles at an Oil-Water Interface. *Soft Matter* **2011**, *7*, 6413–6417.

(19) Tu, F.; Lee, D. Shape-Changing and Amphiphilicity-Reversing Janus Particles with pH-Responsive Surfactant Properties. *J. Am. Chem. Soc.* **2014**, *136*, 9999–10006.

(20) Dendukuri, D.; Pregibon, D. C.; Collins, J.; Hatton, T. A.; Doyle, P. S. Continuous-Flow Lithography for High-Throughput Microparticle Synthesis. *Nat. Mater.* **2006**, *5*, 365–369.

(21) Champion, J. A.; Katare, Y. K.; Mitragotri, S. Making Polymeric Micro- and Nanoparticles of Complex Shapes. *Proc. Natl. Acad. Sci.* **2007**, *104*, 11901–11904.

(22) Jiang, S.; Schultz, M. J.; Chen, Q.; Moore, J. S.; Granick, S. Solvent-Free Synthesis of Janus Colloidal Particles. *Langmuir* **2008**, *24*, 10073–10077.

(23) Roh, K.-H.; Martin, D. C.; Lahann, J. Triphasic Nanocolloids. *J. Am. Chem. Soc.* **2006**, *128*, 6796–6797.

(24) Liu, B.; Zhang, C.; Liu, J.; Qu, X.; Yang, Z. Janus Non-Spherical Colloids by Asymmetric Wet-Etching. *Chem. Commun.* **2009**, *0*, 3871–3873.

(25) Bhaskar, S.; Hitt, J.; Chang, S.-W. L.; Lahann, J. Multicompartmental Microcylinders. *Angew. Chem., Int. Ed.* **2009**, *48*, 4589–4593.

(26) Paunov, V. N. Novel Method for Determining the Three-Phase Contact Angle of Colloid Particles Adsorbed at Air - Water and Oil - Water Interfaces. *Langmuir* **2003**, *19*, 7970–7976.

(27) Pinchasik, B. El; Möhwald, H.; Skirtach, A. G. Mimicking Bubble Use in Nature: Propulsion of Janus Particles due to Hydrophobic-Hydrophilic Interactions. *Small* **2014**, *10*, 2670–2677.

(28) Cayre, O.; Paunov, V. N.; Velev, O. D. Fabrication of Asymmetrically Coated Colloid Particles by Microcontact Printing Techniques. *Journal of Materials Chemistry*, **2003**, *13*, 2445–2450.

(29) Fujimoto, K.; Nakahama, K.; Shidara, M.; Kawaguchi, H. Preparation of Unsymmetrical Microspheres at the Interfaces. *Langmuir* **1999**, *15*, 4630–4635.

(30) Hong, L.; Jiang, S.; Granick, S. Simple Method to Produce Janus Colloidal Particles in Large Quantity. *Langmuir* **2006**, *22*, 9495–9499.

(31) Perro, A.; Reculusa, S.; Ravaine, S.; Bourgeat-Lami, E.; Duguet, E. Design and Synthesis of Janus Micro- and Nanoparticles. *J. Mater. Chem.* **2005**, *15*, 3745–3760.

(32) Bao, H.; Peukert, W.; Klupp Taylor, R. One-Pot Colloidal Synthesis of Plasmonic Patchy Particles. *Adv. Mater.* **2011**, *23*, 2644–2649.

(33) Perro, A.; Duguet, E.; Lambert, O.; Taveau, J.-C.; Bourgeat-Lami, E.; Ravaine, S. A Chemical Synthetic Route towards "Colloidal Molecules". *Angew. Chem., Int. Ed. Engl.* **2009**, *48*, 361–365.

(34) Sundberg, D. C.; Durant, Y. G. Latex Particle Morphology, Fundamental Aspects: A Review. *Polym. React. Eng.* **2003**, *11*, 379–432.

(35) Saito, N.; Nakatsuru, R.; Kagari, Y.; Okubo, M. Formation of "Snowmanlike" Polystyrene/poly(methyl Methacrylate)/toluene Droplets Dispersed in an Aqueous Solution of a Nonionic Surfactant at Thermodynamic Equilibrium. *Langmuir* **2007**, *23*, 11506–11512.

(36) Tanaka, T.; Nakatsuru, R.; Kagari, Y.; Saito, N.; Okubo, M. Effect of Molecular Weight on the Morphology of Polystyrene/poly(methyl Methacrylate) Composite Particles Prepared by the Solvent Evaporation Method. *Langmuir* **2008**, *24*, 12267–12271.

(37) Hu, S. H.; Gao, X. Nanocomposites with Spatially Separated Functionalities for Combined Imaging and Magnetolytic Therapy. *J. Am. Chem. Soc.* **2010**, *132*, 7234–7237.

(38) Okubo, M.; Fujibayashi, T.; Yamada, M.; Minami, H. Micron-Sized, Monodisperse, Snowman/confetti-Shaped Polymer Particles by Seeded Dispersion Polymerization. *Colloid Polym. Sci.* **2005**, *283*, 1041–1045.

(39) Skelhon, T. S.; Chen, Y.; Bon, S. A. F. Synthesis of "Hard–Soft" Janus Particles by Seeded Dispersion Polymerization. *Langmuir* **2014**, *30*, 13525–13532.

(40) Lu, W.; Chen, M.; Wu, L. One-Step Synthesis of Organic-Inorganic Hybrid Asymmetric Dimer Particles via Miniemulsion Polymerization and Functionalization with Silver. *J. Colloid Interface Sci.* **2008**, *328*, 98–102.

(41) Teo, B. M.; Suh, S. K.; Hatton, T. A.; Ashokkumar, M.; Grieser, F. Sonochemical Synthesis of Magnetic Janus Nanoparticles. *Langmuir*, **2011**, *27*, 30–33.

(42) Sheu, H. R.; El-Aasser, M. S.; Vanderhoff, J. W. Uniform Nonspherical Latex Particles as Model Interpenetrating Polymer Networks. *J. Polym. Sci., Part A: Polym. Chem.* **1990**, *28*, 653–667.

(43) Sheu, H. R.; El-Aasser, M. S.; Vanderhoff, J. W. Phase Separation in Polystyrene Latex Interpenetrating Polymer Networks. *J. Polym. Sci., Part A: Polym. Chem.* **1990**, *28*, 629–651.

(44) Kim, J.-W.; Larsen, R. J.; Weitz, D. A. Synthesis of Nonspherical Colloidal Particles with Anisotropic Properties. *J. Am. Chem. Soc.* **2006**, *128*, 14374–14377.

(45) Flory, P. J.; Krigbaum, W. R. Thermodynamics of High Polymer Solutions. *Annual Review of Physical Chemistry*, **1951**, *2*, 383–402.

(46) Huggins, M. L. Some Properties of Solutions of Long-Chain Compounds. *J. Phys. Chem.* **1942**, *46*, 151–158.

(47) Flory, P. J.; Rehner, J. Statistical Mechanics of Cross-Linked Polymer Networks II. Swelling. *J. Chem. Phys.* **1943**, *11*, 521–526.

(48) Morton, M.; Kaizerman, S.; Altier, M. W. Swelling of Latex Particles. *Rubber Chemistry and Technology*, **1959**, *32*, 814–824.

(49) Mock, E. B.; De Bruyn, H.; Hawkett, B. S.; Gilbert, R. G.; Zukoski, C. F. Synthesis of Anisotropic Nanoparticles by Seeded Emulsion Polymerization. *Langmuir* **2006**, *22*, 4037–4043.

(50) Peng, B.; Vutukuri, H. R.; van Blaaderen, A.; Imhof, A. Synthesis of Fluorescent Monodisperse Non-Spherical Dumbbell-like Model Colloids. *Journal of Materials Chemistry*, **2012**, *22*, 21893–21900.

(51) Hoffmann, M.; Lu, Y.; Schrinner, M.; Ballauff, M.; Harnau, L. Dumbbell-Shaped Polyelectrolyte Brushes Studied by Depolarized Dynamic Light Scattering. *J. Phys. Chem. B* **2008**, *112*, 14843–14850.

(52) Tang, C.; Zhang, C.; Liu, J.; Qu, X.; Li, J.; Yang, Z. Large Scale Synthesis of Janus Submicrometer Sized Colloids by Seeded Emulsion Polymerization. *Macromolecules* **2010**, *43*, 5114–5120.

(53) Liu, B.; Liu, J.; Liang, F.; Wang, Q.; Zhang, C.; Qu, X.; Li, J.; Qiu, D.; Yang, Z. Robust Anisotropic Composite Particles with Tunable Janus Balance. *Macromolecules* **2012**, *45*, 5176–5184.

(54) Sacanna, S.; Irvine, W. T. M.; Chaikin, P. M.; Pine, D. J. Lock and Key Colloids. *Nature* **2010**, *464*, 575–578.

(55) Kraft, D. J.; Ni, R.; Smallenburg, F.; Hermes, M.; Yoon, K.; Weitz, D. A.; van Blaaderen, A.; Groenewold, J.; Dijkstra, M.; Kegel, W. K. Surface Roughness Directed Self-Assembly of Patchy Particles into Colloidal Micelles. *Proc. Natl. Acad. Sci.* **2012**, *109*, 10787–10792.

(56) Mokari, T.; Rothenberg, E.; Popov, I.; Costi, R.; Banin, U. Selective Growth of Metal Tips onto Semiconductor Quantum Rods and Tetrapods. *Science* **2004**, *304*, 1787–1790.

(57) Caswell, K. K.; Wilson, J. N.; Bunz, U. H. F.; Murphy, C. J. Preferential End-to-End Assembly of Gold Nanorods by Biotin-Streptavidin Connectors. *J. Am. Chem. Soc.* **2003**, *125*, 13914–13915.

(58) Jackson, A. M.; Myerson, J. W.; Stellacci, F. Spontaneous Assembly of Subnanometre-Ordered Domains in the Ligand Shell of Monolayer-Protected Nanoparticles. *Nat. Mater.* **2004**, *3*, 330–336.

(59) Chen, Q.; Whitmer, J. K.; Jiang, S.; Bae, S. C.; Luijten, E.; Granick, S. Supracolloidal Reaction Kinetics of Janus Spheres. *Science* **2011**, *331*, 199–202.

(60) Nie, Z.; Fava, D.; Kumacheva, E.; Zou, S.; Walker, G. C.; Rubinstein, M. Self-Assembly of Metal-Polymer Analogues of Amphiphilic Triblock Copolymers. *Nat. Mater.* **2007**, *6*, 609–614.

(61) Smoukov, S. K.; Gangwal, S.; Marquez, M.; Velev, O. D. Reconfigurable Responsive Structures Assembled from Magnetic Janus Particles. *Soft Matter* **2009**, *5*, 1285–1292.

(62) Zhang, L.; Zhang, F.; Dong, W.-F.; Song, J.-F.; Huo, Q.-S.; Sun, H.-B. Magnetic-Mesoporous Janus Nanoparticles. *Chem. Commun.* **2011**, *47*, 1225–1227.

(63) Yan, J.; Chaudhary, K.; Chul Bae, S.; Lewis, J. a; Granick, S. Colloidal Ribbons and Rings from Janus Magnetic Rods. *Nat. Commun.* **2013**, *4*, 1516.

(64) Zerrouki, D.; Baudry, J.; Pine, D.; Chaikin, P.; Bibette, J. Chiral Colloidal Clusters. *Nature* **2008**, *455*, 380–382.

(65) Nishi, M.; Nagao, D.; Hayasaka, K.; Ishii, H.; Konno, M. Magnetoresponsive, Anisotropic Composite Particles Reversibly Changing Their Chain Lengths by a Combined External Field. *Soft Matter* **2012**, *8*, 11152–11155.

(66) Sacanna, S.; Rossi, L.; Pine, D. J. Magnetic Click Colloidal Assembly. *J. Am. Chem. Soc.* **2012**, *134*, 6112–6115.

(67) Ma, F.; Wang, S.; Smith, L.; Wu, N. Two-Dimensional Assembly of Symmetric Colloidal Dimers under Electric Fields. *Adv. Funct. Mater.* **2012**, *22*, 4334–4343.

(68) Ma, F.; Wang, S.; Zhao, H.; Wu, D. T.; Wu, N. Colloidal Structures of Asymmetric Dimers via Orientation-Dependent Interactions. *Soft Matter* **2014**, *10*, 8349–8357.

(69) Gangwal, S.; Cayre, O. J.; Velev, O. D. Dielectrophoretic Assembly of Metallodielectric Janus Particles in AC Electric Fields. *Langmuir* **2008**, *24*, 13312–13320.

(70) Gangwal, S.; Pawar, A.; Kretzschmar, I.; Velev, O. D. Programmed Assembly of Metallodielectric Patchy Particles in External AC Electric Fields. *Soft Matter* **2010**, *6*, 1413–1418.

(71) Wang, Y.; Hernandez, R. M.; Bartlett, D. J.; Bingham, J. M.; Kline, T. R.; Sen, A.; Mallouk, T. E. Bipolar Electrochemical Mechanism for the Propulsion of Catalytic Nanomotors in Hydrogen Peroxide Solutions. *Langmuir* **2006**, *22*, 10451–10456.

(72) Howse, J.; Jones, R.; Ryan, A.; Gough, T.; Vafabakhsh, R.; Golestanian, R. Self-Motile Colloidal Particles: From Directed Propulsion to Random Walk. *Phys. Rev. Lett.* **2007**, *99*, 048102.

(73) Gao, W.; Sattayasamitsathit, S.; Orozco, J.; Wang, J. Highly Efficient Catalytic Microengines : Template Electrosynthesis of Polyaniline/Platinum Microtubes. **2011**, 11862–11864.

(74) Jiang, H.-R.; Yoshinaga, N.; Sano, M. Active Motion of a Janus Particle by Self-Thermophoresis in a Defocused Laser Beam. *Phys. Rev. Lett.* **2010**, *105*, 268302.

(75) Gibbs, J. G.; Zhao, Y. P. Autonomously Motile Catalytic Nanomotors by Bubble Propulsion. *Appl. Phys. Lett.* **2009**, *94*, 163104.

(76) Paxton, W. F.; Kistler, K. C.; Olmeda, C. C.; Sen, A.; St Angelo, S. K.; Cao, Y.; Mallouk, T. E.; Lammert, P. E.; Crespi, V. H. Catalytic Nanomotors: Autonomous Movement of Striped Nanorods. *J. Am. Chem. Soc.* **2004**, *126*, 13424–13431.

(77) Zacharia, N. S.; Sadeq, Z. S.; Ozin, G. A. Enhanced Speed of Bimetallic Nanorod Motors by Surface Roughening. *Chem. Commun.* **2009**, 5856–5858.

(78) Laocharoensuk, R.; Burdick, J.; Wang, J. Carbon-Nanotube-Induced Acceleration of Catalytic Nanomotors. *ACS Nano* **2008**, *2*, 1069–1075.

(79) Demirok, U. K.; Laocharoensuk, R.; Manesh, K. M.; Wang, J. Ultrafast Catalytic Alloy Nanomotors. *Angew. Chem., Int. Ed.* **2008**, *47*, 9349–9351.

(80) Kagan, D.; Calvo-Marzal, P.; Balasubramanian, S.; Sattayasamitsathit, S.; Manesh, K. M.; Flechsig, G.-U.; Wang, J. Chemical Sensing Based on Catalytic Nanomotors: Motion-Based Detection of Trace Silver. *J. Am. Chem. Soc.* **2009**, *131*, 12082–12083.

(81) Gibbs, J. G.; Fragnito, N. A.; Zhao, Y. Asymmetric Pt/Au Coated Catalytic Micromotors Fabricated by Dynamic Shadowing Growth. *Appl. Phys. Lett.* **2010**, *97*, 253107.

(82) Wheat, P. M.; Marine, N. A.; Moran, J. L.; Posner, J. D. Rapid Fabrication of Bimetallic Spherical Motors. *Langmuir* **2010**, *294*, 13052–13055.

(83) Ebbens, S.; Tu, M.-H.; Howse, J.; Golestanian, R. Size Dependence of the Propulsion Velocity for Catalytic Janus-Sphere Swimmers. *Physical Review E*, **2012**, *85*, 020401–020404.

(84) Gibbs, J. G.; Kothari, S.; Saintillan, D.; Zhao, Y.-P. Geometrically Designing the Kinematic Behavior of Catalytic Nanomotors. *Nano Lett.* **2011**, *11*, 2543–2550.

(85) Brown, A.; Poon, W. Ionic Effects in Self-Propelled Pt-Coated Janus Swimmers. *Soft Matter* **2014**, 4016–4027.

(86) Ke, H.; Ye, S.; Carroll, R. L.; Showalter, K. Motion Analysis of Self-Propelled Pt-Silica Particles in Hydrogen Peroxide Solutions. *J. Phys. Chem. A* **2010**, *114*, 5462–5467.

(87) Ismagilov, R. F.; Schwartz, A.; Bowden, N.; Whitesides, G. M. Autonomous Movement and Self-Assembly. *Angew. Chem., Int. Ed.* **2002**, *41*, 652–654.

(88) Mei, Y.; Huang, G.; Solovev, A. A.; Ureña, E. B.; Mönch, I.; Ding, F.; Reindl, T.; Fu, R. K. Y.; Chu, P. K.; Schmidt, O. G. Versatile Approach for Integrative and Functionalized Tubes by Strain Engineering of Nanomembranes on Polymers. *Adv. Mater.* **2008**, *20*, 4085–4090.

(89) Solovev, A. A.; Mei, Y.; Ureña, E. B.; Huang, G.; Schmidt, O. G. Catalytic Microtubular Jet Engines Self-Propelled by Accumulated Gas Bubbles. *Small* **2009**, *5*, 1688–1692.

(90) Solovev, A. a.; Sanchez, S.; Pumera, M.; Mei, Y. F.; Schmidt, O. G. Magnetic Control of Tubular Catalytic Microbots for the Transport, Assembly, and Delivery of Micro-Objects. *Adv. Funct. Mater.* **2010**, *20*, 2430–2435.

(91) Manjare, M.; Yang, B.; Zhao, Y.-P. Bubble-Propelled Microjets: Model and Experiment. *J. Phys. Chem. C* **2013**, *117*, 4657–4665.

(92) Fattah, Z.; Loget, G.; Lapeyre, V.; Garrigue, P.; Warakulwit, C.; Limtrakul, J.; Bouffier, L.; Kuhn, A. Straightforward Single-Step Generation of Microswimmers by Bipolar Electrochemistry. *Electrochim. Acta* **2011**, *56*, 10562–10566.

(93) Dong, B.; Zhou, T.; Zhang, H.; Li, C. Y. Directed Self-Assembly of Nanoparticles for Nanomotors. *ACS Nano* **2013**, *7*, 5192–5198.

(94) Manjare, M.; Yang, B.; Zhao, Y.-P. Bubble Driven Quasioscillatory Translational Motion of Catalytic Micromotors. *Phys. Rev. Lett.* **2012**, *109*, 128305.

(95) Gao, W.; Uygun, A.; Wang, J. Hydrogen-Bubble-Propelled Zinc-Based Microrockets in Strongly Acidic Media. *J. Am. Chem. Soc.* **2012**, *134*, 897–900.

(96) Xu, T.; Soto, F.; Gao, W.; Garcia-Gradilla, V.; Li, J.; Zhang, X.; Wang, J. Ultrasound-Modulated Bubble Propulsion of Chemically-Powered Microengines. *J. Am. Chem. Soc.* **2014**, *136*, 8552–8555.

(97) Kline, T. R.; Paxton, W. F.; Mallouk, T. E.; Sen, A. Catalytic Nanomotors: Remote-Controlled Autonomous Movement of Striped Metallic Nanorods. *Angew. Chem., Int. Ed.* **2005**, *44*, 744–746.

(98) Sullivan, A. P.; Kilpatrick, P. K. The Effects of Inorganic Solid Particles on Water and Crude Oil Emulsion Stability. *Ind. Eng. Chem. Res.* **2002**, *41*, 3389–3404.

(99) Hunter, T. N.; Pugh, R. J.; Franks, G. V.; Jameson, G. J. The Role of Particles in Stabilising Foams and Emulsions. *Advances in Colloid and Interface Science*, **2008**, *137*, 57–81.

(100) Gaaseidnes, K.; Turbeville, J. Separation of Oil and Water in Oil Spill Recovery Operations. *Pure Appl. Chem.* **1999**, *71*, 95–101.

(101) Dickinson, E. Food Emulsions and Foams: Stabilization by Particles. *Curr. Opin. Colloid Interface Sci.* **2010**, *15*, 40–49.

(102) Horozov, T.; Binks, B.; Aveyard, R.; Clint, J. Effect of Particle Hydrophobicity on the Formation and Collapse of Fumed Silica Particle Monolayers at the Oil–water Interface. *Colloids Surf., A* **2006**, *282-283*, 377–386.

(103) Ghezzi, F.; Earnshaw, J. C.; Finnis, M.; McCluney, M. Pattern Formation in Colloidal Monolayers at the Air-Water Interface. *J. Colloid Interface Sci.* **2001**, *238*, 433–446.

(104) C. Casagrande, P. Fabre, E. Raphael, M. V. Janus Beads": Realization and Behaviour at Water/Oil Interfaces. *Europhys. Lett.* **1989**, *9*, 251–255.

(105) Ondarçuhu, T.; Fabre, P.; Raphaël, E.; Veyssié, M. Specific Properties Amphiphilic Particles at Fluid Interfaces. *J. Phys. Fr.* **1990**, *51*, 1527–1536.

(106) Jiang, S.; Granick, S. Janus Balance of Amphiphilic Colloidal Particles. *J. Chem. Phys.* **2007**, *127*, 161102.

(107) Hirose, Y.; Komura, S.; Nonomura, Y. Adsorption of Janus Particles to Curved Interfaces. *J. Chem. Phys.* **2007**, *127*, 054707.

(108) Cheung, D. L.; Bon, S. A. F. Stability of Janus Nanoparticles at Fluid Interfaces. *Soft Matter* **2009**, *5*, 3969–3976.

(109) Fan, H.; Resasco, D. E.; Striolo, A. Amphiphilic Silica Nanoparticles at the Decane-Water Interface: Insights from Atomistic Simulations. *Langmuir* **2011**, *27*, 5264–5274.

(110) Binks, B. P.; Fletcher, P. D. I. Particles Adsorbed at the Oil-Water Interface : A Wettability and " Janus " Particles. *Langmuir* **2001**, *17*, 4708–4710.

(111) Akiva, U.; Margel, S. Surface-Modified Hemispherical Polystyrene/polybutyl Methacrylate Composite Particles. *J. Colloid Interface Sci.* **2005**, *288*, 61–70.

(112) Kim, J.-W.; Lee, D.; Shum, H. C.; Weitz, D. A. Colloid Surfactants for Emulsion Stabilization. *Adv. Mater.* **2008**, *20*, 3239–3243.

(113) Park, B. J.; Lee, D. Equilibrium Orientation of Nonspherical Janus Particles at Fluid-Fluid Interfaces. *ACS Nano* **2012**, *6*, 782–790.

(114) Zhang, L.; Zhang, F.; Wang, Y.-S.; Sun, Y.-L.; Dong, W.-F.; Song, J.-F.; Huo, Q.-S.; Sun, H.-B. Magnetic Colloidosomes Fabricated by Fe3O4–SiO2 Hetero-Nanorods. *Soft Matter* **2011**, *7*, 7375–7381.

(115) Ruhland, T. M.; Gröschel, A. H.; Walther, A.; Müller, A. H. E. Janus Cylinders at Liquid-Liquid Interfaces. *Langmuir* **2011**, *27*, 9807–9814.

(116) Glaser, N.; Adams, D. J.; Böker, A.; Krausch, G. Janus Particles at Liquid-Liquid Interfaces. *Langmuir* **2006**, *22*, 5227–5229.

CHAPTER 2

BULK SYNTHESIS OF METAL-ORGANIC HYBRID DIMERS AND THEIR PROPULSION UNDER ELECTRIC FIELDS

Modified from a paper published in *ACS Applied Materials & Interfaces*

Sijia Wang[2], Fuduo Ma[3], Hui Zhao[4], and Ning Wu[5]

2.1 Abstract

Metal-organic hybrid particles have great potential in applications such as colloidal assembly, autonomous micro-robots, targeted drug delivery, and colloidal emulsifiers. Existing fabrication methods, however, typically suffer from low throughput, high operation cost, and imprecise property control. Here, we report a facile and bulk synthesis platform that makes a wide range of metal-organic colloidal dimers. Both geometric and interfacial anisotropy on the particles can be tuned independently and conveniently, which represents a key advantage of this method. We further investigate the self-propulsion of platinum-polystyrene dimers under perpendicularly applied electric fields. In 10^{-4} M potassium chloride (KCl) solution, the dimers exhibit both linear and circular motion with the polystyrene lobes facing towards the moving direction, due to the induced-charge electroosmotic flow surrounding the metal-coated lobes. Surprisingly, in deionized water, the same dimers move with an opposite orientation, i.e., the metallic lobes face the forward direction. This is because of the impact of another type of flow: the electrohydrodynamic flow arising from the induced charges on the conducting substrate. The competition between the electrohydrodynamic flow along the substrate and the induced-charge electroosmotic flow along the metallic lobe determines the propulsion direction of hybrid dimers

[1]Reprinted with permission from *ACS Appl. Mater. Interfaces* **2014**, *6*, 4560–4569.
Copyright 2014 American Chemical Society.
[2,3]Graduate student and [5]Assistant Professor, respectively,
Department of Chemical and Biological Engineering, Colorado School of Mines.
[4]Associate Professor, Department of Mechanical Engineering, University of Nevada.
[2]Particle synthesis and [3]propulsion under electric fields.
[4,5]Development of theoretical models.
[5]Author for correspondence.

under electric fields. Our synthetic approach will provide potential opportunities to study the combined impacts of the geometric and interfacial anisotropy on the propulsion, assembly, and other applications of anisotropic particles.

2.2 Introduction

Particles with anisotropic properties in geometry, interfacial functionality, or chemical composition have attracted a lot of attention recently due to their potential applications in self-assembly,[1] optical display,[2] emulsion stabilization,[3] molecular probes,[4] autonomous motors,[5] or drug delivery.[6] For example, gold nanorods with geometric anisotropy have been used as biomedical imaging agents due to their strong surface plasmon resonance at the near-infrared region.[7] When colloidal particles are functionalized with DNA patches, they behave similarly to the multi-valent atoms and can self-assemble into a variety of colloidal molecules in a controllable fashion.[8]

Among different types of anisotropic particles, the metal-organic hybrid particles[9] are of special interest because (1) the interfacial properties on the metallic and organic regimes can be conveniently tailored due to their complementary difference in surface chemistry and (2) they combine unique properties from both metallic and organic materials such as the electric conductivity, catalytic activity, plasmonic property, etc. The asymmetric interfacial properties can be utilized to induce autonomous motion of hybrid particles in aqueous solutions based on a number of different mechanisms.[10–13] For example, a platinum-polystyrene sphere[14] can move actively in hydrogen peroxide solutions due to the so-called self-diffusiophoresis.[15] The platinum-coated hemisphere catalyzes the decomposition of hydrogen peroxide, while the polystyrene hemisphere remains inert. As a result, there is a concentration gradient of oxygen surrounding the particle, which generates solvent flow and propels the particle. In addition to the difference in

catalytic activity, metallic and polymeric materials have distinguished electric polarizabilities. For example, gold-polystyrene Janus spheres can move laterally under a perpendicularly applied AC electric field,[16] due to the so-called induced-charge electroosmosis.[17,18] The external electric field polarizes the metallic hemisphere and induces mobile ions in the diffusive layer, which move under the applied field and generate a net fluid flow towards the gold-coated part. Previous studies, however, were mostly focused on Janus spheres, which is still symmetric in shape. The combined impacts of geometric and interfacial anisotropy on the self-propulsion of particles remain elusive at this moment.

This is partially because it is challenging to fabricate metal-organic particles in high throughput with narrow polydispersity, which is crucial for practical applications. Conventional strategies[12-16] often rely on templating methods by first depositing a monolayer of particles on a flat substrate. A thin metallic film is then deposited on the particle array via thermal or electron-beam evaporation. Due to the shadowing effect, the top surface of the particles is coated with metal while the bottom half stays intact. This technique is inherently two-dimensional and is associated with low throughput and high operational cost. A three-dimensional templating method based on Pickering emulsion, in principle, could produce large quantities of hybrid particles.[19,20] However, it is usually restricted to spherical particles with carefully-tailored surface properties in order to form Pickering emulsions. The geometric and interfacial anisotropy cannot be modulated independently. Controlled heterogeneous nucleation and growth[21–24] have also been developed for making metal-organic particles. But they are either too small[25,26] for *in situ* observation through optical microscopy or hard to control the morphologies precisely.[22,27,28] Facile synthetic strategy to make microscopic metal-organic particles with tunable anisotropy in both geometry and interfacial property is still missing.

Here we report a bulk synthesis approach to make different types of metal-organic hybrid dimers with independent control of the geometric and interfacial anisotropy. Modified from previously developed seeded-emulsion polymerization,[29–37] we make polystyrene dimers with well-controlled geometric anisotropy that can be characterized by the size ratio between two lobes and bond length. The incorporation of functional silanes during the synthesis stage allows us to combine the sol-gel chemistry[38] and amine-metal complexation[39,40] to grow a variety of metallic films on one of the two lobes selectively. Two key advantages of this synthetic route are that (1) we can systematically tune the geometric and interfacial anisotropy between two lobes in an independent and precise fashion, and (2) it produces hybrid particles with high throughput and reasonable monodispersity. We have also investigated the self-propulsion of the platinum-polystyrene dimers under electric fields. In higher salt concentrations (e.g. 10^{-4} M), we find that the dimers propel with the dielectric lobes facing the forward direction, primarily due to the induced-charge electroosmosis surrounding the metallic lobe. At lower salt concentrations (e.g., in deionized water), they, however, move with the metallic lobes orienting in the propulsion direction, because of stronger electrohydrodynamic flow along the conducting substrate. Moreover, the propulsion speed of a hybrid dimer is very sensitive to its orientation, which can be conveniently tuned by the frequency. Our studies reveal important impacts of the combined geometric and interfacial anisotropy on the electric-field driven propulsion of colloidal particles.

2.3 Experimental Methods

The following sections first introduce the materials we used in this Chapter, and afterwards describe the detailed experimental procedures and characterization methods.

2.3.1 Materials

Styrene, divinylbenzene (DVB), sodium 4-vinylbenzenesulfonate, polyvinylpyrrolidone (PVP, M_w: ~40,000), sodium dodecyl sulfate (SDS), 3-aminopropyltriethoxysilane, trisodium citrate, L-ascorbic acid, fluorescein isothiocyanate and rhodamine 6G are purchased from Sigma-Aldrich. 3-(trimethoxysily) propyl acrylate (TMSPA) is purchased from TCI. Hydrogen tetrachlororaurate(III) trihydrate ($HAuCl_4 \cdot 3H_2O$, 99.9+%), silver nitrate ($AgNO_3$, 99.9+%), and potassium tetrachloroplatinate(II) (K_2PtCl_4, 99.9%) are bought from Alfa Aesar. The thermal initiator V65 is bought from Wako Chemicals. All chemicals are used as received except that both styrene and divinylbenzene are purified by aluminum oxide before usage.

2.3.2 The synthesis of polystyrene (PS) dimers

The synthetic route we use to make colloidal dimers is based on a modification of the methods of Sheu and Kim.[28-36] Typically, spherical PS seed particles are first prepared by the dispersion polymerization in methanol[41] and are cleaned four times via centrifugation (4000 rpm, 30 mins, IEC HT Centrifuge). After that, a mixture of 4 ml 5 wt% PVP aqueous solution, 0.5 ml 2wt% SDS, 1 ml styrene, 0.05 ml DVB, 0.05 ml functional silanes (such as 3-trimethoxysily propyl acrylate), and 0.02 g V65 is emulsified using ultrasonication (Branson digital sonifier 450). The emulsion is then used to swell 1 ml polystyrene seed particles (10 wt% in deionized water) for 24 hours. The swollen seeds are then crosslinked in the reactor at 70°C for another 24 hours. PS dimers are synthesized via a second swelling stage. Again, we use styrene (with variable amount to control the size of the second lobe) to swell 1 ml crosslinked PS seeds (1 wt%) with 4 ml 5 wt% PVP, 0.5 ml 2 wt% SDS, and 2 wt% V65. Subsequently, polymerization is performed at 70 °C for 24 hrs. The synthesized dimers are then cleaned four times via centrifugation.

2.3.3 Selective coating of gold nanoparticles on the crosslinked lobe

During the synthesis of the crosslinked spherical seed particles, different types of functional silane molecules are incorporated in the particles to control the bond length of the dimers. In addition, those silane molecules remain in the crosslinked lobe, which allows us to further attach (3-aminopropyl)-triethoxysilane (APS) on it via the silane coupling chemistry. For example, we mix 0.02 g dimers in 15 ml ethanol solution with 100 µl APS and 3 ml ammonia hydroxide (30% NH_4OH) and stir the mixture for 24 hours at the room temperature.[39] The particles are then washed by ethanol for four times and re-dispersed in water. Once the dimers are functionalized with APS, we mix them with citrate-stabilized gold nanoparticle solutions (Turkevich method[42]) in a sonication bath for 1 hour. We then use track-etched filter papers (Whatman) to completely remove free gold nanoparticles that were suspended in the solution.

2.3.4 Gold/silver and platinum shell growth on gold-coated dimers

To coat an additional layer of silver, we mix 4 ml gold-coated dimers (0.1 wt%) with 0.4 ml 30 mM $HAuCl_4 \cdot 3H_2O/AgNO_3$ by sonication for 10 minutes. Then 70µl formaldehyde is added in the solution, while stirring for 10 minutes. 1 ml NH_4OH (0.3%) is added within 2 minutes afterwards. The solution is kept stirring for 1 hour and allowed standing for another hour. For the shell growth of platinum, we mix 1 ml gold-coated dimers (~10^8 particles/ml) with 0.3 ml 100 mM freshly prepared ascorbic acid solution, followed by adding 2 ml 2 mM K_2PtCl_4 within one hour. If a thicker and more uniform coating is desired, one can re-coat the dimers with 0.3 ml 100 mM ascorbic acid and 2 ml 2 mM K_2PtCl_4 solutions without stirring. Two-step-coating is necessary because if a higher concentration of platinum salt is used (e.g., 5 mM K_2PtCl_4), we lose the capability to coat platinum anisotropically on one lobe only.

2.3.5 Characterization of the hybrid dimers

The surface morphologies of hybrid dimers are characterized by scanning electron microscopy (JEOL JSM-7000F). The element compositions of both lobes are analyzed by the energy dispersive X-ray (EDX). An inverted microscope (Olympus IX71) is used for bright-field and fluorescent microscopy.

2.3.6 Propulsion Pt-PS dimers under electric fields

After synthesis, the Pt-PS dimers are first cleaned four times using centrifugation. They are then dispersed in 10^{-4} M potassium chloride (KCl) solution or in deionized water. The dimers are then injected into the chamber formed by two pieces of indium-tin-oxide (ITO) glasses with an insulating spacer (~100 μm in thickness) to control the separation between top and bottom electrodes. After dimers settle down to the bottom substrate, an AC electric field is applied (RigolDG1022). A high speed camera (SILICON VIDEO® monochrome SV642) is used to record the motion of dimers at 30 frames/sec for at least 30 seconds. We then use Image J[43] to track the dimers' movement and obtain their instantaneous positions.

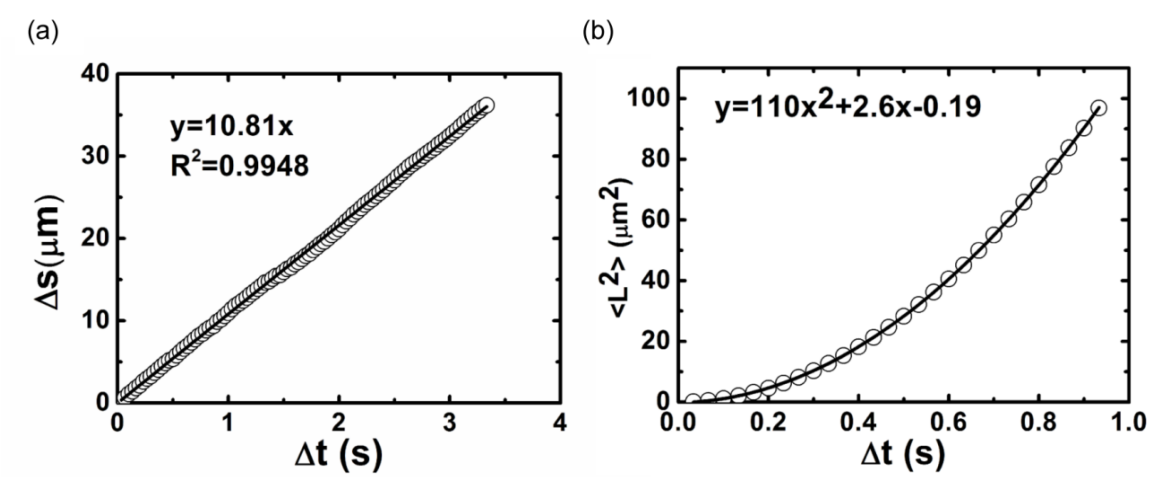

Figure 2.1 Two methods for calculation the speed of dimers. (a) The accumulative displacement of a dimer at E=100 V_{pp}/mm and 2k Hz. (b) The mean square displacement of the dimer following the same trajectory.

Two different methods have been employed to obtain the average velocities of the dimers. As shown in Figure 2.1a, the accumulative displacement of a dimer is plotted vs. time. The average velocity is then calculated from the slope. This method, in principle, works the best when the trajectory is unidirectional and the propulsion velocity is much faster than the Brownian motion. We have also employed a second method which was first proposed by Howse et al[14] Shown in Figure 2.1b, the mean square displacement (MSD) $\langle \Delta L^2 \rangle$ is plotted as a function of time. When Δt is much less than the inverse rotational diffusion coefficient of the dimer τ_R, the curve can be fitted[14] with a quadratic function of Δt

$$\langle \Delta L^2 \rangle = v^2 \Delta t^2 + 4 D_e \Delta t \tag{2.1}$$

where v and D_e are the propulsion speed and the effective diffusion coefficient of a dimer, respectively. We confirm that both methods yield very similar propulsion velocities.

2.4 Results and Discussion

We choose seeded emulsion polymerization to bulk synthesize colloidal polystyrene dimers with both geometric and interfacial anisotropies. The advantage of this method is that we can vary the coating species on the crosslinked lobe simply by changing the metallic precursors, which broaden the applications of the particles into diverse fields. Moreover, we can independently tune the two anisotropies, which can help study the two effects separately. This powerful synthetic platform promotes our understanding to a great extent during our investigation of dimer propulsion. For the first time, we showed both individual and combined effects from geometric and interfacial anisotropies on particle propulsion behaviors under AC electric field.

2.4.1 Synthesis of the metal-organic hybrid dimer

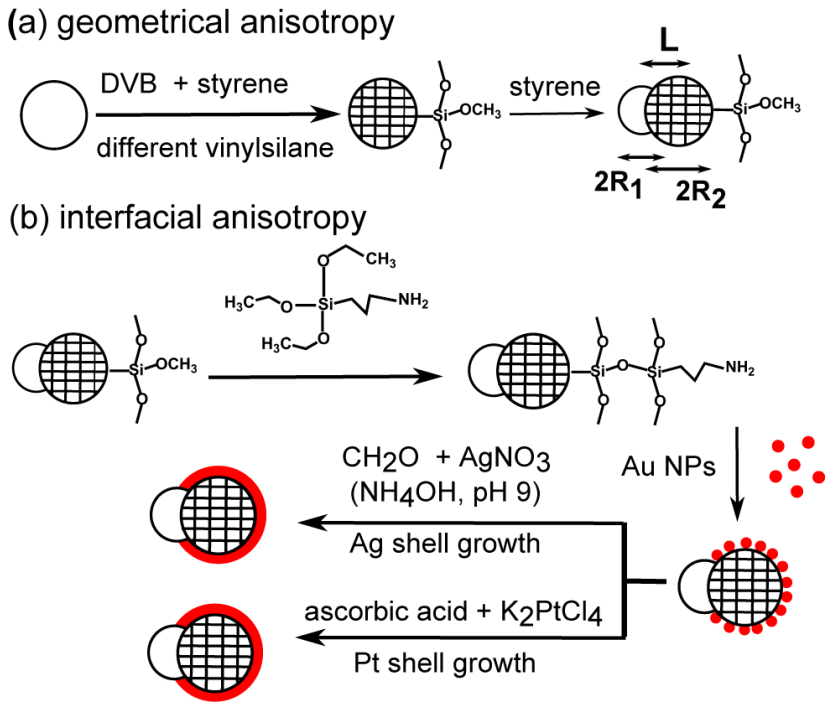

Figure 2.2 The chemical route to synthesizing metal-organic hybrid dimers with independently tunable (a) geometric and (b) interfacial anisotropy.

Figure 2.2 illustrates our overall strategy to synthesize the metal-organic hybrid dimers with independently tunable geometric and interfacial anisotropy. Polystyrene dimers are first synthesized via the seeded emulsion polymerization.[29–37] In brief, spherical polystyrene particles are first crosslinked by adding styrene, divinylbenzene, and different types of functional vinylsilanes. The crosslinked seeds are then swollen with styrene again, where the elastic contraction of the crosslinked polystyrene expels styrene out of the swollen seeds and gives rise to a second lobe. To increase the stability of dimers in water, we have also added co-monomer sodium 4-vinylbenzenesulfonate so that the dimers are negatively charged. As shown in Figure 2.2, both size ratio $\alpha = R_1 / R_2$ and the dimensionless bond length $\beta = L/(R_1 + R_2)$ are important parameters to characterize the geometric anisotropy.

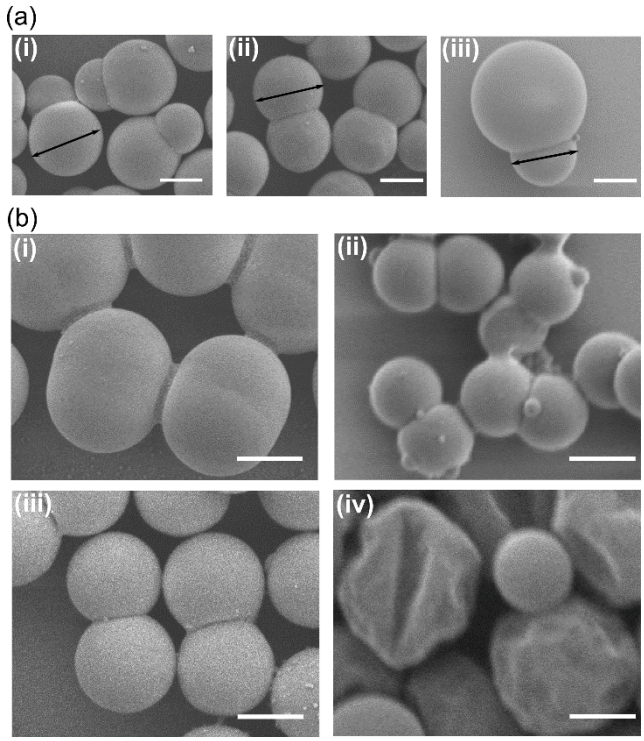

Figure 2.3 Geometric anisotropy of the dimers. (a) The size ratio between two lobes $\alpha = R_1 / R_2$ can be tuned by changing the amount of styrene used to swell the crosslinked particles. The black arrow represents the seed particle, i.e., the original lobe. (b) The dimer bond length $\beta = L / (R_1 + R_2)$ is sensitive to the type of functional vinylsilanes added in the crosslinked seeds: (i) no silane (β = 0.3); (ii) styrylethyl-trimethoxysilane (β =0.7); (iii) trimethoxysilylpropylacrylate (β =0.84); (iv) methacryloxypropyl-trimethoxysilane (β =1). Scale bar for both (a) and (b): 1 μm.

The size ratio α can be controlled by adjusting the relative amount of styrene to the crosslinked seed particles (CPS) during the second swelling stage. As shown in Figure 2.3a, the second lobe diameter increases with increasing amount of styrene while CPS (i.e., the original lobe) does not change its size significantly. We have also found that the incorporation of functional vinylsilanes during the synthesis of CPS has a significant impact on the bond length due to different compatibility between silane molecules and styrene. Shown in Figure 2.3b, when the functionality in the silane molecule changes from styrene to acrylate, the bond length β increases due to an enhanced phase separation during the polymerization of the second lobe. In the case of

methacryloxypropyltrimethoxysilane, styrene barely swells the CPS and the bond length is approximately one, indicating poor compatibility between methacrylate and styrene. We hypothesize that the poorer compatibility between the silane and styrene, more hydrophilic the CPS surface is, which increases the bond length between the two lobes.[44]

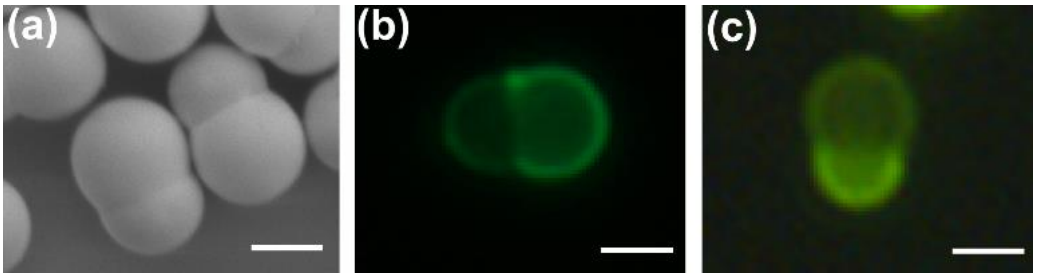

Figure 2.4 Interfacial anisotropy of the dimers. (a) A SEM image of dimers in which the larger lobe is coated with (3-aminopropyl)-triethoxysilane. (b) The fluorescent image of the same dimer after it is coated with neutral FITC dye, which couples strongly with amine groups on the larger lobe. (c) The fluorescent image of the same dimer after it is coated with positively charged rhodamine 6G, which can absorb on negatively charged surfaces. Scale bar: 1μm.

In addition to its impact on the geometric anisotropy, the incorporation of functional silanes in CPS also allows us to create interfacial anisotropy conveniently. For example, we can attach (3-aminopropyl)-triethoxysilane (APS) on the crosslinked lobe using the silane coupling chemistry.[38] The attachment of APS can be confirmed by the fluorescence image in Figure 2.4b, where neutral fluorescein isothiocyanate (FITC) are selectively bonded to the amine group on the original (large) lobe via the isothiocyanate-amine reaction.[33] Alternatively, when we mix dimers with a positively charged dye rodamine 6G, a stronger florescent intensity is observed on the second (smaller) lobe because the amine groups partially neutralize the negative charges on the original lobe (Figure 2.4c).

Since amine groups form complexes with metals, we can further coat a thin layer of pre-synthesized gold nanoparticles (~20nm) selectively on the lobe with APS functionalization, as shown in Figure 2.5a and 2.5b. As a comparison, the control experiment show non-discriminating

coating (Figure 2.5b-iii) on dimers with APS functionalization on both lobes. The surface coverage of gold nanoparticles can be further enhanced by mixing the Au-PS dimers with chloroauric (Au^{III}) acid and formaldehyde (Figure 2.5c). The additional reduction of gold ions (by formaldehyde) on the seeded gold nanoparticles creates more uniform and dense coating on the hybrid dimers, as evidenced by both SEM images and the energy-dispersive X-ray spectroscopy (EDX) results in Figure 2.5c.

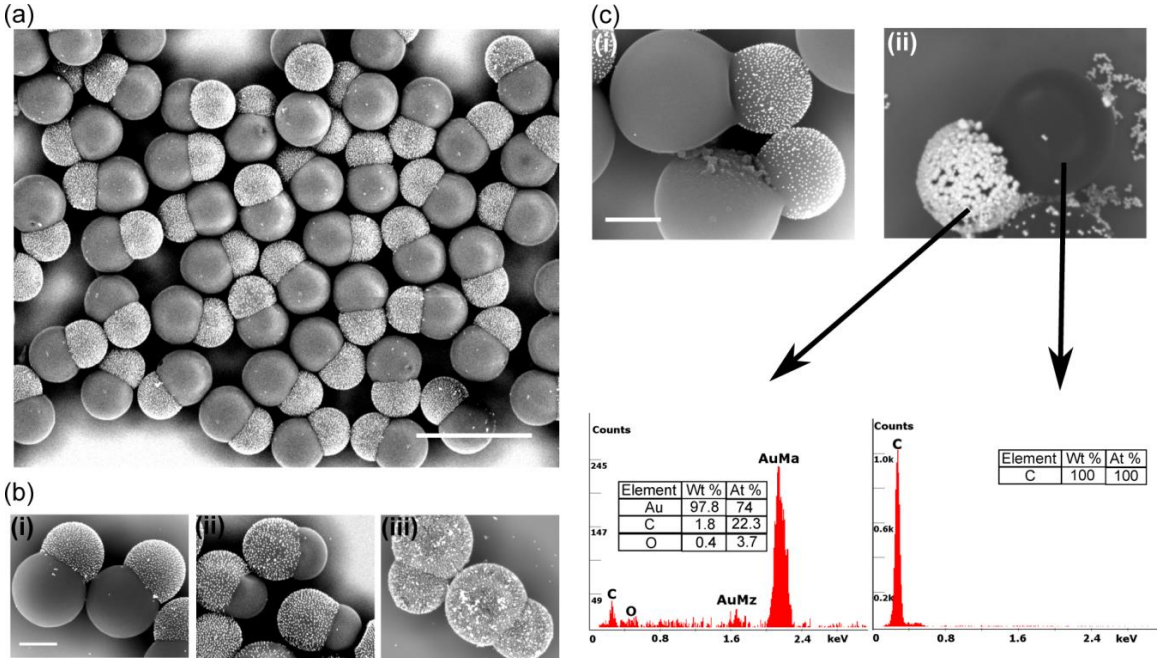

Figure 2.5 Gold coating on dimers. (a) A large field of view of gold-polystyrene hybrid dimers where the brighter lobe is coated with gold nanoparticles. Scale bar: 4μm. (b) Gold nanoparticles can be selectively coated on either smaller (i) or larger (ii) lobes as long as it is functionalized with APS. (iii) When both lobes bear APS, gold nanoparticles are coated uniformly. Scale bar: 1μm. The scale bar is the same for all three images. (c) The surface coverage of gold can be significantly enhanced through a second nucleation and growth stage (ii) on the Au-PS hybrid dimers (i), as evidenced by the element analysis using EDX. Scale bar: 1μm. The scale bar is the same for both images.

The gold nanoparticles on hybrid dimers could be utilized as heterogeneous nucleation sites to promote selective coating of other metals, such as silver and platinum. The former is an excellent candidate for plasmonic materials[45] while the latter is an important catalyst. By suspending Au-PS dimers in silver nitrate solution and using formaldehyde[46] or hydroxylamine hydrochloride[39] as

the reducing agent, we can grow a silver shell with thickness ~100 nm anisotropically (Figure 2.6). We have found that the proper control of the redox speed is critical for selective coating of silver. Homogeneous nucleation of silver in solution can be suppressed by choosing a milder reducing agent (e.g., formaldehyde), limiting the maximal salt concentration (<5mM), and adding ammonia hydroxide dropwise to carefully control the solution pH.

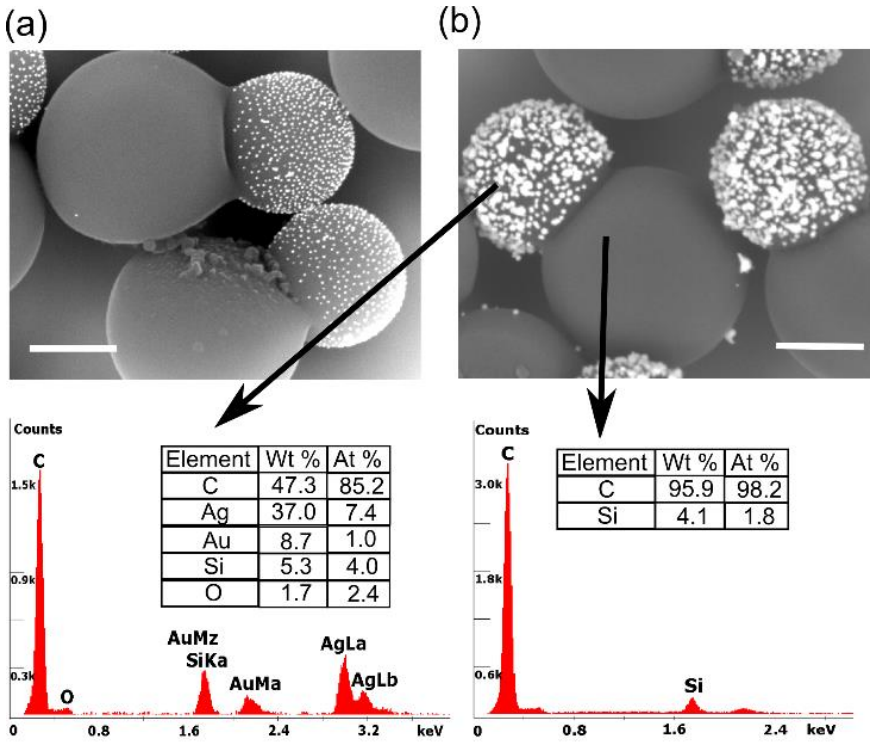

Figure 2.6 Silver coating on dimer. (a) The SEM image of gold nanoparticles coated on dimers. (b) Silver can be further coated on the Au-PS dimer, as shown in the corresponding EDX analyses. Scale bar: 1μm. The Si signal arises from the silicon substrate used for preparing SEM samples.

We can adopt a similar strategy to grow a platinum shell on the dimers although a milder reducing agent than formaldehyde is necessary. Otherwise, black precipitates would form within five minutes even at neutral pH. Therefore, we choose ascorbic acid as the reducing agent.[47–49] With properly adjusted pH, reaction temperature, and the concentration ratio between dimers and metal salts, we have successfully achieved a selective coating of platinum, as shown in Figure 2.7a.

Although keeping lower ascorbic acid concentration helps maintaining the anisotropic coating due to a lower reaction speed, its concentration needs to be high enough to ensure good colloidal stability during the shell growth. However, this limited redox speed prevents platinum from coating a complete shell in one step. Therefore multiple growth steps are required for dense coating. Both room and low temperatures (e.g., ice bath) yield satisfactory coatings on the selected lobe during the first step (Figure 2.7a), but low temperature is necessary in the second growth step to reduce the extent of platinum deposition on the other lobe (Figure 2.7a-ii and iv).

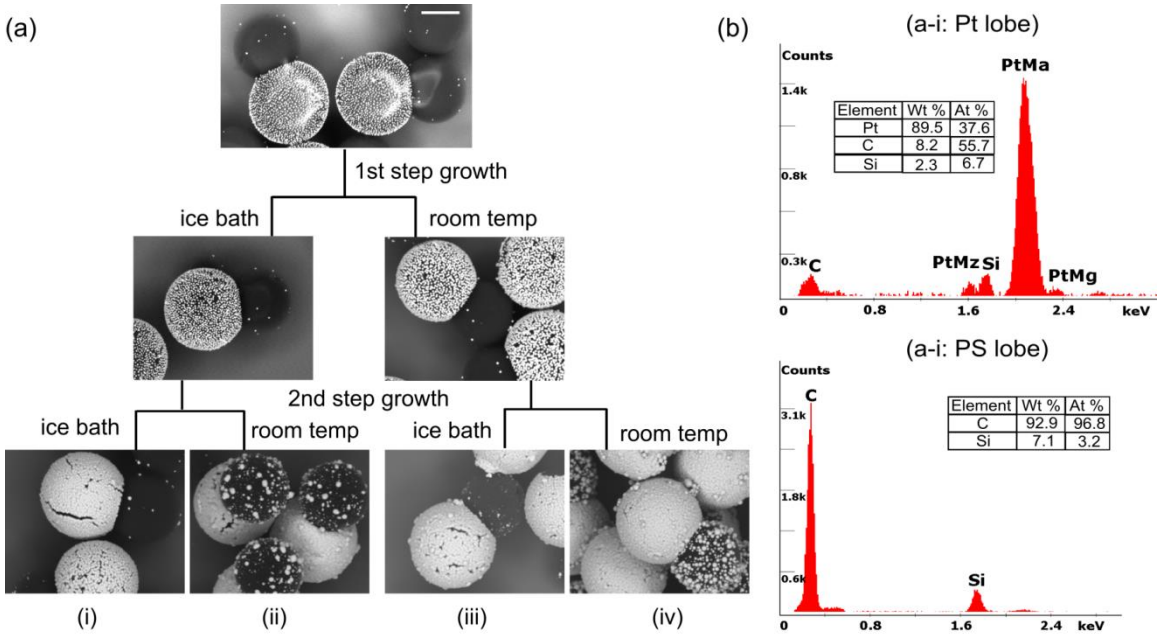

Figure 2.7 Platinum coating on dimers. (a) The effect of deposition temperature on the surface coverage of the platinum coating. Two-step growth made more uniform and denser coating of platinum if the conditions are correct, e.g., (i) and (iii). Scale bar: 1μm. Scale bar is the same for all the images. (b) The EDX analysis on the platinum-coated and polystyrene lobes. The Si signal arises from the silicon substrate used for preparing SEM samples.

In summary, we have developed a versatile and bulk-synthesis strategy to make metal-organic hybrid dimers with tunable geometric and interfacial anisotropy. We demonstrate our concept by three types of metallic coatings: gold, silver, and platinum, and it should be readily extended to other types of inorganic materials too. Compared with the commonly used templating

methods for making Janus spheres,[11,12,14] our bulk-synthesis strategy has the great potential for high throughput and low cost. Moreover, the combined asymmetry in both geometric shape and interfacial property on our dimers allows us to investigate their impacts on the self-propulsion of micro-particles in a fluidic environment. In the following, we will report the electric-field driven propulsion of platinum-polystyrene dimers. The self-propulsion of dimers due to asymmetric catalytic reactions (e.g., in hydrogen peroxide) will be presented in Chapter 3.

2.4.2 Propulsion of hybrid dimers under electric fields

The synthesized Pt-PS dimers are first dispersed in deionized water. An appropriate amount of salt (e.g., potassium chloride) is then added to control the Debye length. We first examine the propulsion of hybrid dimers in 10^{-4} M salt water under AC electric fields. At ~2 kHz, dimers align parallel to the substrate (i.e., lying dimers) except a few are perpendicular (i.e., standing dimers). We find that all lying dimers move horizontally, while both standing dimers and uncoated polystyrene dimers only exhibit Brownian motions. We also notice that a moving dimer always orients its polystyrene lobe towards the propelling direction. Based on the recorded images, we calculate the propulsion velocities at different field strengths and frequencies. We find that the velocity of lying dimers scales well with the square of the field strength, i.e., $u \propto E_0^2$.

Our observations can be explained based on the theory of the induced-charge electrophoresis.[17,18] As shown in Figure 2.8, the platinum-coated lobe is much more polarizable than the bare polystyrene lobe because of the metallic conductivity. Under external fields, the polarized platinum lobe induces diffusive charges surrounding it. Those ions can respond to the applied field and generate the so-called "induced-charge electroosmotic (ICEO)" flow of solvent from the pole to the equator of the particle. While Figure 2.8 only illustrates the solvent flow during one half period of the AC field, the flow direction does not change during the second half period

because both the applied field and the induced-charges will change their signs. For a metallic sphere, the quadrupolar solvent flow does not generate a net movement of the particle because of the symmetry. But for Pt-PS dimers, the ICEO flow is much stronger along the platinum-coated lobe than the dielectric (polystyrene) lobe. Such a broken symmetry[18] in the interfacial polarizability induces the propulsion of dimers along the long axis, *i.e.*, the x-direction. Therefore, the hydrodynamic shear will push the dimer with its dielectric lobe oriented forward, regardless of its relative sizes. This directional movement is consistent with both ICEO theory[18] and experiments for Janus spheres.[16]

Our chemically synthesized Pt-PS dimers, unlike Janus spheres, are anisotropic in both geometry and interfacial property. This combined anisotropy has profound impacts on the propulsion of particles that have not been observed before. For example, previous studies[16] mainly reported linear motions because the metal film was E-beam evaporated uniformly on one half surface of the polystyrene spheres. We, however, have observed both linear and circular motions for our dimers (Figure 2.8a). The circular motion could be attributed to potentially non-uniform platinum coating on the lobe. As depicted in Figure 2.8c, if one hemisphere of the small lobe has slightly denser coating than the other half, asymmetric ICEO flow along the y-direction could also be generated. Different from the IECO flow in x-direction, the y-direction flow is perpendicular to the dimer's long axis. Therefore, a torque would be generated, which makes the dimer move counterclockwise, as shown in Figure 2.8c. Because of the chemical deposition method employed here, the platinum coating on the smaller lobe is far from perfectly uniform, as can be seen clearly in Figure 2.7. Even a slight imbalance on the uniformity between left and right hemispheres could cause the circular motion. In fact, we observe equal populations of clockwise and counterclockwise motions due to the stochastic nature of coating. This ICEO flow in the y-direction is, however, a

secondary effect compared with the ICEO flow in the x-direction, which arises from the anisotropy in polarizability between metallic and dielectric lobes. Therefore, the circular motion is manifested more significantly at higher field strengths. Even when dimers underwent the circular motion they still keep their orientations with the dielectric lobe pointing forward, again because the primary and strong ICEO flow is along the x-direction.

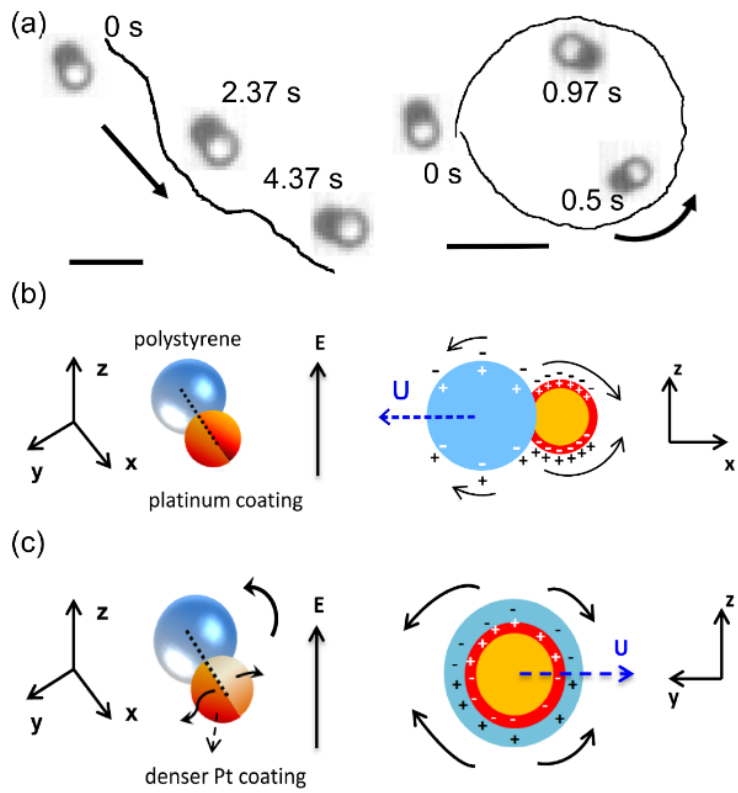

Figure 2.8 Propulsion of Pt-PS dimers under AC electric field. (a) The linear (100 V_{pp}/mm, 2 kHz) and circular (200 V_{pp}/mm, 2 kHz) motions of Pt-PS dimers. Several optical snapshots show the dimer's orientation at different time. The dark sphere represents the platinum-coated lobe. Scale bars for both trajectories: 10 μm. The dimer itself is about 2 μm. The platinum-coated lobe (R_1=0.85 μm) is smaller than the dielectric lobe (R_2=0.95 μm). (b) The polarizability difference between the platinum-coated and polystyrene lobes generates an ICEO flow that propels the dimer laterally with its polystyrene lobe oriented along the forward direction. The $x-y$ plane is parallel to the bottom substrate, and the electric field is applied in the z-direction. (c) The circular motion of dimers could be attributed to the non-uniform coating of platinum on the smaller lobe.

After confirming the behavior in high salt concentration, we also investigate the propulsion of Pt-PS dimers in deionized water. The behavior of our dimers is surprising. First, about 50% of

the lying dimers orient to the opposite direction now, i.e., the platinum-coated lobe orients toward the propelling direction (Figure 2.9a). When we plot the velocity vs. the field strength, it still scales with E_0^2. Second, although the rest of the dimers still orient in the same direction to what is predicted by the ICEO theory (i.e., the polystyrene lobe faces forward), the speed reduces dramatically. This is unexpected since the ICEO velocity should remain almost unchanged when the salt concentration is reduced.[16,50]

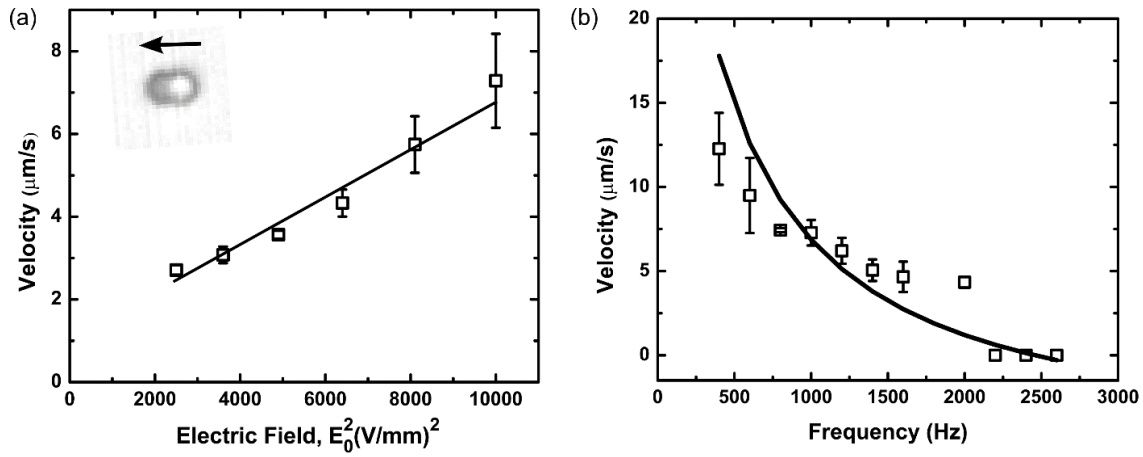

Figure 2.9 Propulsion speed as a function of electric field strength and frequency. (a) Velocity of Pt-PS dimers in DI water (16 Vpp and 2 kHz). The arrow indicates the propulsion direction, which is opposite to Figure 2.8. (b) Frequency dependence of the velocity. The solid curve is the theoretical prediction based on eqn 2.2 with f $\approx$0.0055.

Here we hypothesize that there exists a second type of flow, i.e., the electrohydrodynamic (EHD) flow along the conducting substrate. It can compete with the ICEO and propel our dimers into the opposite direction under certain experimental conditions. The EHDF on a conducting substrate was first proposed by Trau, Ristenpart, Aksay, and Saville.[51–54] Under applied electric fields, an excess amount of surface charges can be induced within the diffusive layer near the conducting substrate. Although the external field is perpendicular to the substrate, the polarization of the particle distorts its local field and creates a tangential component that is parallel to the substrate. This tangential field acts on the induced charges and causes an EHDF along the

substrate. In fact, this flow can be strong enough to entrain all neighboring particles and to form close-packed aggregates.[51]

Although the EHDF is essentially an induced-charge electroosmosis along the electrode, there are some subtle differences between EHDF and ICEO on the particle. For example, ICEO around a dielectric particle is negligible. Although EHDF is initiated from the conducting substrate, it has impacts on both dielectric and metallic particles, as long as they are close to the substrate. Also, the emergence of the tangential field is different between EHDF and ICEO. In EHDF, the tangential field component arises from the polarization field of the particle's induced dipole. Therefore, the polarization coefficient K, especially its imaginary part K'' (which represents the phase lag between the dipole field and the applied field) is an important parameter in EHDF. Based on the theory of EHDF,[54] it can be further shown that the EHDF velocity near a spherical particle is[55]

$$U_{EHDF} \sim f \frac{K''\kappa D}{\omega} \frac{\varepsilon\varepsilon_0 E_0^2}{\mu} \tag{2.2}$$

where f is a prefactor that depends on the distance between the particle and the electrode and ω is the frequency. Based on Eq. 2.2, we can calculate the EHDF velocities acting on both lobes. By further combing the ICEO velocity on the metallic lobe, the net velocity of the dimer at different frequencies is plotted by the solid line in Figure 2.9b. Our calculation fits the experimental data reasonably well. Detailed analyses can be found in our recent publication.[56]

2.5 Conclusions

We report a bulk-synthesis strategy to make metal-organic hybrid dimers with both geometric and interfacial anisotropy. By changing the type of functional vinylsilanes in the crosslinked seed particles and the amount of styrene in the swelling stage, we can tune the

geometric anisotropy such as the bond length $L/(R_1 + R_2)$ from 0.3 to 1 and the size ratio R_1/R_2 from 0.45 to 1. By taking advantage of the amine-metal complexation, gold nanoparticles can be coated selectively on the crosslinked lobe, forming metal-organic hybrid dimers. Dense metallic shells such as gold, silver, and platinum can be further grown on the gold-seeded lobe due to enhanced heterogeneous nucleation. Among various types of reducing agents, the chemical with lower reduction speed (e.g., formaldehyde for gold/silver and ascorbic acid for platinum) can make hybrid dimers with excellent contrast in surface coating between two lobes. With the complementary difference in surface chemistry between the metallic and organic lobes, it is possible to further modify the interfacial properties on asymmetric particles, such as the hydrophobicity, surface charge, catalytic activity, etc. Such a synthetic platform will allow facile tuning of geometric and interfacial anisotropy on a wide range of metal-organic hybrid dimers, which offers abundant opportunities to study their specific and synergistic impacts on self-assembly, multi-tasking and self-motile motors, colloidal emulsifiers, etc.

Once having synthesized the platinum-polystyrene dimers, we further investigate the self-propulsion of those particles under perpendicularly applied electric fields. In higher salt concentrations (e.g., 10^{-4} M KCl solution), the hybrid dimers exhibited both linear and circular motions. This is due to the significant contrast in the electric polarizability between metal-coated and polystyrene lobes, where the induced-charge electroosmotic flow surrounding the metal-coated lobe propelled the dimer with its polystyrene lobe facing towards the moving direction. The same dimer, however, can move with the opposite orientation in deionized water, i.e., the dimer orients its metal-coated lobe towards the propelling direction. Although the velocities in both cases scale with the square of the applied field, their frequency dependence are rather different. We argue that an additional electroosmotic flow, the electrohydrodynamic flow arising from the induced

charges along the conducting substrate, can also propel the dimer. Depending on both frequency and salt concentration, the competition between the electrohydrodynamic and the induced-charge electroosmosis can influence the orientation of the dimer during its propulsion. Interestingly, the propulsion speed of the dimer can be tuned by its orientation too. When it lies on the substrate, it moves due to the asymmetric EHD and ICEO flow. The flow asymmetry disappears when it stands on the substrate (i.e., aligns parallel to the applied field). Therefore, the synergistic effect of both geometric and interfacial anisotropy can be utilized to control both propulsion and orientation of colloidal dimers.

2.6 Acknowledgement

This work was supported by the start-up funds from Colorado School of Mines and National Science Foundation (CBET-1336893).

References

(1) Sacanna, S.; Irvine, W. T. M.; Chaikin, P. M.; Pine, D. J. Lock and Key Colloids. *Nature* **2010**, *464*, 575–578.

(2) Nisisako, T.; Torii, T.; Takahashi, T.; Takizawa, Y. Synthesis of Monodisperse Bicolored Janus Particles with Electrical Anisotropy Using a Microfluidic Co-Flow System. *Adv. Mater.* **2006**, *18*, 1152–1156.

(3) Tanaka, T.; Okayama, M.; Minami, H.; Okubo, M. Dual Stimuli-Responsive "Mushroom-Like" Janus Polymer Particles as Particulate Surfactants. *Langmuir* **2010**, *0*, 11732–11736.

(4) Choi, J.; Zhao, Y.; Zhang, D.; Chien, S.; Lo, Y.-H. Patterned Fluorescent Particles as Nanoprobes for the Investigation of Molecular Interactions. *Nano Lett.* **2003**, *3*, 995–1000.

(5) Paxton, W. F.; Kistler, K. C.; Olmeda, C. C.; Sen, A.; St Angelo, S. K.; Cao, Y.; Mallouk, T. E.; Lammert, P. E.; Crespi, V. H. Catalytic Nanomotors: Autonomous Movement of Striped Nanorods. *J. Am. Chem. Soc.* **2004**, *126*, 13424–13431.

(6) Kagan, D.; Laocharoensuk, R.; Zimmerman, M.; Clawson, C.; Balasubramanian, S.; Kang, D.; Bishop, D.; Sattayasamitsathit, S.; Zhang, L.; Wang, J. Rapid Delivery of Drug Carriers Propelled and Navigated by Catalytic Nanoshuttles. *Small* **2010**, *6*, 2741–2747.

(7) Tong, L.; Wei, Q.; Wei, A.; Cheng, J.-X. Gold Nanorods as Contrast Agents for Biological Imaging: Optical Properties, Surface Conjugation and Photothermal Effects. *Photochem. Photobiol.* **2009**, *85*, 21–32.

(8) Wang, Y.; Wang, Y.; Breed, D. R.; Manoharan, V. N.; Feng, L.; Hollingsworth, A. D.; Weck, M.; Pine, D. J. Colloids with Valence and Specific Directional Bonding. *Nature* **2012**, *491*, 51–55.

(9) Perro, A.; Reculusa, S.; Ravaine, S.; Bourgeat-Lami, E.; Duguet, E. Design and Synthesis of Janus Micro- and Nanoparticles. *J. Mater. Chem.* **2005**, *15*, 3745–3760.

(10) Wilson, D. A.; Nolte, R. J. M.; Hest, J. C. M. Van. Autonomous Movement of Platinum-Loaded Stomatocytes. *Nat. Chem.* **2012**, *4*, 268–274.

(11) Ke, H.; Ye, S.; Carroll, R. L.; Showalter, K. Motion Analysis of Self-Propelled Pt-Silica Particles in Hydrogen Peroxide Solutions. *J. Phys. Chem. A* **2010**, *114*, 5462–5467.

(12) Gibbs, J. G.; Zhao, Y. P. Autonomously Motile Catalytic Nanomotors by Bubble Propulsion. *Appl. Phys. Lett.* **2009**, *94*, 163104–3.

(13) Chang, S. T.; Paunov, V. N.; Petsev, D. N.; Velev, O. D. Remotely Powered Self-Propelling Particles and Micropumps Based on Miniature Diodes. *Nat. Mater.* **2007**, *6*, 235–240.

(14) Howse, J. R.; Jones, R. A. L.; Ryan, A. J.; Gough, T.; Vafabakhsh, R.; Golestanian, R. Self-Motile Colloidal Particles: From Directed Propulsion to Random Walk. *Phys. Rev. Lett.* **2007**, *99*, 048102–048104.

(15) Anderson, J. L.; Prieve, D. C. Diffusiophoresis Caused by Gradients of Strongly Adsorbing Solutes. *Langmuir* **1991**, *7*, 403–406.

(16) Gangwal, S.; Cayre, O.; Bazant, M.; Velev, O. Induced-Charge Electrophoresis of Metallodielectric Particles. *Phys. Rev. Lett.* **2008**, *100*, 1–4.

(17) Squires, T. M.; Bazant, M. Z. Induced-Charge Electro-Osmosis. *J. Fluid Mech.* **2004**, *509*, 217–252.

(18) Squires, T. M.; Bazant, M. Z. Breaking Symmetries in Induced-Charge Electro-Osmosis and Electrophoresis. *J. Fluid Mech.* **2006**, *560*, 65–101.

(19) Liu, B.; Wei, W.; Qu, X.; Yang, Z. Janus Colloids Formed by Biphasic Grafting at a Pickering Emulsion Interface. *Angew. Chem., Int. Ed.* **2008**, *47*, 3973–3975.

(20) Liu, B.; Zhang, C.; Liu, J.; Qu, X.; Yang, Z. Janus Non-Spherical Colloids by Asymmetric Wet-Etching. *Chem. Commun.* **2009**, *0*, 3871–3873.

(21) Xing, S.; He, J.; Liu, X.; Chen, H. A Symmetry-Adapted Shell Transformation of Core-Shell Nanoparticles for Binary Nanoassembly. *Chem. Commun.* **2011**, *47*, 12533–12535.

(22) Perro, A.; Duguet, E.; Lambert, O.; Taveau, J.-C.; Bourgeat-Lami, E.; Ravaine, S. A Chemical Synthetic Route towards "Colloidal Molecules". *Angew. Chem., Int. Ed.* **2009**, *48*, 361–365.

(23) Yu, H.; Chen, M.; Rice, P. M.; Wang, S. X.; White, R. L.; Sun, S. Dumbbell-like Bifunctional Au-Fe3O4 Nanoparticles. *Nano Lett.* **2005**, *5*, 379–382.

(24) Shi, W.; Sahoo, Y.; Zeng, H.; Ding, Y.; Swihart, M. T.; Prasad, P. N. Anisotropic Growth of PbSe Nanocrystals on Au–Fe3O4 Hybrid Nanoparticles. *Adv. Mater.* **2006**, *18*, 1889–1894.

(25) Chen, T.; Yang, M.; Wang, X.; Tan, L. H.; Chen, H. Controlled Assembly of Eccentrically Encapsulated Gold Nanoparticles. *J. Am. Chem. Soc.* **2008**, *130*, 11858–11859.

(26) Ohnuma, A.; Cho, E. C.; Camargo, P. H. C.; Au, L.; Ohtani, B.; Xia, Y. A Facile Synthesis of Asymmetric Hybrid Colloidal Particles. *J. Am. Chem. Soc.* **2009**, *131*, 1352–1353.

(27) Zhang, C.; Liu, B.; Tang, C.; Liu, J.; Qu, X.; Li, J.; Yang, Z. Large Scale Synthesis of Janus Submicron Sized Colloids by Wet Etching Anisotropic Ones. *Chem. Commun.* **2010**, *46*, 4610–4612.

(28) Lu, W.; Chen, M.; Wu, L. One-Step Synthesis of Organic-Inorganic Hybrid Asymmetric Dimer Particles via Miniemulsion Polymerization and Functionalization with Silver. *J. Colloid Interface Sci.* **2008**, *328*, 98–102.

(29) Sheu, H. R.; El-Aasser, M. S.; Vanderhoff, J. W. Uniform Nonspherical Latex Particles as Model Interpenetrating Polymer Networks. *J. Polym. Sci., Part A: Polym. Chem.* **1990**, *28*, 653–667.

(30) Sheu, H. R.; El-Aasser, M. S.; Vanderhoff, J. W. Phase Separation in Polystyrene Latex Interpenetrating Polymer Networks. *J. Polym. Sci., Part A: Polym. Chem.* **1990**, *28*, 629–651.

(31) Kim, J.-W.; Larsen, R. J.; Weitz, D. A. Synthesis of Nonspherical Colloidal Particles with Anisotropic Properties. *J. Am. Chem. Soc.* **2006**, *128*, 14374–14377.

(32) Tang, C.; Zhang, C.; Liu, J.; Qu, X.; Li, J.; Yang, Z. Large Scale Synthesis of Janus Submicrometer Sized Colloids by Seeded Emulsion Polymerization. *Macromolecules* **2010**, *43*, 5114–5120.

(33) Kim, J.-W.; Lee, D.; Shum, H. C.; Weitz, D. A. Colloid Surfactants for Emulsion Stabilization. *Adv. Mater.* **2008**, *20*, 3239–3243.

(34) Park, J.-G.; Forster, J. D.; Dufresne, E. R. High-Yield Synthesis of Monodisperse Dumbbell-Shaped Polymer Nanoparticles. *J. Am. Chem. Soc.* **2010**, *132*, 5960–5961.

(35) Yoon, K.; Lee, D.; Kim, J. W.; Kim, J.; Weitz, D. A. Asymmetric Functionalization of Colloidal Dimer Particles with Gold Nanoparticles. *Chem. Commun.* **2012**, 9056–9058.

(36) Mock, E. B.; De Bruyn, H.; Hawkett, B. S.; Gilbert, R. G.; Zukoski, C. F. Synthesis of Anisotropic Nanoparticles by Seeded Emulsion Polymerization. *Langmuir* **2006**, *22*, 4037–4043.

(37) Mock, E. B.; Zukoski, C. F. Emulsion Polymerization Routes to Chemically Anisotropic Particles. *Langmuir* **2010**, *26*, 13747–13750.

(38) Plueddemann, E. P. *Silane Coupling Agents*; Springer Science & Business Media, **1982**.

(39) Graf, C.; Van Blaaderen, A. Metallodielectric Colloidal Core−Shell Particles for Photonic Applications. *Langmuir* **2002**, *18*, 524–534.

(40) Xue, J.; Wang, C.; Ma, Z. A Facile Method to Prepare a Series of SiO2@Au Core/shell Structured Nanoparticles. *Mater. Chem. Phys.* **2007**, *105*, 419–425.

(41) Zhang, F.; Cao, L.; Yang, W. Preparation of Monodisperse and Anion-Charged Polystyrene Microspheres Stabilized with Polymerizable Sodium Styrene Sulfonate by Dispersion Polymerization. *Macromol. Chem. Phys.* **2010**, *211*, 744–751.

(42) Turkevich, J.; Stevenson, P. C.; Hillier, J. A Study of the Nucleation and Growth Processes in the Synthesis of Colloidal Gold. *Discuss. Faraday Soc.* **1951**, *11*, 55–75.

(43) Abramoff, M. D.; Magalhães, P. J.; Ram, S. J. Image Processing with ImageJ. *Biophotonics Int.* **2004**, *11*, 36–42.

(44) Feng, Y.; He, J.; Wang, H.; Tay, Y. Y.; Sun, H.; Zhu, L.; Chen, H. An Unconventional Role of Ligand in Continuously Tuning of Metal-Metal Interfacial Strain. *J. Am. Chem. Soc.* **2012**, *134*, 2004–2007.

(45) Jensen, T. R.; Malinsky, M. D.; Haynes, C. L.; Van Duyne, R. P. Nanosphere Lithography: Tunable Localized Surface Plasmon Resonance Spectra of Silver Nanoparticles. *J. Phys. Chem. B* **2000**, *104*, 10549–10556.

(46) Yong, K.-T.; Sahoo, Y.; Swihart, M. T.; Prasad, P. N. Synthesis and Plasmonic Properties of Silver and Gold Nanoshells on Polystyrene Cores of Different Size and of Gold–silver Core–shell Nanostructures. *Colloids Surf., A* **2006**, *290*, 89–105.

(47) Montero, M. A.; de Chialvo, M. R. G.; Chialvo, A. C. Electrocatalytic Activity of Core-Shell Au@Pt Nanoparticles for the Hydrogen Oxidation Reaction. *Int. J. Hydrogen Energy* **2011**, *36*, 3811–3816.

(48) Li, J.-F.; Yang, Z.-L.; Ren, B.; Liu, G.-K.; Fang, P.-P.; Jiang, Y.-X.; Wu, D.-Y.; Tian, Z.-Q. Surface-Enhanced Raman Spectroscopy Using Gold-Core Platinum-Shell Nanoparticle Film Electrodes: Toward a Versatile Vibrational Strategy for Electrochemical Interfaces. *Langmuir* **2006**, *22*, 10372–10379.

(49) Lu, L.; Sun, G.; Xi, S.; Wang, H.; Zhang, H.; Wang, T.; Zhou, X. A Colloidal Templating Method To Hollow Bimetallic Nanostructures. *Langmuir* **2003**, *19*, 3074–3077.

(50) Levitan, J. A.; Devasenathipathy, S.; Studer, V.; Ben, Y.; Thorsen, T.; Squires, T. M.; Bazant, M. Z. Experimental Observation of Induced-Charge Electro-Osmosis around a Metal Wire in a Microchannel. *Colloids and Surfaces A: Physicochemical and Engineering Aspects*, **2005**, *267*, 122–132.

(51) Trau, M.; Saville, D. A.; Aksay, I. A. Field-Induced Layering of Colloidal Crystals. *Science*, **1996**, *272*, 706–709.

(52) Trau, M.; Saville, D. a; Aksay, I. a. Assembly of Colloidal Crystals at Electrode Interfaces. *Langmuir* **1997**, *13*, 6375–6381.

(53) Ristenpart, W. D.; Aksay, I. A.; Saville, D. A. Assembly of Colloidal Aggregates by Electrohydrodynamic Flow: Kinetic Experiments and Scaling Analysis. *Phys. Rev. E* **2004**, *69*, 021405.

(54) Ristenpart, W. D.; Aksay, I. A.; Saville, D. A. Electrohydrodynamic Flow around a Colloidal Particle near an Electrode with an Oscillating Potential. *Journal of Fluid Mechanics*, **2007**, *575*, 83–109.

(55) Ma, F. D.; Zhao, H.; Wu, D.; Wu, N. Propulsion of Dielectric Particles under Electric Fields. *Manuscr. Prep.*

(56) Wang, S.; Ma, F.; Zhao, H.; Wu, N. Bulk Synthesis of Metal–Organic Hybrid Dimers and Their Propulsion under Electric Fields. *ACS Appl. Mater. Interfaces* **2014**, *6*, 4560–4569.

CHAPTER 3

SELECTING THE SWIMMING MECHANISMS OF COLLOIDAL PARTICLES: BUBBLE PROPULSION VS. SELF-DIFFUSIOPHORESIS

Modified from a paper published in *Langmuir*

Sijia Wang[2] and Ning Wu[3]

3.1 Abstract

Bubble propulsion and self-diffusiophoresis are two common mechanisms that can drive autonomous motion of micro-particles in hydrogen peroxide. Although micro-tubular particles, when coated with platinum in their interior concave surfaces, can propel due to the formation and release of bubbles from one end, the convex Janus particles usually do not generate any visible bubble. They move primarily due to the self-diffusiophoresis. Coincidentally, the platinum film on those particles were typically coated by physical evaporation. In this paper, we use a simple chemical deposition method to make platinum-polystyrene Janus dimers. Surprisingly, those particles are propelled by periodic growth and collapse of bubbles on the platinum-coated lobes. We find that both high catalytic activity and rough surface are necessary to change the propulsion mode from self-diffusiophoresis to bubble propulsion. Our Janus dimers, with combined geometric and interfacial anisotropy, also exhibit distinctive motions at the respective stages of bubble growth and collapse, which differ by six orders of magnitude in time. Our study not only provides insight into the link between self-diffusiophoresis and bubble propulsion, but also reveals the intriguing impacts of the combined geometric and interfacial anisotropy on self-propulsion of particles.

[1]Reprinted with permission from *Langmuir* **2014**, *30*, 3477–3486.
Copyright 2014 American Chemical Society.
[2]Graduate student and [3]Assistant Professor, respectively,
Department of Chemical and Biological Engineering, Colorado School of Mines.
[2]Experiments and [2,3]data analysis.
[3]Author for correspondence

3.2 Introduction

Nature assembles relatively simple molecular building blocks into well-defined units of exquisite complexity and functionality. For example, a white blood cell, the "soldier" in our immune system, can sense, chase, and engulf bacteria with their delicately designed biomolecular sensors and motors. Equally intelligent synthetic machines, although extremely difficult to make, have been dreamed over long time for targeted drug delivery,[1–3] self-motile sensors,[4] and miniaturized surgeons.[5] Over the last decade, a variety of synthetic micro-motors has been developed based on different propulsion mechanisms, including the self-diffusiophoresis,[6–8] bubble recoil,[9–12] self-electrophoresis,[13,14] magnetic field,[15,16] the Marangoni effect,[17–19] and enzymatic reactions.[20–23] Detailed studies based on surface science, fluid mechanics, electrokinetics, and material chemistry have enhanced our fundamental understanding and advanced this field significantly.

Among different types of propulsion strategies, the self-diffusiophoresis and bubble propulsion, using hydrogen peroxide as the fuel, have been studied widely.[6,7,24–26] For example, when a Janus platinum-polystyrene sphere is immersed in hydrogen peroxide solutions, the platinum-coated hemisphere catalyzes the decomposition of hydrogen peroxide into water and oxygen, while the polystyrene hemisphere remains inert. The particle propels with a linear velocity of ~μm/s. Although bubble propulsion[25] was proposed as a possible mechanism, no visible bubble has been found using optical microscopy. It is now widely accepted that the particle motion is primarily governed by the so-called self-diffusiophoresis.[6,27,28] The asymmetric reaction surrounding the Janus sphere generates a concentration gradient of oxygen, as well as a gradient in interfacial pressure. To balance this pressure gradient, solvent flow ensues and propels the particle. Contrary to the convex Janus particles, micro-tubes, when coated with platinum in their

interior concave surfaces, were propelled by the accumulation and release of bubbles from one end.[10,29] Compared with self-diffusiophoresis, the propulsion speed driven by bubble recoil can be as high as 1 mm/s.[10] Such a high speed is advantageous to overcome the background fluid flow in blood vessels. Unlike self-diffusiophoresis, bubble propulsion remains powerful in high ionic strengths, which is crucial for biomedical applications.

Although it is relatively easy to understand the accumulation and release of bubbles in a confined space (e.g., in micro-tubes), the fate of nanobubbles surrounding convex spheres is largely unknown. Except one recent report on large particles (~20 μm),[11] no microscopic bubble was observed. Coincidently, the platinum films on those particles were typically deposited via physical (e.g., E-beam or thermal) evaporation. No chemical deposition has been employed. Therefore, it remains an open question whether one can tailor the platinum surface so that the automotion of convex particles can be switched from self-diffusiophoresis to bubble propulsion. Besides its potential in applications, a fundamental understanding on the interconnectedness between self-diffusiophoresis and bubble propulsion is necessary.

Here we show a simple strategy to chemically synthesize platinum-polystyrene Janus dimers. Unlike the physical evaporation method, those particles can be propelled by periodic growth and collapse of bubbles on the platinum-coated lobes. The same method can essentially switch the autonomous displacement of a convex particle from self-diffusiophoresis to bubble propulsion. We perform systematic studies to show that both high catalytic activity and rough surface are necessary for nucleating, pinning, and stabilizing bubble growth on the platinum surfaces. As a result of the combined anisotropy in both particle geometry and catalytic activity, colloidal dimers also exhibit complex propulsion behavior. In particular, they do not move

monotonically in one direction during the whole cycle of bubble nucleation, growth, and collapse, because of the combined effects of particle location and fluid flow.

3.3 Experimental Methods

The following sections first introduce the materials we used in this Chapter, and afterwards describe the detailed experimental procedures and characterization methods.

3.3.1 Materials

Styrene, divinylbenzene (DVB), sodium 4-vinylbenzenesulfonate, polyvinyl-pyrrolidone (PVP, M_w: ~40,000), sodium dodecyl sulfate (SDS), 3-aminopropyltriethoxysilane, trisodium citrate, and L-ascorbic acid are purchased from Sigma-Aldrich. 3-(trimethoxysily) propyl acrylate (TMSPA) is purchased from TCI. Hydrogen tetrachlororaurate(III) trihydrate ($HAuCl_4 \cdot 3H_2O$, 99.9+%), and potassium tetrachloroplatinate(II) (K_2PtCl_4, 99.9%) are bought from Alfa Aesar. The thermal initiator V65 is bought from Wako Chemicals. All chemicals are used as received except that both styrene and divinylbenzene are purified by aluminum oxide before usage.

3.3.2 Selective coating of gold nanoparticles on the crosslinked lobe

The synthesis of the polystyrene (PS) dimers can be found in section 2.3.2, Chapter 2. We attach (3-aminopropyl)-triethoxysilane (APS) to the crosslinked lobe in dimers by mixing 0.02 g dimers in 15 ml ethanol solution with 100 µl APS and 3 ml NH4OH (30%) and stirring for 24 hours at the room temperature.[30] The particles are then washed by ethanol for four times and re-dispersed in water. The citrate-stabilized gold nanoparticles are made via the Turkevich method.[31] To coat the gold nanoparticles on the dimers, we mix 3 ml (0.3 wt%) APS-coated dimers with gold nanoparticles (0.05 wt% in 30 ml) in a sonication bath for 1 hour. We use track-etched filter papers to completely remove free gold nanoparticles suspended in the solution. The coated gold

nanoparticles on the crosslinked lobe can promote heterogeneous nucleation for further growth of a thicker metallic shell, such as platinum.[38]

3.3.3 Deposition of the platinum (Pt) shell on gold-coated dimers

We mix 1 ml gold nanoparticles-coated dimer solution (10^8 particles/ml) with 0.3 ml 100 mM ascorbic acid (freshly prepared), followed by adding 2 ml 2 mM K_2PtCl_4 within one hour.[32] The solution is allowed to sit for one day. If a thicker and denser platinum shell is desired, we can re-coat the dimers with 0.3 ml 100 mM ascorbic acid and 2 ml 2 mM K_2PtCl_4 without stirring.

3.3.4 Synthesis of polystyrene particles with rough surfaces

We swell 1 ml polystyrene seed particles[33] (10wt%) with an emulsion of 4 ml 5wt% PVP, 0.5 ml 2wt% SDS, 1 ml styrene, 0.05 ml DVB, 0.05 ml 3-(trimethoxysilyl)propyl methacrylate, and 0.02 g V65 for 24 hours. The swollen particles are polymerized in the reactor at 70°C for 24 hours. The surface of the polystyrene particles become corrugated because of the mechanical buckling during the polymerization. If we do not add 3-(trimethoxysilyl) propyl methacrylate, the particle surface is smooth.

3.3.5 E-beam evaporation of platinum on polystyrene spheres

We first deposit 0.1wt% polystyrene spheres (1.4 μm in methanol) on a silica wafer. Spin-coating at 3000 rpm for 50 s make a sub-monolayer of particle arrays. A thin platinum film (~10 nm) is then evaporated onto the top surfaces of the particles using an E-beam evaporator (Temescal BJD-1800). After evaporation, we remove the platinum-coated polystyrene spheres from the substrate by rinsing with deionized water.

3.3.6 Characterization of the platinum-polystyrene (Pt-PS) particles

We put a droplet of particle solution on a silicon wafer and let it dry naturally for SEM (JEOL JSM-7000F) characterization. Occasionally, an aluminum foil is used for energy dispersive

X-ray (EDX) spectrum analyses. Optical observations are performed on an inverted microscope (Olympus IX71).

3.3.7 Propulsion of Pt-PS dimers in hydrogen peroxide

Pt-PS particles (spheres or dimers) in solutions with different hydrogen peroxide concentrations are pipetted into a chamber, which is made of a perforated PDMS gel on a glass slide (treated by Piranha solution). We observe large amounts of bubble generation after sealing the chamber with a cover slip. The dimers are floated to the top because of the bubble generation, which prevent accurate characterization of their propulsion. Therefore, for most of the experiments, we leave the chamber open without a cover slip and allow solvent evaporation. A high speed camera (SILICON VIDEO® monochrome SV642) is used to record the motion of dimers at 300 frames/s for at least 30 seconds and ImageJ[34] is used to analyze the moving behavior of dimers. Occasionally, an ultra-high speed camera (phantom V711) is used to capture the motion of particles up to 680,000 frames per second.

3.3.8 Measurement of the oxygen production rate

We put the same amount of Pt-PS Janus spheres (4×10^7 particles), both with chemically and physically deposited platinum shell, into separated vials of 10 ml 5% H_2O_2 solution and collect the generated oxygen by using cylinders filled with water initially. Since the oxygen has a low solubility in water, it continuously push out water in the cylinder. The volume change in the cylinder is then recorded periodically.

3.4 Results and Discussion

The actual swimming mechanisms of micron- or even nanometer-sized objects are often obscure due to the lack of characterization techniques. Currently, the mechanism of self-diffusiophoresis is still under hot debate because of the inconsistent experimental observations.

We utilized different platinum deposition strategies on micron-sized colloids and observed distinct propulsion behaviors. To the best of our knowledge, the comparison between particles propelled by self-diffusiophoresis and particles propelled by bubbles at micron size scale has never been reported in previous literature. We also reveals novel phenomena at bubble burst moment, when linear motions behave entirely oppositely to circular motions.

3.4.1 Synthesis of the platinum-polystyrene hybrid dimers.

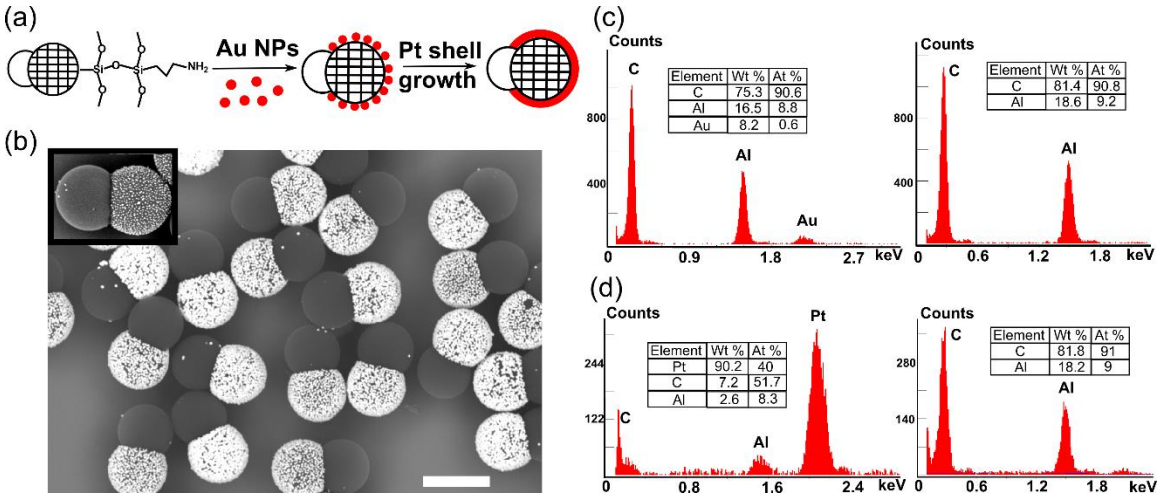

Figure 3.1 Synthesis of platinum-polystyrene dimers. (a) The procedure for making platinum-polystyrene hybrid dimers. (b) A representative SEM of the Pt-PS dimers. Scale bar: 2 µm. Inset: a polystyrene dimer with one lobe coated by gold nanoparticles (~20 nm). (c) The energy dispersive X-ray spectrum of the polystyrene dimer where one lobe is coated with gold nanoparticles (left) and the other lobe is polystyrene (right). The Al signal comes from the aluminum foil, which is used as a substrate for sample preparation. (d) The energy dispersive X-ray spectrum of the Pt-PS dimer where one lobe is coated with platinum (left) and the other lobe is polystyrene (right). The Au signal is below the detection limit of the instrument.

Figure 3.1a illustrates the synthetic route we adopt to make platinum-polystyrene (Pt-PS) hybrid dimers.[35] We first make polystyrene dimers by employing the seeded emulsion polymerization.[36,37] During the synthesis, functional silane molecules (e.g., 3-trimethoxysilypropylacrylate) are incorporated and they remain in the crosslinked lobe only, which creates an anisotropy in surface functionality between two lobes. This anisotropy allows us to further attach (3-aminopropyl)-triethoxysilane (APS) on the crosslinked lobe by exploiting the

silane coupling chemistry.[38] Subsequently, we coat a sub-monolayer of gold nanoparticles (~20 nm) since amines can form complexes with metals (inset in Figure 3.1b, EDX results in Figure 3.1C). This pre-coating step is crucial because those gold particles can promote heterogeneous nucleation and growth of other metallic materials,[35] such as platinum. By using ascorbic acid as the reducing agent for potassium tetrachloroplatinate(II) (K_2PtCl_4), we can synthesize Pt-PS dimers as shown in Figure 3.1b. Combined with the EDX results in Figure 3.1d, it clearly demonstrates the selective coating of platinum on one lobes in all dimers. It is noted that our method is a bulk-synthesis strategy, where metallic salts are chemically reduced into thin metal films on particles.[38] Such an approach can significantly improve the throughput of making self-propelling particles, since previous efforts were typically based on physical evaporation of a thin platinum film on a templated monolayer of spherical particles.[6,7,25] More importantly, our dimers are anisotropic in both geometry and interfacial property. This combined anisotropy has profound impacts on the self-propulsion of particles as will be discussed subsequently.

3.4.2 Bubble-propulsion vs. self-diffusiophoresis of Pt-PS particles

Figure 3.2 shows a summary of the particles we have tested in hydrogen peroxide solution. They show different propulsion behavior due to different methods of platinum deposition and/or surface roughness, as we will elaborate later. Before reporting the self-propulsion of our synthesized Pt-PS dimers (*particle d* in Figure 3.2), we perform a control experiment by suspending Pt-PS Janus spheres (*particle a* in Figure 3.2) in hydrogen peroxide solutions. The synthesis of Pt-PS Janus spheres is described in the experimental section. Figure 3.3a illustrates the trajectory and snapshots of a Pt-PS Janus sphere (*particle a* in Figure 3.2) in 5% hydrogen peroxide solution. Consistent with the literature,[7,25,6] we observe an active propulsion of the Pt-PS sphere without any detectable bubble (Figure 3.4a). We have also found that its motion can be

characterized by a short-time linear displacement and a long-time enhanced random motion[6], consistent with the commonly agreed propulsion mechanism: the so-called self-diffusiophoresis.[26] The calculated propulsion speed (~ 1.7 μm/s) is also comparable to previous reports.[6,7]

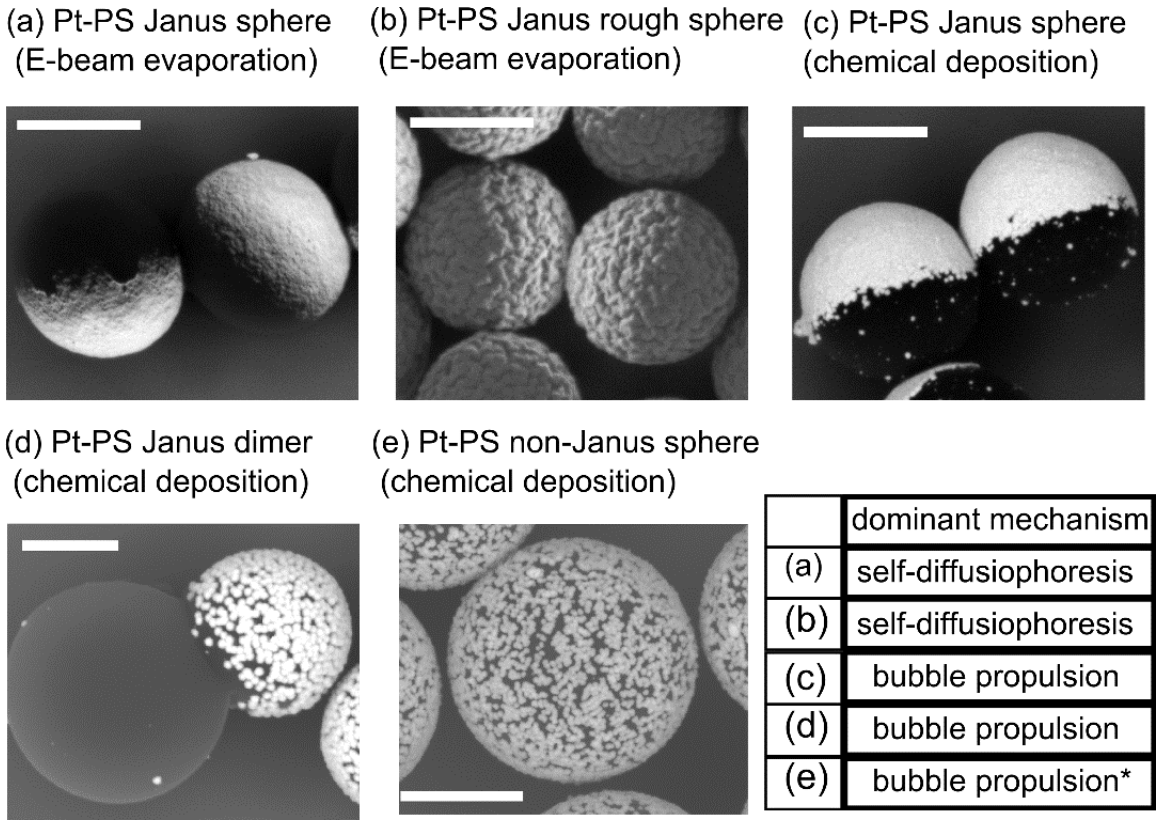

	dominant mechanism
(a)	self-diffusiophoresis
(b)	self-diffusiophoresis
(c)	bubble propulsion
(d)	bubble propulsion
(e)	bubble propulsion*

Figure 3.2 A summary of particles that have been tested in hydrogen peroxide solution and their corresponding swimming mechanisms. The * indicates that the dominant propulsion mechanism depends on the surface roughness of the particle. Scale bar: 1 μm.

Next we suspend our synthesized Pt-PS dimers (*particle d* in Figure 3.2) in 5% hydrogen peroxide solution under the same experimental condition. To our surprise, we consistently observe the nucleation, pinning, growth, and collapse of microscopic bubbles (~3-12 μm in diameter) on the platinum-coated lobes. Although we do observe the growth of multiple bubbles on the same particle, most of the particles (over 90%) only have one large bubble. In the beginning, many platinum active sites could generate oxygen nuclei and potentially pin them. However, once a

particular site starts to form a microscopic bubble, it will probably attract other small nucleus through Oswald ripening and grow bigger, as captured by an ultra-high speed camera (Figure 3.3).

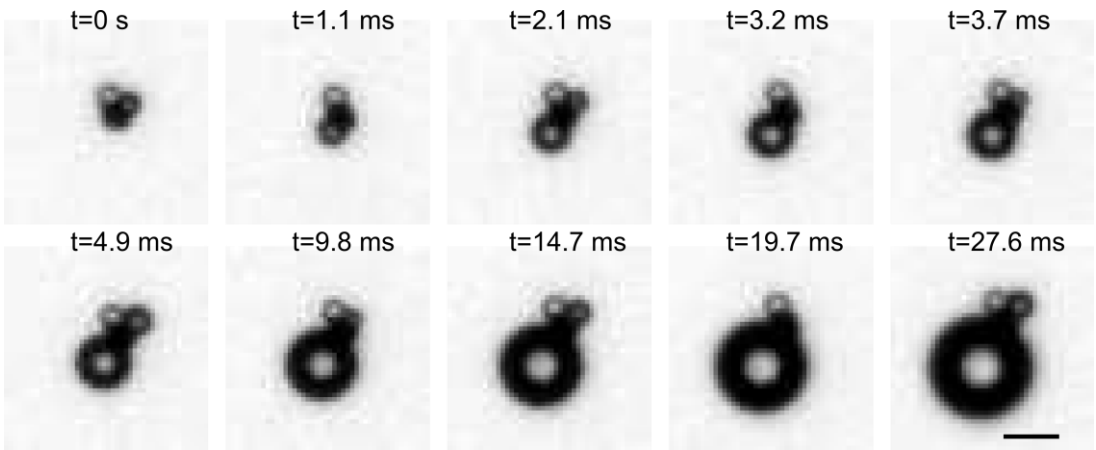

Figure 3.3 Snapshots of a dimer with two bubble nucleation sites. Scale bar: 5 µm.

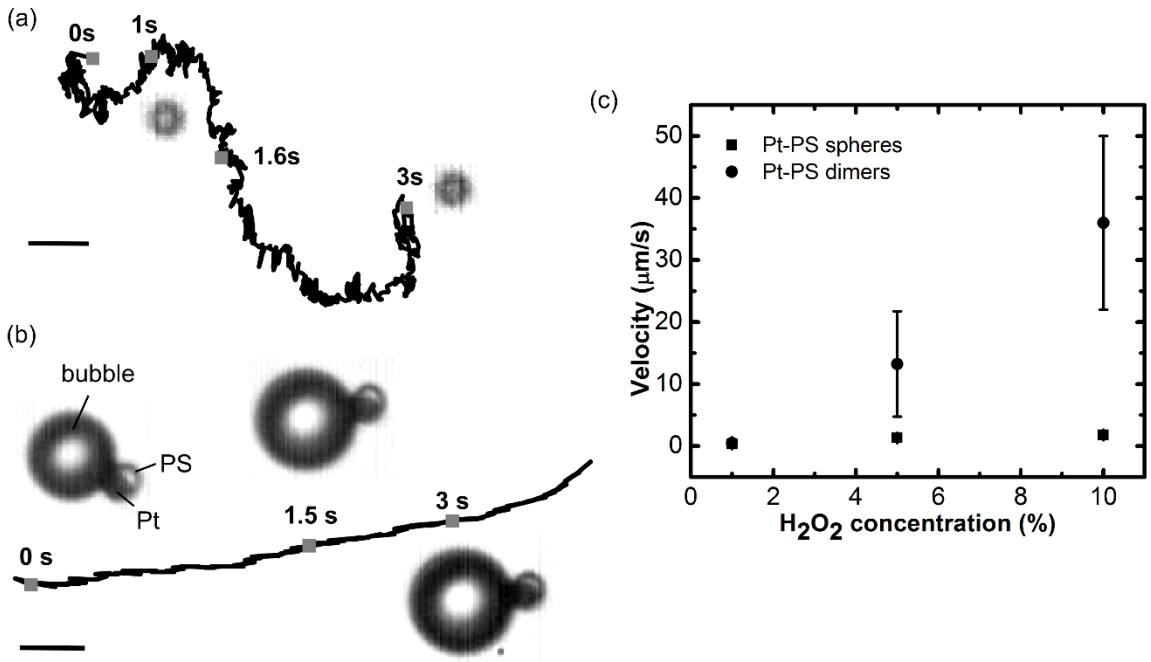

Figure 3.4 Trajectories and velocities of Pt-PS Janus spheres and Pt-PS hybrid dimers in hydrogen peroxide solutions. (a) The trajectory of a (physically evaporated) Pt-PS sphere (particle a in Figure 2) in 5% H2O2 solution. Scale bar: 1 µm. The snapshots show no evidence of microscopic bubbles. (b) The trajectory of a (chemically deposited) Pt-PS dimer (particle d in Figure 2) in 5% H2O2 solution. Scale bar: 5 µm. The snapshots show that the dimer is propelled by a bubble that grows and collapses periodically on the platinum-coated lobe. (c) Velocities of the dimers and spheres at different hydrogen peroxide concentrations.

Figure 3.4b illustrates a typical trajectory of the bubble-propelled dimer with several instantaneous snapshots. It can be seen that the dimer always orients itself with the platinum-coated lobe facing backward. The speed of the Pt-PS dimers can be as high as ~40 μm/s in 10% H_2O_2, or equivalently 20 body length per second. It is at least one order of magnitude higher than the self-diffusiophoresis of Pt-PS spheres, which is of comparable size to the dimers. Clearly, the dominant propulsion mechanism for Pt-PS dimers is due to bubble growth and collapse. Although diffusiophoresis could be present simultaneously, its effect is negligible.

Having observed the striking difference between our chemically synthesized Pt-PS dimers and the physically evaporated Pt-PS spheres, one would naturally wonder whether it is due to the geometric difference between dimers and spheres. Therefore, we further coat an additional thin layer of platinum on the evaporated platinum surface of the Pt-PS spheres (*particle c* in Figure 3.2), by exploiting our chemical deposition method in Figure 3.1a. Here the gold coating step is not necessary, since the evaporated platinum itself promotes the chemical reduction of platinum on its own surface. Interestingly, we now observe that the new Pt-PS spheres can be propelled by the periodic growth and collapse of bubbles. Therefore, particle geometry is not important.

Bubble propulsion has been observed for micro-tubular particles,[10,22] where oxygen bubbles are formed within and escaped from a confined space. Our experiments, however, demonstrate the bubble propulsion on convex particles in open space. More importantly, we discover a method to select the swimming mechanisms of Janus particles: from self-diffusiophoresis to bubble propulsion simply by changing the way of platinum deposition. In fact, although self-diffusiophoresis has been widely accepted as the major propulsion mechanism for Janus Pt-PS spheres, nanobubbles should always form in the solution. Understanding the fate of

those nanobubbles and the interconnectedness between self-diffusiophoresis and bubble propulsion is one of the fundamental questions that have not been explored before.[39]

As can be seen from the SEM images (Figure 3.2) of the platinum surfaces prepared by two different methods, the physically evaporated platinum is very smooth, while the chemically deposited platinum consists of percolating nanoparticles (~80 nm). In addition, its surface is far from perfect with lots of defects and cracks. Based on our observations, we hypothesize that the E-beam evaporated and chemically deposited platinum have different catalytic activity and surface roughness. Both could significantly affect the nucleation, pinning, and growth of oxygen bubbles, which lead to dramatically different propulsion mechanisms.

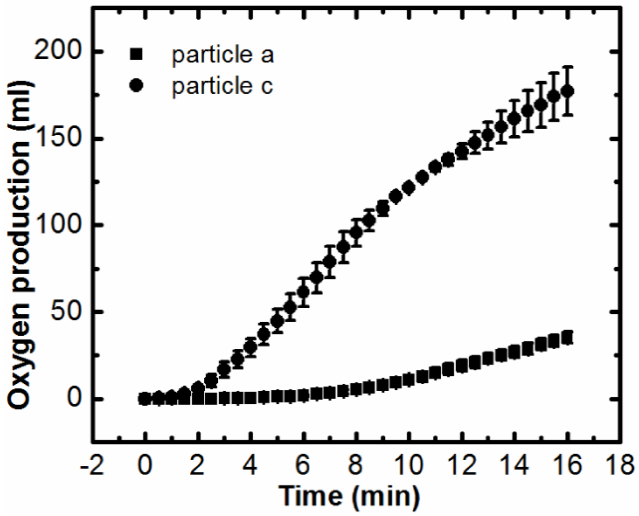

Figure 3.5 The amount of oxygen produced by two types of Pt-PS Janus spheres in separate vials of 10 ml 5% hydrogen peroxide solution. Particle a: the hemispherical platinum is E-beam evaporated. Particle c: the hemispherical platinum is chemically deposited. Both types of particles have identical sizes (~1.4 μm) and similar surface coverage.

To test our hypothesis, we first examine the catalytic activities between two types of platinum surfaces, i.e., the *particles a and c* in Figure 3.2. The particles c are made via chemical deposition of a conformal layer of platinum on particles a, which have been coated by using the E-beam evaporation. By examining the SEM images, we confirm that both types of particles have

similar surface coverage of platinum. We put the same amount of particle a and particle c into two separate vials of 10 ml 5% H_2O_2 solution, and then record the oxygen production rate in each vial (see details in the experimental section). Our measurement is reported in Figure 3.5.

It is interesting to note that both particles have relatively small oxygen production rate during the "incubation" stage, although particle c reaches the constant production rate (~2 minutes) much faster than particle a (~9 minutes), which may be due to the different oxidative states of the platinum.[40] The oxygen production rate for particle a is ~4.2 ml/min for a total of 4×10^7 particles, while the same amount of Particle c produces oxygen at a much higher rate of ~16 ml/min. The decreasing oxygen production rate of particle c at the later stage is simply due to the depletion of hydrogen peroxide (from initially 5% to 1% after 10 minutes). Based on our measurement, we can estimate that the oxygen production rate per particle c is ~10^{-13} mol/s, e.g., 0.1 moles/s·m^2. Considering the oxygen diffusion coefficient (2.1×10^{-5} cm^2/s) and the solubility of oxygen in water (2.375×10^{-4} mol/L), we can estimate that the oxygen diffusion rate from a microscopic bubble (radius: ~2 μm) to the bulk solution is ~10^{-14} mol/s. Therefore, the oxygen production rate is about one order of magnitude higher than the diffusion rate for our chemically synthesized Pt-PS dimers. Clearly, such a high catalytic activity will generates a large amount of oxygen locally, causing supersaturation in the solution. This favors the heterogeneous nucleation and growth of microscopic bubbles on the platinum surface, which justifies our observation.

The enhanced catalytic activity on the chemically deposited platinum could be due to (1) the attached surface functionality during synthesis or (2) higher densities of active sites on the platinum surface. To further elucidate the possible reason, we try five types of commonly-used reducing or capping agents and study their impacts on the catalytic activity. They are ascorbic acid, formic acid, sodium citrate, polyvinylpyrrolidone (PVP, M_w: ~10,000), and 3-mercaptopropionic

acid. The first three are reducing agents for platinum salts, but they could also remain on the platinum surface during the chemical synthesis. The last two are capping agents that can be attached on platinum after chemical synthesis or physical evaporation. We find that all of the reducing agents can consistently make chemically deposited Pt-PS particles that are propelled by bubbles. When we mix each of those reducing agents with the physically evaporated Pt-PS particles, their propulsion remains to be driven by the self-diffusiophoresis and no microscopic bubble is observed. The physical absorption of PVP on the chemically-deposited or physically-evaporated particles does not change their dominant propulsion modes and speeds. However, when we replace the existing ligand on the chemically deposited platinum by 3-mercaptopropionic acid, we no longer observe the bubble propulsion. In fact, the oxygen production rate is significantly reduced. A similar result is also observed when we attach 3-mercaptopropionic acid on the freshly evaporated platinum. Those results are expected because sulfur is a well-known catalyst poison[41,42] for platinum. It can chemisorb onto and react with the active catalytic sites. Therefore, our findings have shown that, except for 3-mercaptopropionic acid, other common types of reducing or capping agent do not affect the catalytic activity on both chemically deposited and physically evaporated platinum surfaces. This leads to the possibility that the different catalytic activities could originate from different densities of active sites due to two types of deposition methods. It is known that low-coordinated surface atomic sites is primarily responsible for high catalytic activity due to the change of local electronic structures.[43,44] Since nanoparticles have a much larger surface-to-volume ratio than the extended smooth surface by physical evaporation, we expect that the density of surface defects and kinks (hence the active sites) is higher on the chemically deposited surfaces. Although full characterization of the active sites on the platinum surface is challenging and beyond

the scope of this paper, previous experiments and theoretical calculation are consistent with our argument.[45]

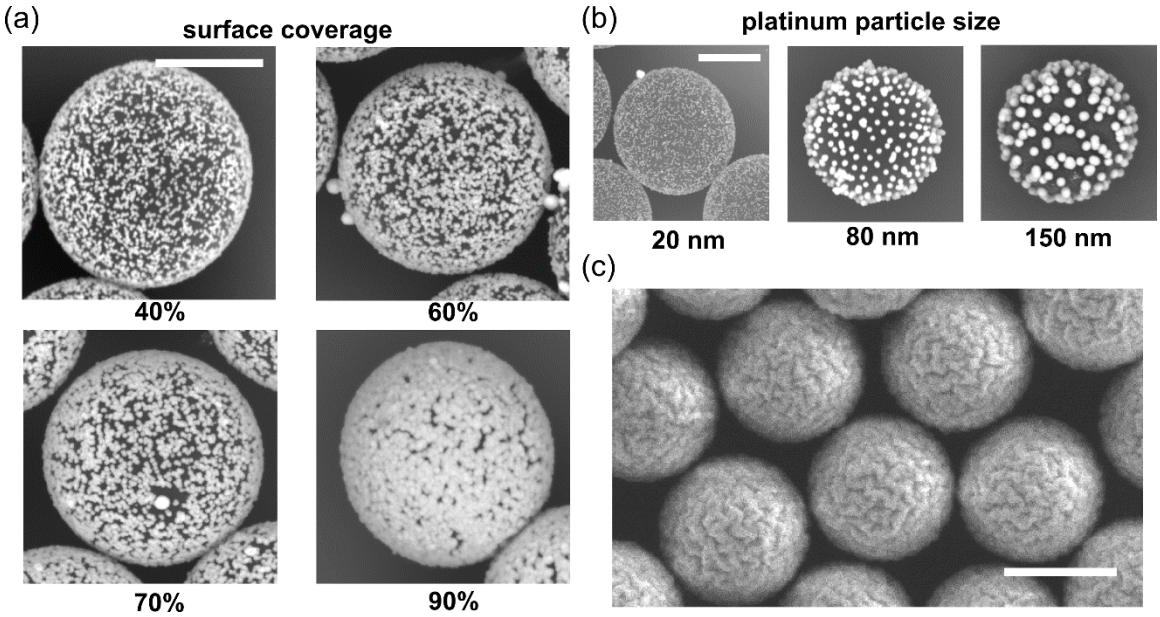

Figure 3.6 Platinum coated polystyrene spheres with different surface roughness. (a) Polystyrene spheres are unifromly coated with platinum particles (~40 nm) with different surface coverage. Bubble propulsion is observed on spheres with 60%, 70%, and 90% surface coverage. (b) Polystyrene spheres coated with platinum nanoparticles of different sizes. Bubble propulsion is observed on spheres coated with ~150 nm nanoparticles. (c) Rough polystrene spheres coated with platinum by E-beam evaporation. Scale bars: 1 µm.

Now we confirm that the chemically deposited platinum has a higher catalytic activity than the physically evaporated platinum and the former can produce more oxygen nuclei. After the bubbles are nucleated heterogeneously, they, however, need to adhere to and grow on the particle surface without detachment. Not every sites behave equally, as can be clearly seen in Figure 3.3. Since it is known that the geometric defects on a rough surface help pin three-phase (gas, liquid, and solid) contact lines,[46,47] we decide to study the effect of surface roughness on the chemically deposited platinum film. We perform a first set of experiments by tuning the surface coverage of platinum nanoparticles (~40 nm) that are uniformly coated on the entire surface of polystyrene spheres, as shown in Figure 3.6a. They are also *particles e* in Figure 3.2. Different surface coverage

is achieved by varying the concentration of metal precursor and the reaction time during the coating. For spheres with 40% surface coverage, we do not observe the formation of any bubble that can be detected optically. Bubbles, however, are clearly observed on spheres with 60%, 70%, and 90% surface coverage. The particles propel vigorously with periodic bubble growth and collapse although those polystyrene spheres are coated uniformly with platinum nanoparticles. This result itself is significant because anisotropy (which is always difficult to make) is no longer necessary if the particle is propelled by bubbles. Since the reactivity difference between 40% and 60% covered spheres is small, this transition from self-diffusiophoresis to bubble propulsion should be attributed by stronger adhesion and larger amount of pinning points for bubble nuclei. As clearly seen on the sphere with 90% surface coverage, those large geometric voids and defects could help pin the contact line and prevent the detachment of the bubble.

In a second set of experiments, we first synthesize different sizes of platinum nanoparticles[48] and then attach them to polystyrene spheres with similar but relatively low surface coverage (~30%) as shown in Figure 3.6b. Since the catalytic activity of a nanoparticle depends on its surface area-to-volume ratio,[49] small platinum nanoparticles should facilitate the formation of bubbles. On the contrary, we find that only the spheres coated with large platinum nanoparticles (~150 nm) can generate and pin bubbles on the surface. No bubble is observed for the other two types of spheres. This experiment further proves that the high catalytic activity is a necessary but non-sufficient condition for bubble propulsion. Since a layer of larger platinum particles forms rougher surfaces than smaller particles with the same surface coverage, they can promote heterogeneous nucleation and pin bubbles more effectively. We note that the platinum particle size in Figure 3.6a is ~40 nm, which is smaller than 150 nm. However, high enough surface coverage of smaller particles can still provide sufficient and strong pinning points. If the surface coverage

is low, then the particles size needs to be large enough to make a rough surface for strong pinning as evidenced in Figure 3.6b.

Given the importance of surface roughness, can we switch the motion of physically evaporated Pt-PS spheres from self-diffusiophoresis to bubble propulsion simply by changing its surface roughness? We perform a third set of experiments to answer this question. As shown in Figure 3.6c, we first make polystyrene particles with rough surfaces (see details in the experimental section). We then coat a thin layer of platinum on them using the E-beam evaporator (they are also *particles b* in Figure 3.2). However, none of them shows the nucleation of bubbles on their surfaces and they are still propelled by the self-diffusiophoresis. Therefore, surface roughness itself is also necessary but not sufficient. Based on our investigations in Figures 3.2-3.6, we conclude that two conditions are required for making bubble-propelled *convex* micro-motors: high catalytic activity and rough surface on the platinum film. The former is necessary for generating large amounts of bubble nucleus and ensuring oversaturation, and the latter is important for pinning and stabilizing the bubbles once they nucleate on the particle surface. It is noted that, however, when the motor is *concave*, e.g., rolled-up or templated tubes, bubble propulsion is observed even if the platinum is physically evaporated. This is because oxygen production is within a confined space, where local gas concentration can be well beyond its saturation concentration before oxygen can escape from one end of the tubes.

3.4.3 The motion of Pt-PS dimers driven by periodic bubble growth and collapse

After illuminating the mechanisms of tunable propulsion on the synthesized Pt-PS dimers, we further investigate their motion behaviors which are heavily influenced by the geometric anisotropy. In general, we observe three fundamental types of motion: the linear, clockwise, and counterclockwise motion, all depending on the location where the bubble grows. As shown in

Figure 3.7a, when the bubble is grown along the long axis of the dimer, linear motion is observed. Circular motions typically happen when the bubble is situated away from the axis. As shown in Figure 3.7b and 3.7c, the dimer and bubble together form left- and right-handed mirror images. Such a broken symmetry generates a torque on the dimer which determines its rotational direction. During the circular motion, the dimer's orientation keeps changing too. As shown in Figure 3.8, the speed of its internal rotation is ~6.51±0.27 radian/s, approximately equal to the particle's angular velocity ~6.56±0.61 radian/s. Therefore, the dimer itself changes its orientation 360° after one round of rotation. The coupling between its internal rotation and circular motion indicates that the torque generated by the periodic bubble growth and collapse is the only driving force for rotation. We observe approximately equal numbers of clockwise and counterclockwise motion, since where a bubble grows on the particle is a stochastic process. The geometric anisotropy on the dimers plays an important role here, too. When we use a Pt-PS sphere, we only observe linear motions. It is expected since the center of the bubble always lies on the axis of spherical particles. Therefore, our dimers are fundamentally different from the Janus spheres because of the additional geometric anisotropy.

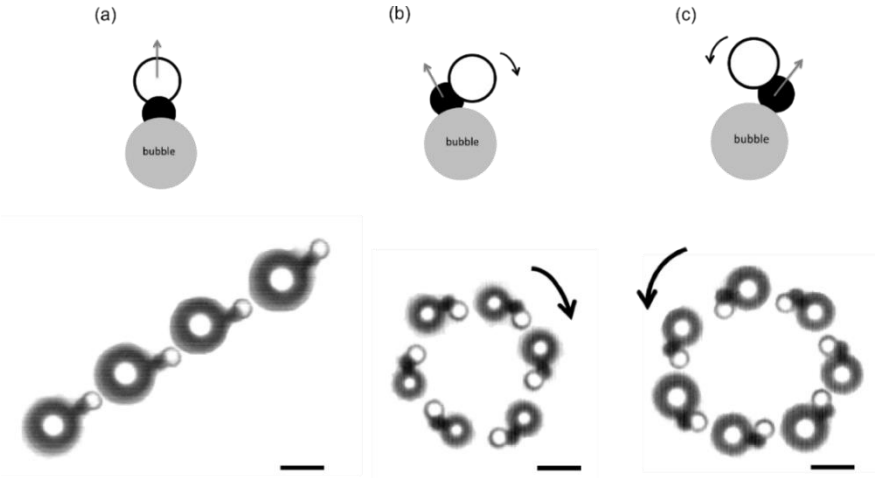

Figure 3.7 Three types of motion of the Pt-PS hybrid dimers: (a) linear, (b) clockwise, and (c) counterclockwise motion. Scale bar: 5 μm.

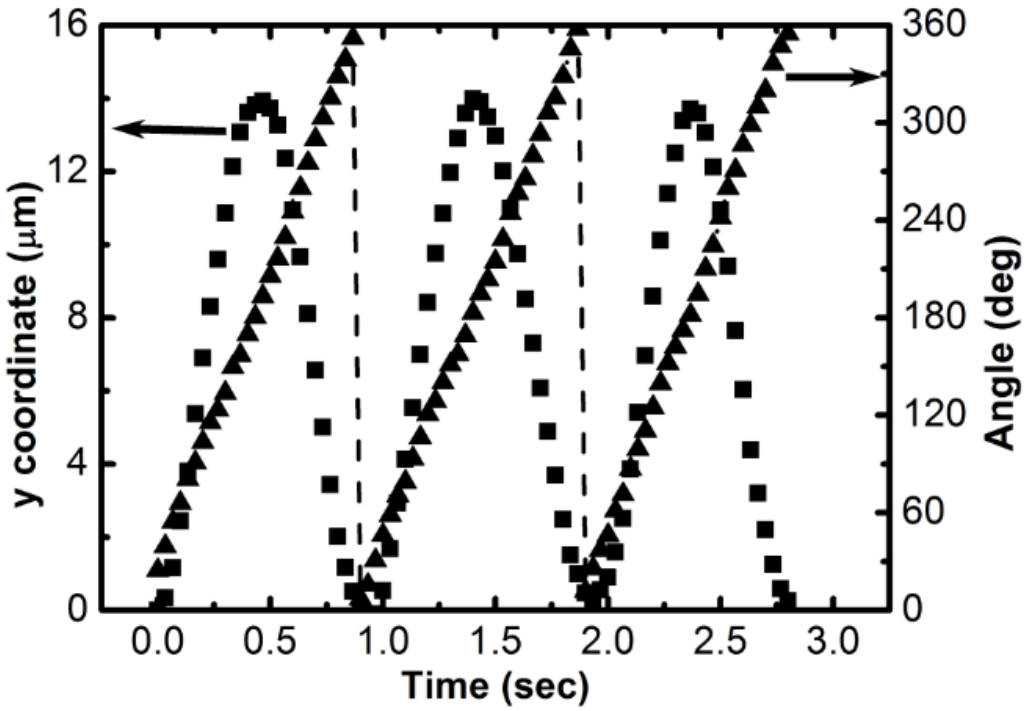

Figure 3.8 Change of the angle (triangle) between the dimer's long axis and the horizontal reference line as a function time. Also shown is the change of particle positions (the y-coordinate) as a function of time (square).

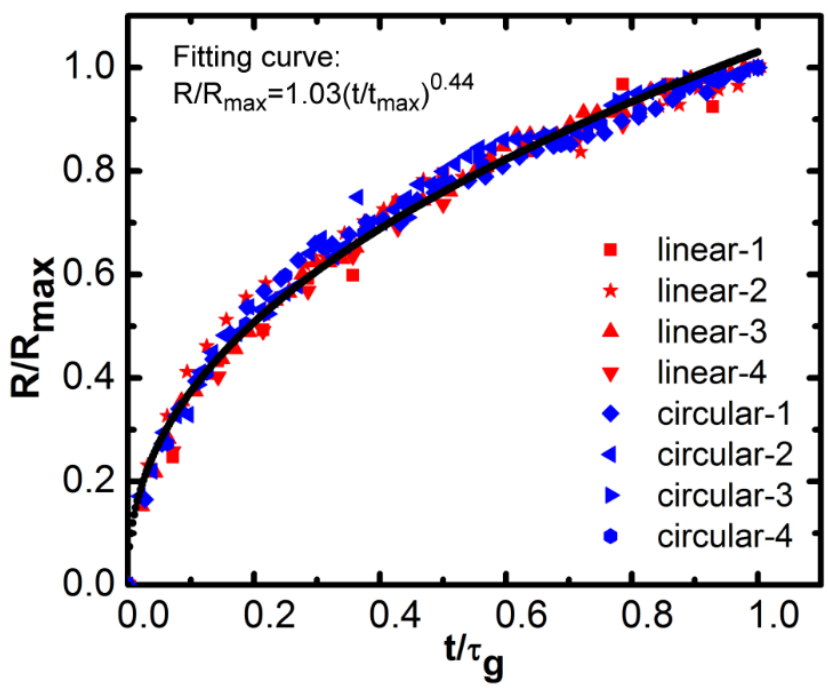

Figure 3.9 The time dependence of the bubble radius during both linear and circular motions. R_{max} is the maximal bubble radius and τ_g is the time scale for bubble growth (see text for details).

For both linear and circular motions, the growth of bubbles follows a master time dependence curve, as shown in Figure 3.9. The fitting reveals a power law relationship: $R \propto t^{0.44}$. The exponent is 0.44 +/- 0.02 (with a 95% confidence interval), close to 1/2, which suggests that the bubble growth is diffusion controlled. Here we develop a heuristic theory to explain it. We assume that the bubble growth is due to the diffusion of oversaturated gas (generated by platinum coating surrounding the pinning point of the bubble) towards the bubble. Applying the conservation of mass to the microscopic bubble of radius R, we obtain

$$\frac{dn}{dt} = 4\pi R^2 D \left.\frac{\partial c}{\partial r}\right|_{r=R} \tag{3.1}$$

where n is the number of moles in the bubble, D is the diffusivity of the gas, and c is the local gas concentration. The diffusion flux can be approximated $\sim DC_s / R$, where C_s is the gas solubility. The number of moles n can be related to both pressure and volume by applying the ideal gas law

$$\frac{dn}{dt} = \frac{d(PV)}{kT} = \frac{d\left[\left(P_\infty + 2\gamma / R\right)4\pi R^3\right]}{3kT} \tag{3.2}$$

where P_∞ is the atmosphere pressure, γ is the liquid-gas interfacial tension, k is the ideal gas constant, and T is the temperature. Here, we have assumed that the pressure inside the bubble is in equilibrium with pressure outside and Laplace pressure, i.e., the viscous stress at the bubble interface is neglected.

Combining Equation (3.1) and Equation (3.2), we obtain a differential equation that governs the bubble growth

$$\frac{d\bar{R}}{d\bar{t}} = \frac{\tau_g 2kTDC_s}{R_{\max}^2 P_\infty} \frac{1}{2\left(\bar{R} + 4\gamma / 3R_{\max} P_\infty\right)} \tag{3.3}$$

Equation (3.3) has been non-dimensionalized, where $\bar{R} = R / R_{\max}$ and $\bar{t} = t / \tau_g$. Without solving Equation (3.3), we can learn some characteristic information about the bubble growth. For example, the time scale for bubble growth τ_g is related to other parameters by $\tau_g \sim R_{\max}^2 P_\infty / 2kTDC_s$. If we assume that the maximal bubble radius $R_{\max}$ is ~5 μm, τ_g is then on the order of one second, which is close to our experimental observation. As a comparison, the time scale for bubble collapse is $\tau_c \sim R\sqrt{\rho / P_\infty}$ according to the Rayleigh-Plesset equation[50],

$$\mathrm{P} - P_\infty = \rho R \frac{d^2 R}{dt^2} + \frac{3}{2}\rho \left(\frac{dR}{dt}\right)^2 + \frac{4\mu}{R} \cdot \frac{dR}{dt} + \frac{2\gamma}{R} \tag{3.4}$$

where P, ρ, and μ are the pressure inside the bubble, the density of water, and the viscosity of water, respectively. For a microscopic bubble of ~5 μm, τ_c is on the order of micro-second, which is also confirmed by us with the help of an ultra-high speed camera. Therefore, the bubble growth and collapse time are different in about six orders of magnitude. A second interesting feature from Equation (3.3) is the parameter $\alpha = 4\gamma / 3R_{\max} P_\infty$, which is essentially the ratio between the Laplace pressure and the atmosphere pressure. When $\alpha \ll 1$, the surface tension effect is negligible, and $d\bar{R} / d\bar{t} \propto \bar{R}^{-1}$. Clearly, in this situation, one recovers the 1/2 law, i.e., $\bar{R} \propto \bar{t}^{1/2}$. In our experiments, α is about 0.2. Therefore, the surface tension is important especially during the initial growth stage where the bubble radius is less than one micron. Any non-negligible α will make the radius growth deviate from the square-root-of-time relationship, which perhaps explains our exponent of 0.44.

After discovering the enormously different time scales between bubble growth and collapse, we decide to use a high speed camera to investigate the motion of dimers, which reveals an interesting phenomenon. The linearly propelled dimer does not move in one direction

monotonically. During the whole cycle of the bubble nucleation, growth, and collapse, the dimer moves forward most of the time except when the bubble collapses. At that moment, the dimer is pulled back. In Figure 3.10a, we plot both bubble size and the instantaneous particle displacement vs. time. The particle displacement remains largely positive until the moment when the bubble radius shrinks to zero. A large negative displacement at that specific time simply means that the dimer is pulled back, presumable due to the backflow of the solvent.[11] Because of the extremely short interval for bubble collapse, the displacement of 3 μm means a velocity of ~3 m/sec, an extremely high speed. However, when a dimer moves circularly, we observe the opposite phenomenon. As shown in Figure 3.10b, when a bubble collapses, the circularly propelled dimer is pushed forward, characterized by a large positive displacement. The striking difference between the "pull-back" and "push-forward" movement during the bubble collapse moment is intriguing. We confirm that they are closely linked to whether the particle undergoes the linear or circular motion by examining more than twenty videos for each type of motion. Before attempting to explain the difference, we report another finding based on our image analyses.

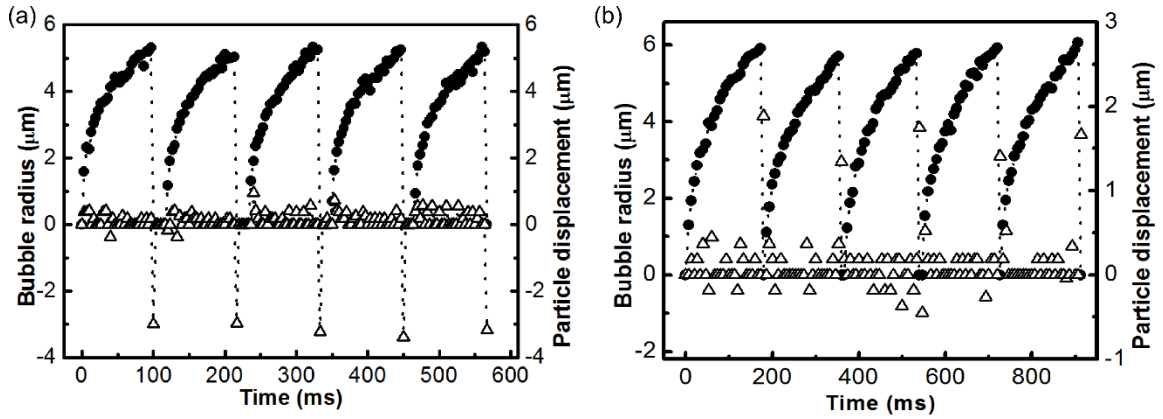

Figure 3.10 The plot of the bubbles radius (circle) and the particle's instantaneous displacement (triangle) versus time in (a) the linear motion and (b) the circular motion.

Figure 3.11 shows that the accumulative movement of the dimer as a function of time, accompanied by the radius growth for both linear and circular motion. We find that during the

bubble growing stage, the center of the bubble remains stationary. Therefore, the dimer is passively pushed forward during the bubble growth. In Figure 3.11a, the accumulative displacement of the linearly propelled dimer follows the bubble growth curve closely, which indicates that the dimer is located close to the central plane of the bubble, i.e., $\theta \sim 90^{\circ}$. Therefore, when the bubble grows to a bigger size than the dimer, the dimer would be lifted from the substrate. However, for the circular motion (Figure 3.11b), we find that the dimer's displacement follows about one third of the bubble radius increase, which indicates that the dimer is actually located below the central plane of the bubble. With an angle $\theta \sim 20^{\circ}$, it is located very close to the substrate. The optical observations also support this argument since at the later stage of the bubble growth, the dimer is located at a different focus plane compared with the central plane of the bubble.

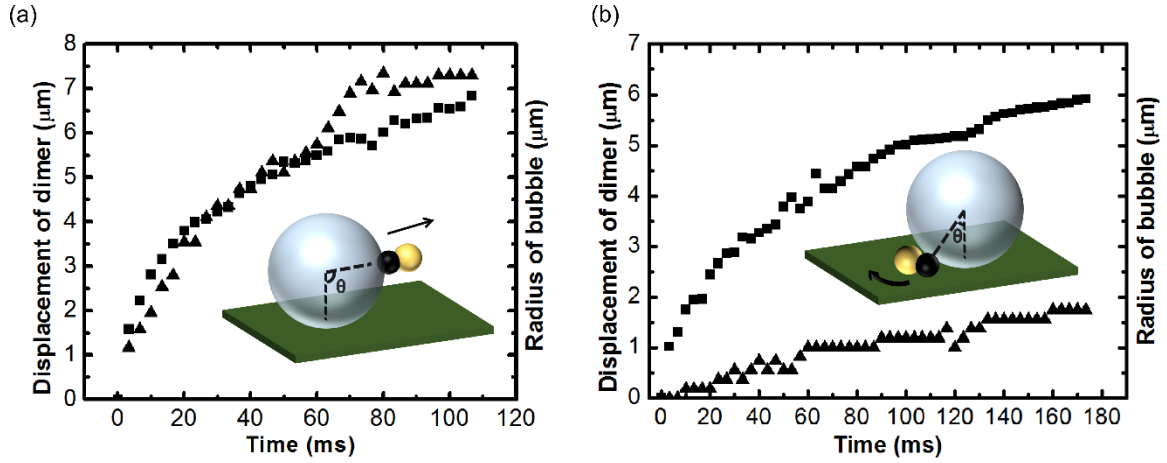

Figure 3.11 The accumulative displacement of dimers (triangle) and the bubble radius (square) versus time for (a) linear motion and (b) circular motion. The insets show the position of the dimer (black: the platinum-coated lobe; yellow: the polystyrene lobe) relative to the bubble. The green represents the substrate.

The different locations of linearly and circularly propelled dimers could explain their distinct behavior at the bubble burst moment. As illustrated schematically in Figure 3.12a, since the bubble is close to the solid substrate, it will collapse asymmetrically compared with an isotropic shrinkage in the bulk.[51,52] It is known that this asymmetric collapse is accompanied by the development of a high speed liquid "micro-jet"[53–55] at the later stage. The liquid jet will eventually

penetrate the interior surface of the bubble and cause an impulsive impact to the substrate (Figure 3.12b). In fact, this micro-jet is the reason why high speed turbines can be damaged by bubble cavitations.[54] Immediately after the bubble disappears, there will be a development of vortex rings [55,56] because of the micro-jet, as illustrated in Figure 3.12c. Therefore, the dimer that is close to the substrate (during circular motion) will experience an outward water flow, which pushes it away from the center of the bubble.[53] For a lineally propelled dimer, it is far away from the substrate. So it will experience an inward water flow, which pulls it towards the center of the collapsed bubble.

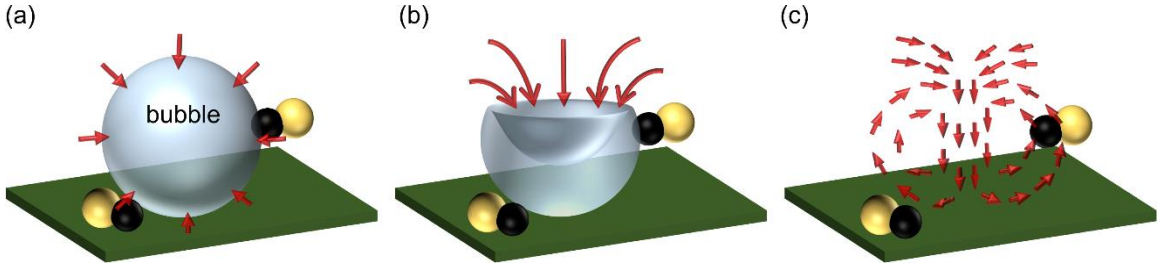

Figure 3.12 A schematics showing the solvent flow during the moment of the bubble collapse. Red arrows indicate the solvent flow. (a) The bubble collapses asymmetrically due to the influence of a solid substrate. (b) A micro-jet is developed, which will eventually penetrate the interior surface of the bubble and cause an impulsive impact to the substrate. (c) Vortex rings form immediately after the bubble collapses. Depending on the relative locations of the dimers, they can be pushed away or pulled towards the center.

Since the bubble collapse takes on the order of microseconds, we utilize an ultra-high speed camera (phantom v711) with 680,000 frames per second to capture the motion of dimers. Figure 3.13a and b show a few consecutive snapshots during and immediately after the collapse of bubbles for both linearly and circularly propelled dimers. Their accumulative displacement are calculated based on the image analyses and are summarized in Figure 3.13. Clearly, the dimer exhibiting a linear motion has the largest negative displacement between 0 μs and 1.5 μs, i.e., immediately following the bubble collapse. The dimer exhibiting a circular motion, however, shows continuous positive displacement long after the collapse of the bubble. This difference in timing of the "pull-

back" and “push-forward” is consistent with our schematics in Figure 3.12. The inward water flow can initiate earlier, while the outward flow along the substrate happens after the bubble collapses. It is also interesting to notice that the appearance of the bright spots and the development of shock waves when the bubble collapses. Such a dramatic change in pressure (and possibly temperature) within an extremely short interval can release a large amount of energy.

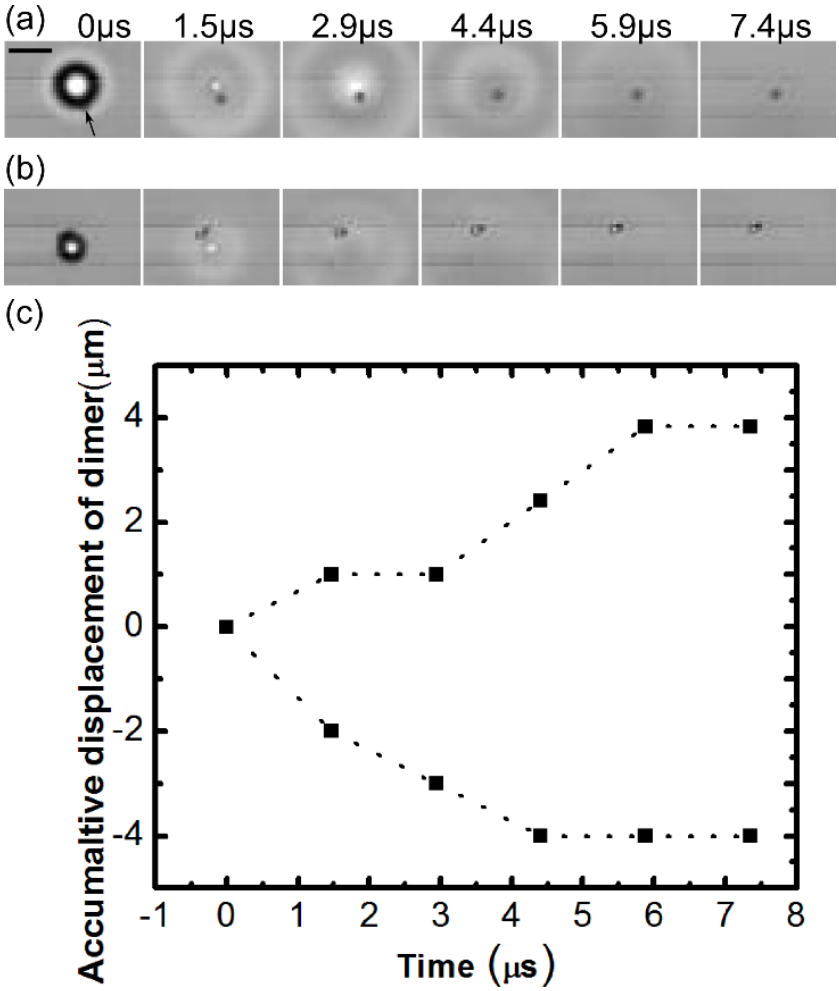

Figure 3.13 Bubble collapse moments captured by an ultra-high speed camera in linear and circular motions. Snapshots of the dimer during and immediately after the bubble collapse in (a) linear and (b) circular motions. (c) The accumulative displacement of dimers vs. time. The solid squares represent the circularly moved dimer, while the triangles correspond to the linearly propelled dimer. Scale bar: 5μm.

3.5 Conclusions

We utilize a bulk synthesis method to fabricate platinum-polystyrene dimers chemically and study their self-propulsion in hydrogen peroxide solutions. Simply by changing the way of platinum deposition, we can switch the dominant swimming mechanism of the Janus particles from self-diffusiophoresis to bubble propulsion. When the platinum is physically evaporated, the particle moves without any visible bubble, consistent with the self-diffusiophoresis mechanism. When the platinum is chemically deposited, the particle is propelled by periodic growth and collapse of bubbles. Through series of systematic investigations, we find that the chemically deposited platinum has higher catalytic activity and rougher surface than the physically evaporated platinum. Both properties are important for making bubble-propelled convex micro-motors. The former is necessary for generating large amounts of bubble nuclei and ensuring oversaturation, and the latter is crucial for pinning and stabilizing the growth of bubbles once they nucleate on the platinum surface.

Because of the combined anisotropy in particle geometry and catalytic activity, our hybrid dimers exhibit linear and circular motions, depending on the location where the bubble is grown. Both motions share some common features during the bubble growth stage. Since the center of the bubble remains stationary, particles are passively pushed forward. The growth of bubbles follows a square-root relationship with time, indicating a diffusion-controlled process. However, the dimer is lifted away from the substrate during linear motion and is close to the substrate in circular motion. This difference causes the dimers behave distinctively at the moment of the bubble collapse, which occurs within microseconds. The dimer is pulled back if it undergoes a linear motion, while it is pushed forward in the circular motion. This is because when the bubble collapses asymmetrically

due to the influence of the solid substrate, vortex rings develop. The resulting solvent flow could push or pull the dimers depending on the particle locations to the substrate.

In summary, our study reveals a simple method to select the propulsion mode of micro-motors, as well as the intriguing impacts of the combined geometric and interfacial anisotropy on propulsion. The hybrid polystyrene-platinum dimers also represent a new type of micro-motors. Compared with Janus spheres and tubular particles, the additional (polystyrene) lobe can be conveniently modified to encapsulate drugs or reactive agents. Combined with the bubble propulsion, the dimers could be an excellent candidate for building smart vehicles for targeted delivery through active propulsion. We are currently investigating along these lines.

3.6 Acknowledgement

We thank Jason Trevithick for his help on the analyses of some experimental data. This work was partially supported by the start-up funds of Colorado School of Mines. Additional acknowledgment is made to the Donors of the American Chemical Society Petroleum Research Fund.

References

(1) Ozin, G. A.; Manners, I.; Fournier-Bidoz, S.; Arsenault, A. Dream Nanomachines. *Adv. Mater.* **2005**, *17*, 3011–3018.

(2) Wang, J.; Gao, W. Nano/Microscale Motors: Biomedical Opportunities and Challenges. *ACS Nano* **2012**, *6*, 5745–5751.

(3) Ebbens, S. J.; Howse, J. R. In Pursuit of Propulsion at the Nanoscale. *Soft Matter*, **2010**, *6*, 726–738.

(4) Hunt, H. K.; Armani, A. M. Label-Free Biological and Chemical Sensors. *Nanoscale* **2010**, *2*, 1544–1559.

(5) Fernandes, R.; Gracias, D. H. Toward a Miniaturized Mechanical Surgeon. *Mater. Today* **2009**, *12*, 14–20.

(6) Howse, J. R.; Jones, R. A. L.; Ryan, A. J.; Gough, T.; Vafabakhsh, R.; Golestanian, R. Self-Motile Colloidal Particles: From Directed Propulsion to Random Walk. *Phys. Rev. Lett.* **2007**, *99*, 048102–048104.

(7) Ke, H.; Ye, S.; Carroll, R. L.; Showalter, K. Motion Analysis of Self-Propelled Pt-Silica Particles in Hydrogen Peroxide Solutions. *J. Phys. Chem. A* **2010**, *114*, 5462–5467.

(8) Valadares, L. F.; Tao, Y.-G.; Zacharia, N. S.; Kitaev, V.; Galembeck, F.; Kapral, R.; Ozin, G. A. Catalytic Nanomotors: Self-Propelled Sphere Dimers. *Small* **2010**, *6*, 565–572.

(9) Wu, Y.; Wu, Z.; Lin, X.; He, Q.; Li, J. Autonomous Movement of Controllable Assembled Janus Capsule Motors. *ACS Nano* **2012**, *6*, 10910–10916.

(10) Gao, W.; Sattayasamitsathit, S.; Orozco, J.; Wang, J. Highly Efficient Catalytic Microengines: Template Electrosynthesis of Polyaniline/platinum Microtubes. *J. Am. Chem. Soc.* **2011**, *133*, 11862–11864.

(11) Manjare, M.; Yang, B.; Zhao, Y.-P. Bubble Driven Quasioscillatory Translational Motion of Catalytic Micromotors. *Phys. Rev. Lett.* **2012**, *109*, 128305–5.

(12) Ju, G.; Cheng, M.; Xiao, M.; Xu, J.; Pan, K.; Wang, X.; Zhang, Y.; Shi, F. Smart Transportation Between Three Phases Through a Stimulus-Responsive Functionally Cooperating Device. *Adv. Mater.* **2013**, *25*, 2915–2919.

(13) Paxton, W. F.; Kistler, K. C.; Olmeda, C. C.; Sen, A.; St Angelo, S. K.; Cao, Y.; Mallouk, T. E.; Lammert, P. E.; Crespi, V. H. Catalytic Nanomotors: Autonomous Movement of Striped Nanorods. *J. Am. Chem. Soc.* **2004**, *126*, 13424–13431.

(14) Hong, Y.; Blackman, N. M. K.; Kopp, N. D.; Sen, A.; Velegol, D. Chemotaxis of Nonbiological Colloidal Rods. *Phys. Rev. Lett.* **2007**, *99*, 178103–178104.

(15) Sundararajan, S.; Lammert, P. E.; Zudans, A. W.; Crespi, V. H.; Sen, A. Catalytic Motors for Transport of Colloidal Cargo. *Nano Lett.* **2008**, *8*, 1271–1276.

(16) Solovev, A. A.; Sanchez, S.; Pumera, M.; Mei, Y. F.; Schmidt, O. G. Magnetic Control of Tubular Catalytic Microbots for the Transport, Assembly, and Delivery of Micro-Objects. *Adv. Funct. Mater.* **2010**, *20*, 2430–2435.

(17) Hanczyc, M. M.; Toyota, T.; Ikegami, T.; Packard, N.; Sugawara, T. Fatty Acid Chemistry at the Oil-Water Interface: Self-Propelled Oil Droplets. *J. Am. Chem. Soc.* **2007**, *129*, 9386–9391.

(18) Lagzi, I.; Soh, S.; Wesson, P. J.; Browne, K. P.; Grzybowski, B. A. Maze Solving by Chemotactic Droplets. *J. Am. Chem. Soc.* **2010**, *132*, 1198–1199.

(19) Xiao, M.; Cheng, M.; Zhang, Y.; Shi, F. Combining the Marangoni Effect and the pH-Responsive Superhydrophobicity-Superhydrophilicity Transition to Biomimic the Locomotion Process of the Beetles of Genus Stenus. *Small* **2013**, *9*, 2509–2514.

(20) Vicario, J.; Eelkema, R.; Browne, W. R.; Meetsma, A.; La Crois, R. M.; Feringa, B. L. Catalytic Molecular Motors: Fuelling Autonomous Movement by a Surface Bound Synthetic Manganese Catalase. *Chem. Commun.* **2005**, 3936–3938.

(21) Pantarotto, D.; Browne, W. R.; Feringa, B. L. Autonomous Propulsion of Carbon Nanotubes Powered by a Multienzyme Ensemble. *Chem. Commun.* **2008**, 1533–1535.

(22) Sanchez, S.; Solovev, A. A.; Mei, Y.; Schmidt, O. G. Dynamics of Biocatalytic Microengines Mediated by Variable Friction Control. *J. Am. Chem. Soc.* **2010**, *132*, 13144–13145.

(23) Mano, N.; Heller, A. Bioelectrochemical Propulsion. *J. Am. Chem. Soc.* **2005**, *127*, 11574–11575.

(24) Wilson, D. A.; Nolte, R. J. M.; Hest, J. C. M. Van. Autonomous Movement of Platinum-Loaded Stomatocytes. *Nat. Chem.* **2012**, *4*, 268–274.

(25) Gibbs, J. G.; Zhao, Y. P. Autonomously Motile Catalytic Nanomotors by Bubble Propulsion. *Appl. Phys. Lett.* **2009**, *94*, 163104–3.

(26) Anderson, J. L.; Prieve, D. C. Diffusiophoresis Caused by Gradients of Strongly Adsorbing Solutes. *Langmuir* **1991**, *7*, 403–406.

(27) Rückner, G.; Kapral, R. Chemically Powered Nanodimers. *Phys. Rev. Lett.* **2007**, *98*, 150603–150604.

(28) Ebbens, S.; Tu, M.-H.; Howse, J.; Golestanian, R. Size Dependence of the Propulsion Velocity for Catalytic Janus-Sphere Swimmers. *Physical Review E*, **2012**, *85*, 020401–020404.

(29) Solovev, A. a; Xi, W.; Gracias, D. H.; Harazim, S. M.; Deneke, C.; Sanchez, S.; Schmidt, O. G. Self-Propelled Nanotools. *ACS Nano* **2012**, *6*, 1751–1756.

(30) Graf, C.; Van Blaaderen, A. Metallodielectric Colloidal Core−Shell Particles for Photonic Applications. *Langmuir* **2002**, *18*, 524–534.

(31) Turkevich, J.; Stevenson, P. C.; Hillier, J. A Study of the Nucleation and Growth Processes in the Synthesis of Colloidal Gold. *Discuss. Faraday Soc.* **1951**, *11*, 55–75.

(32) Lu, L.; Sun, G.; Xi, S.; Wang, H.; Zhang, H.; Wang, T.; Zhou, X. A Colloidal Templating Method To Hollow Bimetallic Nanostructures. *Langmuir* **2003**, *19*, 3074–3077.

(33) Zhang, F.; Cao, L.; Yang, W. Preparation of Monodisperse and Anion-Charged Polystyrene Microspheres Stabilized with Polymerizable Sodium Styrene Sulfonate by Dispersion Polymerization. *Macromol. Chem. Phys.* **2010**, *211*, 744–751.

(34) Abramoff, M. D.; Magalhães, P. J.; Ram, S. J. Image Processing with ImageJ. *Biophotonics Int.* **2004**, *11*, 36–42.

(35) Wang, S.; Ma, F.; Zhao, H.; Wu, N. Bulk Synthesis of Metal–Organic Hybrid Dimers and Their Propulsion under Electric Fields. *ACS Appl. Mater. Interfaces* **2014**, *6*, 4560–4569.

(36) Sheu, H. R.; El-Aasser, M. S.; Vanderhoff, J. W. Phase Separation in Polystyrene Latex Interpenetrating Polymer Networks. *J. Polym. Sci., Part A: Polym. Chem.* **1990**, *28*, 629–651.

(37) Kim, J.-W.; Larsen, R. J.; Weitz, D. A. Synthesis of Nonspherical Colloidal Particles with Anisotropic Properties. *J. Am. Chem. Soc.* **2006**, *128*, 14374–14377.

(38) Plueddemann, E. P. *Silane Coupling Agents*; Springer Science & Business Media, **1982**.

(39) Mirkovic, T.; Zacharia, N. S.; Scholes, G. D.; Ozin, G. A. Fuel for Thought: Chemically Powered Nanomotors out-Swim Nature's Flagellated Bacteria. *ACS Nano* **2010**, *4*, 1782–1789.

(40) Okamoto, H.; Horii, K.; Fujisawa, A.; Yamamoto, Y. Oxidative Deterioration of Platinum Nanoparticle and Its Prevention by Palladium. *Exp. Dermatol.* **2012**, *21*, 5–7.

(41) Zhao, G.; Sanchez, S.; Schmidt, O. G.; Pumera, M. Poisoning of Bubble Propelled Catalytic Micromotors: The Chemical Environment Matters. *Nanoscale* **2013**, *5*, 2909–2914.

(42) Koningsberger, D.; Miller, J. The Origin of Sulfur Tolerance in Supported Platinum Catalysts: The Relationship between Structural and Catalytic Properties in Acidic and Alkaline Pt/LTL. *J. Catal.* **1996**, *162*, 209–219.

(43) Greeley, J.; Nørskov, J. K.; Mavrikakis, M. Electronic Structure and Catalysis on Metal Surfaces. *Annu. Rev. Phys. Chem.* **2002**, *53*, 319–348.

(44) Zambelli, T.; Wintterlin, J.; Trost, J.; Ertl, G. Identification of the "Active Sites" of a Surface-Catalyzed Reaction. *Science* **1996**, *273*, 1688–1690.

(45) Chang, L. Y.; Barnard, A. S.; Gontard, L. C.; Dunin-Borkowski, R. E. Resolving the Structure of Active Sites on Platinum Catalytic Nanoparticles. *Nano Lett.* **2010**, *10*, 3073–3076.

(46) Quéré, D. Wetting and Roughness. *Annual Review of Materials Research*, **2008**, *38*, 71–99.

(47) Kalinin, Y. V; Berejnov, V.; Thorne, R. E. Contact Line Pinning by Microfabricated Patterns: Effects of Microscale Topography. *Langmuir* **2009**, *25*, 5391–5397.

(48) Bigall, N. C.; Härtling, T.; Klose, M.; Simon, P.; Eng, L. M.; Eychmüller, A. Monodisperse Platinum Nanospheres with Adjustable Diameters from 10 to 100 Nm: Synthesis and Distinct Optical Properties. *Nano Lett.* **2008**, *8*, 4588–4592.

(49) Semagina, N.; Kiwi Minsker, L. Recent Advances in the Liquid-Phase Synthesis of Metal Nanostructures with Controlled Shape and Size for Catalysis. *Catalysis Reviews*, **2009**, *51*, 147–217.

(50) Plesset, M. S.; Prosperetti, A. Bubble Dynamics and Cavitation. *Annu. Rev. Fluid Mech.* **1977**, *9*, 145–185.

(51) Blake, J. R.; Keen, G. S.; Tong, R. P.; Wilson, M. Acoustic Cavitation: The Fluid Dynamics of Non-Spherical Bubbles. *Philos. Trans. R. Soc., A* **1999**, *357*, 251–267.

(52) Chen, J.; Han, B.; Li, B.; Shen, Z.-H.; Lu, J.; Ni, X.-W. The Collapse of a Bubble against Infinite and Finite Rigid Boundaries for Underwater Laser Propulsion. *J. Appl. Phys.* **2011**, *109*, 083101–083108.

(53) Junge, L.; Ohl, C. D.; Wolfrum, B.; Arora, M.; Ikink, R. Cell Detachment Method Using Shock-Wave-Induced Cavitation. *Ultrasound Med. Biol.* **2003**, *29*, 1769–1776.

(54) Franc, J. P.; Michel, J. M. *Fundamentals of Cavitation*; Fluid mechanics and its applications; Kluwer Academic Publishers: Dordrecht, the Netherlands, **2006**.

(55) Jing, L.; Guangneng, D.; Jian, L. Two-Dimensional Simulation of the Collapse of Vapor Bubbles Near a Wall. *J. Fluids Eng.* **2008**, *130*, 91301–91304.

(56) Brujan, E. A.; Keen, G. S.; Vogel, A.; Blake, J. R. The Final Stage of the Collapse of a Cavitation Bubble close to a Rigid Boundary. *Phys. Fluids* **2002**, *14*, 85–92.

CHAPTER 4

BICOMPARTMENTAL PHASE TRANSFER VEHICLES BASED ON COLLOIDAL DIMERS

Modified from a paper published in *ACS Applied Materials & Interfaces*

Sijia Wang[2] and Ning Wu[3]

4.1 Abstract

Colloidal particles have been used extensively for stabilizing oil-water interfaces in petroleum, food, and cosmetics industries. They have also demonstrated promising potential in the encapsulation and delivery of drugs. Our work is motivated by challenging applications that require protecting and transporting active agents across the water-oil interfaces, such as delivering catalysts to underground oil phase through water flooding for *in situ* cracking of crude oil. In this paper, we successfully design, synthesize, and test a unique type of bi-compartmental targeting vehicle that encapsulates catalytic molecules, finds and accumulates at oil-water interface, releases the catalysts towards the oil phase, and performs hydrogenation reaction of unsaturated oil. This vehicle is based on colloidal dimers that possess structural anisotropy between two compartments. We encapsulate active species such as fluorescent dye and catalytic molecules in one lobe which consists of uncrosslinked polymers, while the other polymeric lobe is highly crosslinked. Although dimers are dispersible in water initially, the uncrosslinked lobe swells significantly upon contact with a trace amount of oil in aqueous phase. The dimers then become amphiphilic, migrate towards, and accumulate at the oil-water interface. As the uncrosslinked lobe swells and eventually dissolves in oil, the encapsulated catalysts are fully released. We also show that hydrogenation of

[1]Reprinted with permission from *ACS Appl. Mater. Interfaces* **2014**, *6*, 20164–20170.
Copyright 2014 American Chemical Society.
[2]Graduate student and [3]Assistant Professor, respectively,
Department of Chemical and Biological Engineering, Colorado School of Mines.
[2]Primary researcher and author.
[3]Author for correspondence.

unsaturated oil can be performed subsequently with high conversion efficiency. By further creating the interfacial anisotropy on the dimers, we can reduce the catalyst release time from hundred hours to thirty minutes. Our work demonstrates a new concept in making colloidal emulsifiers and phase-transfer vehicles that are important for encapsulation and sequential release of small molecules across two different phases.

4.2 Introduction

Colloidal particles that are partially wettable to both oil and water tend to adsorb at an oil-water interface. Once adsorbed, they are very stable due to the high energy barrier of desorption,[1] which offers a great advantage over molecular surfactants. As such, micro- and nano-particles have long been used in the petroleum, cosmetic, food, and pharmaceutical industries[2–11] to stabilize emulsions and foams against coalescence. However, the stabilization energy of a particle with homogenous surface properties depends sensitively on its contact angle at the interface,[12] which is often difficult to tune precisely.

Better control of the particle wettability can be achieved if its surface can be tailored differently on two sides of the particle, i.e., the so-called Janus particle.[13–17] For example, when one side is coated with hydrophilic molecules and the other side is hydrophobic, the Janus particle can mimic the amphiphilic nature of molecular surfactants faithfully. Recent work using Janus spheres as colloidal emulsifiers[18–20] have shown significant advantages over isotropic particles. The spherical geometry, however, is still far from ideal. It is widely known that the geometric balance between the hydrophilic and lipophilic parts of molecular surfactants largely dictates different morphologies that they can pack into and influences their emulsification behavior.[21] Motivated by this, very recently, Park and Lee[22,23] performed theoretical calculations on the attachment energy of colloidal dimers, whose interfacial and geometric asymmetry can be, in

principle, tailored independently. They have found that amphiphilic dimers can adopt upright or tilted orientations at the oil-water interface, depending on the relative difference in both diameter and hydrophilicity between two lobes. Recent experiments appear to support the theoretical findings.[24,25]

Although most studies focused primarily on the adsorption of particles at oil-water interfaces, in many applications it is also important to transfer species such as molecules and nanoparticles across the interface.[26–29] For example, drug-carrying vehicles that can enter various types of biological barriers from plasma can revolutionize modern diagnostic and therapeutic technologies. Our research here is motivated by a similar problem facing the petroleum industry in extracting unconventional hydrocarbons such as heavy oil.[30] In spite of its immense resource, only 15% percent of yearly oil production is from heavy oil due to its notoriously high viscosity. Conventional water flooding fails because less viscous water can easily find pathways to flow through a reservoir (i.e., the fingering effect) and leave pockets of oil behind. Even if heavy oil is extracted to the surface, its viscosity must be kept low for transportation in pipelines. Therefore, the Society of Petroleum Engineers[30,31] has recently identified that downhole delivery of nanocatalysts for *in-situ* conversion of heavy oil into a lighter grade could be a game-changing technology. The central task for realizing *in-situ* cracking is the delivery of catalytic species into the oil phase through downhole porous media. This process has two competing constraints: the catalysts must first be dispersed in water and then delivered underground through water flooding; later they need to accumulate in the oil phase for subsequent catalytic reactions such as low-temperature oxidation or partial hydrogenation. It is particularly challenging for catalysts since they usually are not amphiphilic in nature. Surface functionalization could be detrimental to their catalytic activities.[32]

Here, we design, synthesize, and test a unique type of bi-compartmental targeting vehicle that can fulfill this challenging task for oil-phase delivery of catalysts. As shown in Figure 4.1, the targeting vehicle is designed based on a two-compartmental polystyrene particle where one non-crosslinked compartment encapsulates the catalysts. The other compartment consists of highly crosslinked polymer. Although the vehicle is hydrophilic and dispersible in water initially, it can become amphiphilic because the non-crosslinked compartment swells in oil easily. This will enable the vehicle to transport through the aqueous phase; seek and then attach to the oil-water interface. Furthermore, the non-crosslinked compartment is designed to swell significantly and dissolve in oil eventually, which will facilitate the targeted release of catalysts into the oil phase.

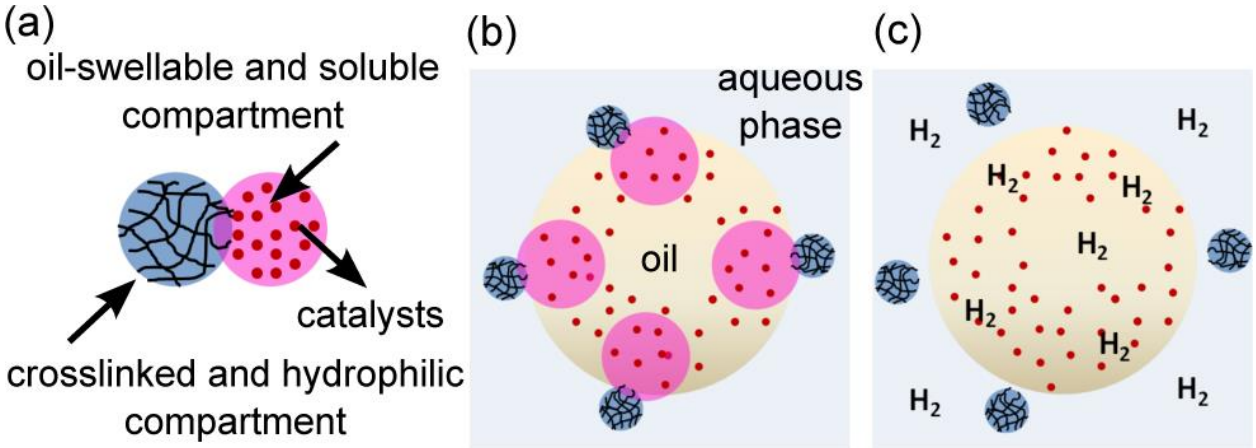

Figure 4.1 A schematic of the bi-compartmental vehicle (colloidal dimer) targeted for delivering catalysts to oil phase underground. (a) One compartment is hydrophilic and highly crosslinked, while the other one is non-crosslinked and oil-swellable. (b) The vehicle transports through water flooding, adsorbs at the oil-water interface, and swells significantly in oil. (c) The hydrophobic compartment eventually dissolves in oil and releases catalysts for subsequent hydrogenation.

4.3 Experimental Methods

The following sections first introduce the materials we used in this Chapter, and afterwards describe the detailed experimental procedures and characterization methods.

4.3.1 Chemicals

Styrene, divinylbenzene (DVB), sodium 4-vinylbenzenesulfonate, polyvinylpyrrolidone (PVP, M_w: ~40,000), sodium dodecyl sulfate (SDS), 3-aminopropyltriethoxysilane, Oil Red O, chlorotris(triphenylphosphine)rhodium(I) (the Wilkinson's catalyst), palladium(II) acetate ($Pd(OAc)_2$), and n-dodecyltriethoxysilane are purchased from Sigma-Aldrich. 3-(trimethoxysily) propyl acrylate (TMSPA) is purchased from Tokyo Chemical Industry (TCI). The thermal initiator V65 is bought from Wako Chemicals. All chemicals are used as received except that both styrene and divinylbenzene are purified by aluminum oxide before usage.

4.3.2 Synthesis of polystyrene dimers

The synthetic route we use to make colloidal dimers is based on seeded emulsion polymerization.[33] We prepare the seed polystyrene (PS) spheres by dispersion polymerization.[34] After we clean the PS seeds four times via centrifugation at 4000 rpm (30 minutes), we can further use these seeds for making crosslinked PS spheres. In brief, we use a tip sonicator (Branson digital sonifier 450) to make an aqueous emulsion. The aqueous phase consists of 4 ml 5 wt% PVP and 0.5 ml 2 wt% SDS. The oil phase is made up of 1 ml styrene, 0.05 ml DVB, 0.05 ml 3-trimethoxysily propyl acrylate, and 0.02 g V65. We mix the emulsion with 1 ml PS seeds (10 wt%) for 24 hours, then put the swollen seeds in an oil bath (70°C) for another 24 hours for polymerization. We then clean these crosslinked PS via centrifugation for four times again. By further swelling the crosslinked PS with an emulsion of styrene, PS dimers can be formed. We can tune the size of the newly formed lobe (i.e., the second lobe) by adjusting the amount of styrene to swell the crosslinked PS seeds. Finally, we perform polymerization at 70 °C overnight to solidify the second (non-crosslinked) lobe.

4.3.3 Dye/catalyst encapsulation

To encapsulate Oil Red O, palladium(II) acetate, or the Wilkinson catalysts in the non-crosslinked lobe, we mix 0.5 ml styrene, 2 wt% V65, and variable amounts (from 20 mg/ml to 100 mg/ml) of the above molecules. They are emulsified in an aqueous solution of 4 ml 5 wt% PVP and 0.5 ml 2 wt% SDS. The emulsion is then used to swell 1 ml crosslinked PS seeds (10 wt%) for ~ 24 hours. Subsequently, polymerization is performed at 70 °C for another 24 hours. The synthesized dimers are then cleaned four times via centrifugation.

4.3.4 Surface modification

The incorporation of vinylsilane molecules (e.g., TMSPA) in the crosslinked lobe allows us to modify its surface properties after the dimer encapsulation and synthesis. For example, we add 1 ml 0.1 wt% dimers and 100 µl n-dodecyltriethoxysilane into an ethanol/water mixture (95:5 vol%), with stirring for 24 hours at room temperature. We then wash the particles by methanol four times via centrifugation (2000 rpm for 20 minutes).

4.3.5 Rhodamine 6G coating on polystyrene dimers

We mix 1 ml dimer (0.5 wt%) with 12.5 µl Rhodamine 6G solution (0.25 wt%) overnight. Then we centrifuge the particles four times before taking fluorescent images.

4.3.6 Biphasic delivery

We put equal amount (1-2 ml) of toluene and water in a glass vial. Dimers with different encapsulated molecules are then injected to the water phase. Typically, the vial is sit on the bench without disturbance during the delivery. Occasionally, we put the vial on a rotator with constant rotation of 50 rpm to accelerate the delivery time.

4.3.7 Hydrogenation of olefin

We mix 40 µl octene, styrene, or butyl acrylate with 2 ml toluene, as the oil phase. After the catalyst molecules are released from the dimers, we collect 1 ml of the upper oil phase, dilute it 10 times with toluene, and carry out the hydrogenation reactions in a closed chamber, where hydrogen gas is injected at 2 bar. The hydrogenation takes place at 80 °C for 1 hour.

4.3.8 Characterization

The morphologies of conventional dimers are characterized by scanning electron microscopy (JEOL JSM-7000F). To ensure dye encapsulation, dimers are also imaged by fluorescent microscopy. The encapsulation efficiency of the Wilkinson's catalysts in the dimers is determined by the following procedures. Since the equipment (ICP-OES Perkin-Elmer Optima 5300 DV) we use is only capable of quantifying the metal ion concentration in aqueous solution, we need to dissolve the metal salts in water. After all the catalysts in the dimers are delivered to the oil phase, we take 10 µl liquid from the oil phase and dilute it with 990 µl toluene. We then evaporate all toluene in 1 ml of the above solution (with 100 times dilution of the original oil phase) at 50 °C. Subsequently we add 5 ml water and 2 ml 30% hydrogen peroxide in the vial and heat for 1 hour (100 °C). This process can be repeated for multiple times until a clear solution is obtained, when the organic compounds in the catalytic molecules are fully decomposed. We then add 10 ml 2% HNO_3 to dissolve the metal ions in aqueous solution. Afterwards, we use inductively coupled plasma optical emission spectroscopy (ICP-OES Perkin-Elmer Optima 5300 DV) to measure the metal concentration in the solution. Finally we calculate the catalyst encapsulation efficiency based on the amount of metal salts delivered to the oil phase and the amount of particles we injected in the vial. In the calculation, we assume that all catalysts in the dimers are released to the oil phase. To quantify the degree of conversion of olefins, we use a Gas Chromatography-Mass

Spectrometry (GC-MS Varian 1200L) with triple quad analyzer to analyze the compositions of the oil phase after the hydrogenation experiments.

4.4 Results and Discussion

For the first time, we utilize particles without any surface modification to act as colloidal surfactants. Different from conventional application as colloidal emulsifiers, colloidal polystyrene dimers with swellability contrast between two lobes, perform phase transfer delivery of active agents. This is one innovative demonstration among numerous applications of colloidal surfactants, and can be one of the solutions for enhanced oil recovery. Meanwhile, the preparation of this bicompartmental phase transfer vehicle is quite facile, low cost, and high output. We also develop different approaches to improve the phase transfer efficiency of the colloidal polystyrene dimers.

4.4.1 Dimer synthesis and active-agent encapsulation

Figure 4.2 summarizes the synthetic routes we follow to make both conventional polystyrene dimers and those encapsulated with different kinds of active agents. The conventional dimers are synthesized based on a seeded emulsion polymerization method.[33,35–39] We first swell polystyrene spheres with styrene, divinylbenzene, and a small amount of vinylsilane (e.g., 3-(trimethoxysily) propyl acrylate) to make crosslinked polystyrene spheres, i.e., the seeds. In the second stage, styrene is used again to swell the seeds.

As shown in Figure 4.2a, the elastic energy of the crosslinked polymer prevents itself from isotropic swelling, induces a phase separation between the monomer and the seeds, and gives rise to the second (monomer) lobe. Further polymerization will solidify the second lobe and generate dimers with high monodispersity. To prevent dimer aggregation in water, we add a small amount of ionic monomer (e.g., sodium 4-vinylbenzenesulfonate) when synthesizing the crosslinked

seeds. Interestingly, when we swell the seeds with styrene again, some poly(sodium 4-styrenesulfonate) chains migrate towards the second lobe. This is evidenced by the fluorescent image in Figure 4.2a, where the positively charged fluorophores (Rhodamine 6G) are absorbed uniformly on both lobes. The surface charges arising from sulfonate functional groups stabilize polystyrene dimers in water. Although the dimer has very similar surface and bulk compositions in both lobes, their physical properties are inherently different. One lobe is made of highly crosslinked (e.g., 5%-20%) polymer while the other lobe primarily consists of linear chains. Later we will exploit this property for oil-phase delivery of catalytic molecules.

As shown in Figure 4.2b and 4.2c, the synthetic recipe for conventional dimers can be conveniently modified to encapsulate different kinds of oil-soluble molecules in the second and non-crosslinked lobe. As a proof of principle, we mix styrene with a fluorescent molecule Oil Red O (ORO), which is then used to swell the crosslinked seed particles. The fluorescent image in Figure 4.2b clearly demonstrates the selective encapsulation of ORO in the second lobe. The large-field SEM image in Figure 4.2b also shows that the encapsulation does not interfere with the dimer synthesis in general and the particle monodispersity can be preserved. We further apply the similar synthetic strategy to encapsulate two other types of molecular catalysts $Pd(OAc)_2$ and $RhCl(PPh_3)_3$. Both of them are common catalysts for hydrogenation of alkenes. When $Pd(OAc)_2$ is loaded close to its solubility limit in styrene (~5 mg/ml), the second lobe undergoes significant buckling (Figure 4.2c-i) during the polymerization stage. This is probably caused by the poor compatibility between polystyrene and $Pd(OAc)_2$.[40] The morphologies of dimers that encapsulate $RhCl(PPh_3)_3$), however, are similar to conventional dimers (Figure 4.2c-ii).

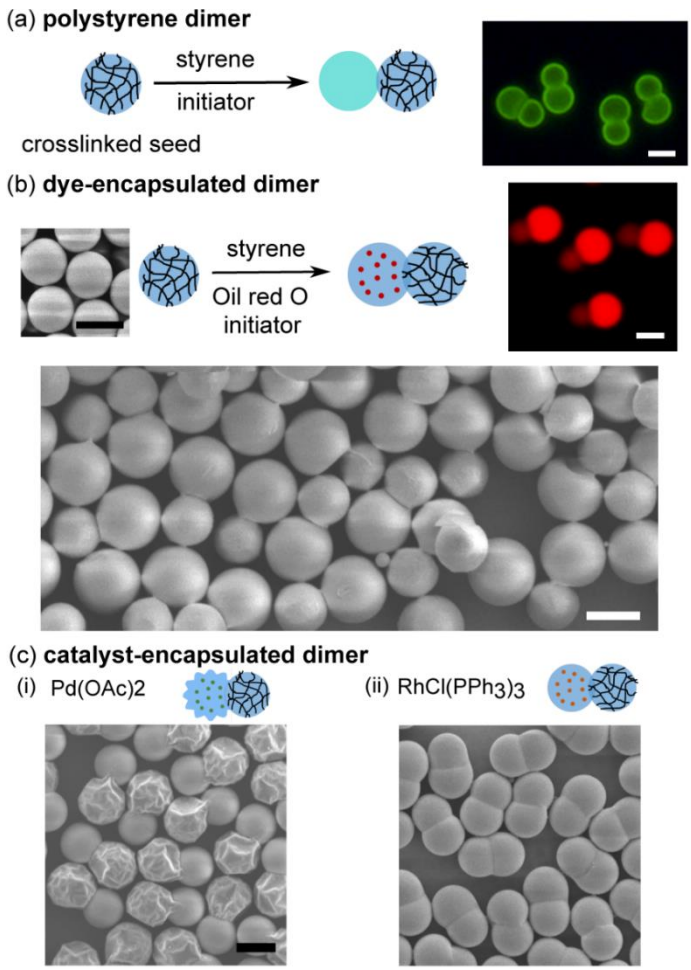

Figure 4.2 The synthetic route of polystyrene dimers encapsulating different molecules. (a) Synthesis of conventional polystyrene dimers. Fluorescent image shows that the negatively charged dimers absorb positively charged fluorophores (i.e., Rhodamine 6G) uniformly. (b) The fluorescent image shows selective encapsulation of Oil red O in the uncrosslinked lobe. The SEM image shows the large-field view of polymerized dimers. (c) Encapsulation of two molecular catalysts in the uncrosslinked lobe. Scale bar for all images: 2 µm.

4.4.2 Structural emulsifier

We first study the behavior of the conventional polystyrene dimers (without any encapsulation or surface modification) in a mixture of toluene and water. Since the dimers possess a uniform distribution of sulfonate groups on their surfaces, they are well dispersed in the aqueous phase initially (Figure 4.3a). They sediment to the bottom of the vial within ~1 day because of their large sizes (~1.6 µm for both lobes) and higher density (~1.05 g/cm^3) than water. Afterwards,

they surprisingly migrate to the water-toluene interface. After ~72 hours, no particle is left at the bottom and both oil and water phases are clear. Essentially all dimers are trapped at the interface. To understand what happens, we examine the shape of dimer particles using an optical microscope.

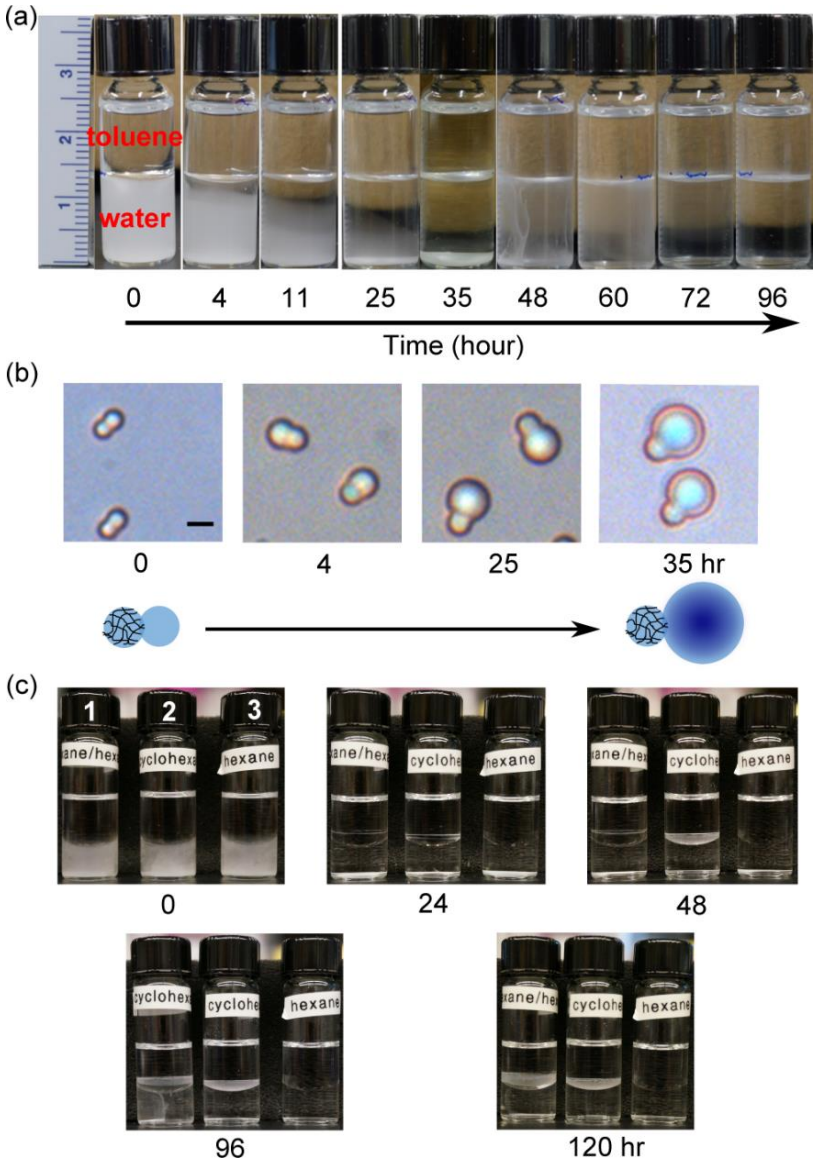

Figure 4.3 Conventional polystyrene dimers in oil-water biphasic mixture. (a) Time evolution of the conventional polystyrene dimers in water/toluene biphasic solution. The scales on the ruler are in inches. (b) Optical image of dimers at the interface in different time. The non-crosslinked lobe absorbs oil significantly. Scale bar: 2 μm. (c) Oil phase composition affects the migration of polystyrene dimers towards the interface. At time zero, the upper phases in three vials are (1) 50%:50% mixture of cyclohexane and hexane, (2) 100% cyclohexane, and (3) 100% hexane, respectively. The bottom phase is water (with dimers) in all vials.

Figure 4.3b shows that the dimers are symmetric initially. As time progresses, one of the lobes becomes significantly larger due to swelling by toluene, while the other lobe barely changes its size. Therefore, the autonomous movement of our dimers towards the toluene-water interface can be understood by the physical anisotropy in the dimers. Toluene, although immiscible with water, has a small solubility of 0.52 g/L at 25°C. The trace amount of toluene in water preferentially swells the non-crosslinked lobe because of the much favorable mixing enthalpy between toluene and linear polystyrene chains.[41,42] When sufficient amount of toluene is absorbed in one lobe, the dimer not only becomes amphiphilic but lighter than water. For instance, if the non-crosslinked lobe doubles its size from 1.6 μm to 3.2 μm due to swelling, the dimer density will change from 1.05 g/cm^3 to 0.91 g/cm^3. Buoyancy can drive the particles towards the toluene-water interface. Since the crosslinked lobe is non-swollen and remains hydrophilic, the dimers stay at the interface.

Our experiment demonstrates that the conventional polystyrene dimers can be used as colloidal emulsifier even without modifying its surface property. We note that it represents a different kind of emulsifier than other kinds of colloidal surfactants, which often need to have a contact angle close to 90º.[15–17,38,43,44] Our dimers are hydrophilic initially and they can be easily dispersed in aqueous phase. They, however, quickly convert into amphiphilic particles by absorbing even a trace amount of oil. In fact, the amphiphilicity becomes quite strong since oil essentially soaks into one of the lobes while the other remains hydrophilic. Because the behavior of our dimers is primarily due to the structural difference (i.e., crosslinked vs. non-crosslinked) between two lobes, we coin them structural emulsifiers. Another noticeable difference between our dimers and conventional emulsifiers is the buoyancy effect since the oil-swollen particles can

become lighter than water, which helps them find the oil phase under natural conditions in underground reservoirs.

We notice that the structural emulsifier works under two conditions: (1) colloids need to be swollen by oil at least partially; (2) oil must have some solubility in water. When we change the upper oil phase into linear hydrocarbons, such as hexane, our dimers remain settled at the bottom of the vials because of its negligible solubility in water (9.5mg/L) and poor compatibility with polystyrene (Figure 4.3c). However, when the oil phase is an equal volume mixture of toluene and hexane, or cyclohexane and hexane, the dimers are able to move towards the water-oil interface. Since crude oil is often a mixture of linear, cyclo, and aromatic hydrocarbons,[45,46] our dimers could find potential applications in enhanced oil recovery. Moreover, the concept presented here can be extended to other oil-water systems if the particle is made of copolymers with both linear and aromatic repeating units, so that it can be swollen by both types of hydrocarbons. Furthermore, unlike conventional colloidal stabilizers whose interfacial properties are homogeneous, the surface properties of two lobes on the dimer particle can be modified independently, which will be discussed later.

4.4.3 Oil phase delivery and hydrogenation

The initially hydrophilic nature of our dimers makes them easily dispersible in water. This is advantageous because those dimers can be transported underground through water flooding, which is commonly used to displace residual oil in reservoir formation. With encapsulated molecular catalysts in the non-crosslinked lobe, our dimer becomes a delivery vehicle that can both find oil and release catalysts to the oil phase for *in-situ* cracking. To demonstrate this concept, we first test the oil-phase delivery of dye molecules.

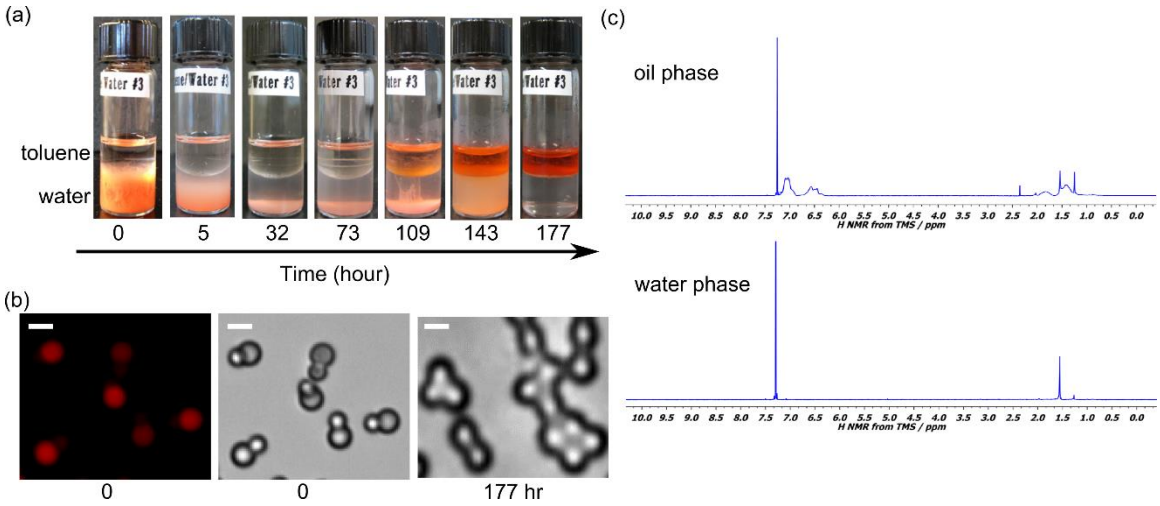

Figure 4.4 Oil phase delivery by dye encapsulated dimers. (a) Time evolution of the Oil Red O encapsulated dimers in a mixture of toluene and water. (b) When t=0, both fluorescent and bright-field microscopy images show that the dye is encapsulated in the large and non-crosslinked lobe. At t~177 hrs, the non-crosslinked lobes eventually dissolve in the oil phase. Scale bar for all images: 2 µm. (c) 1H NMR spectra of both oil and water phases. Note that the peak around 7.24 ppm in both images corresponds to the solvent chloroform we use for NMR characterization. The peak near 1.55 ppm corresponds to the residual water.

Shown in Figure 4.4, the dye is initially encapsulated in the non-crosslinked (larger) lobe, rendering the water phase red. The particles gradually move towards the interface when they are swollen by trace amount of toluene in water. Once they are at the interface, the dye molecules diffuse out of the non-crosslinked lobe into the oil phase. 100% phase transfer is complete after ~ one week when the water phase becomes clear. By examining the particles at the final stage (Figure 4.4b), we find that the non-crosslinked lobes eventually disappear, indicating that they dissolve completely in the oil phase. The NMR spectra shown in Figure 4.4c further demonstrate that polystyrene chains (as characterized by the expected resonance for the aromatic protons peaks near 7.1 and 6.6 ppm) can be found in the oil phase but not the water phase. We note that the dissolvability of the non-crosslinked lobe will allow potential encapsulation and release of much larger species such as catalytic nanoparticles in addition to molecular catalysts, which will be tested in future.

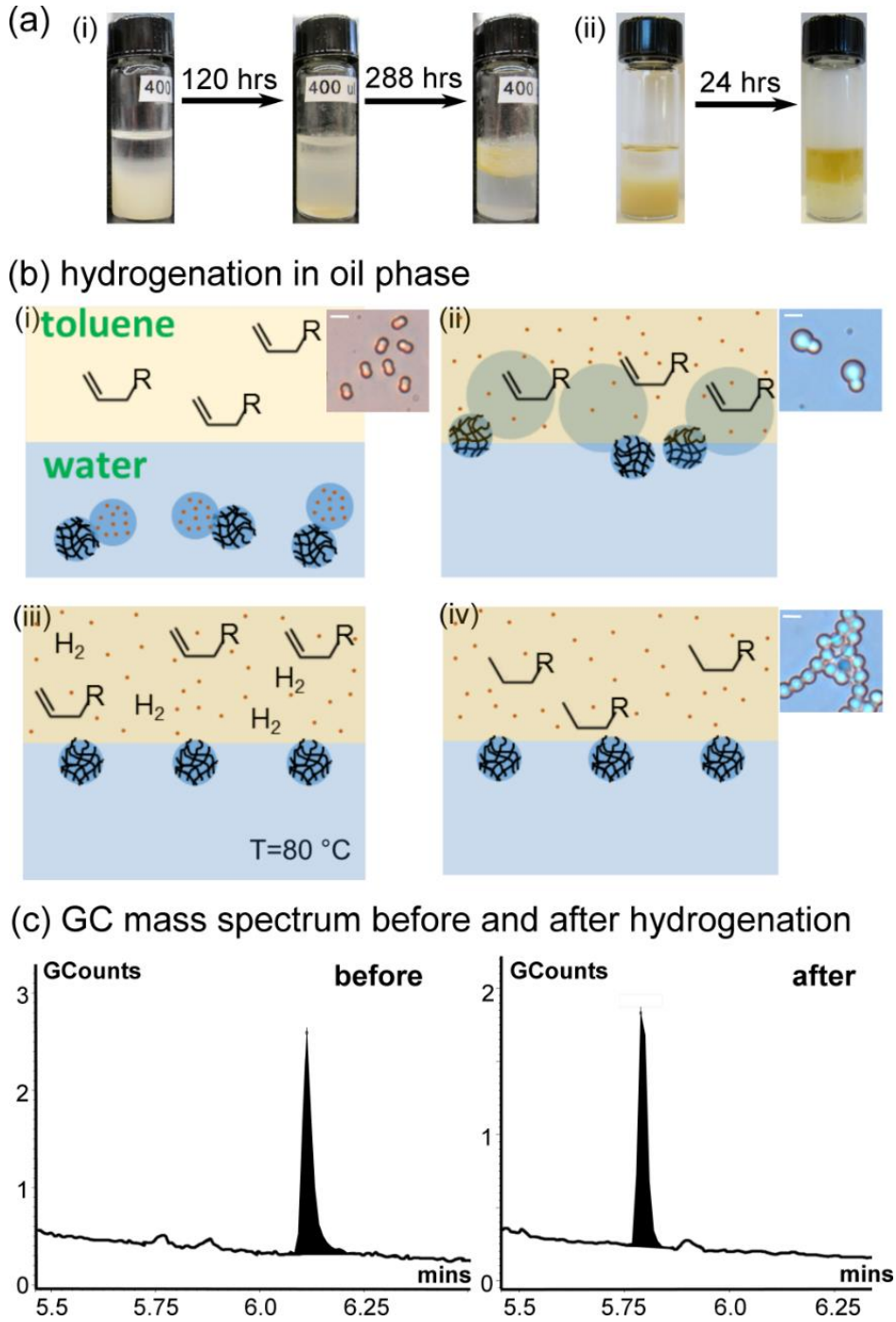

Figure 4.5 Oil-Phase delivery of the Wilkinson's catalyst and hydrogenation reaction. (a) $RhCl(PPh_3)_3$ encapsulated in dimers is transported from water (bottom phase) to oil (top phase). The glass vial was (i) put on a bench without disturbance or (ii) put on a rotator with a constant rotation speed of 50 rpm. (b) Schematics illustrate the oil-phase delivery and hydrogenation using dimers. Red dots represent the catalysts. The insets show corresponding microscopy images of the particles. Scale bar: 2 µm. (c) GC mass spectra of the substrate (styrene) and product (ethylbenzene) before and after the hydrogenation of styrene.

We further investigate the oil-phase delivery of organometallic salts which can catalyze the hydrogenation of olefins. Although two salts ($Pd(OAc)_2$ and $RhCl(PPh_3)_3$) have been encapsulated successfully, we primarily focus on the latter (i.e., the Wilkinson's catalyst) because it has higher solubility (10 wt%) in styrene. We inject dimer particles into the aqueous phase in a vial where oil is separated on the top. We then use two different methods to test the oil-phase delivery of catalysts: a static process where the vial sits still on a bench (similar to the dye release experiment, Figure 4.5a-i) and a dynamic process where the vial is put on a rotator and is subject to a constant rotation speed of 50 rpm (Figure 4.5a-ii). Clearly, rotation induces a mild degree of mixing, which significantly decreases the amount of time (10 times faster) for complete release of the catalysts. In fact, this release time can be further decreased by at least two orders of magnitude when we modify the surface property of the dimers, which will be shown later. The amount of Wilkinson's catalysts in the oil phase can be determined by the inductively coupled plasma optical emission spectroscopy. For 1 ml 1 wt% dimers, they deliver ~ 486 ppm catalysts in 2 ml toluene. This corresponds to ~ 12% encapsulation efficiency. Considering that many small polystyrene spheres are formed during the second stage of the dimer synthesis (because of the homogeneous nucleation effect), we believe that catalysts are also encapsulated in these small particles which are then separated from dimers during centrifugation.

After the catalysts are delivered into the oil phase, we perform the hydrogenation reaction for three different kinds of α-olefins, i.e., styrene as a model for aromatics, octene for linear hydrocarbons, and butyl acrylate for unsaturated esters. 40 µl of olefins is each dissolved in separated vials of 2 ml toluene where the Wilkinson catalysts have already been delivered through dimers (see experimental methods for details). The mixtures are then heated to 80 °C under 2 bar of hydrogen gas (Figure 4.5b). After one hour, we stop the reaction and take the oil phase for GC-

mass spectrometry. As shown in Figure 4.5c, we find that both styrene and octene reach 100% conversion to ethylbenzene and octane, respectively. For butyl acrylate, its conversion to butyl propionate is ~84.5%. Clearly, the high conversion rates prove that our dimer system is capable of performing oil-phase catalytic reactions by delivering the encapsulated catalysts from water to oil.

4.4.4 Dimer surface modification

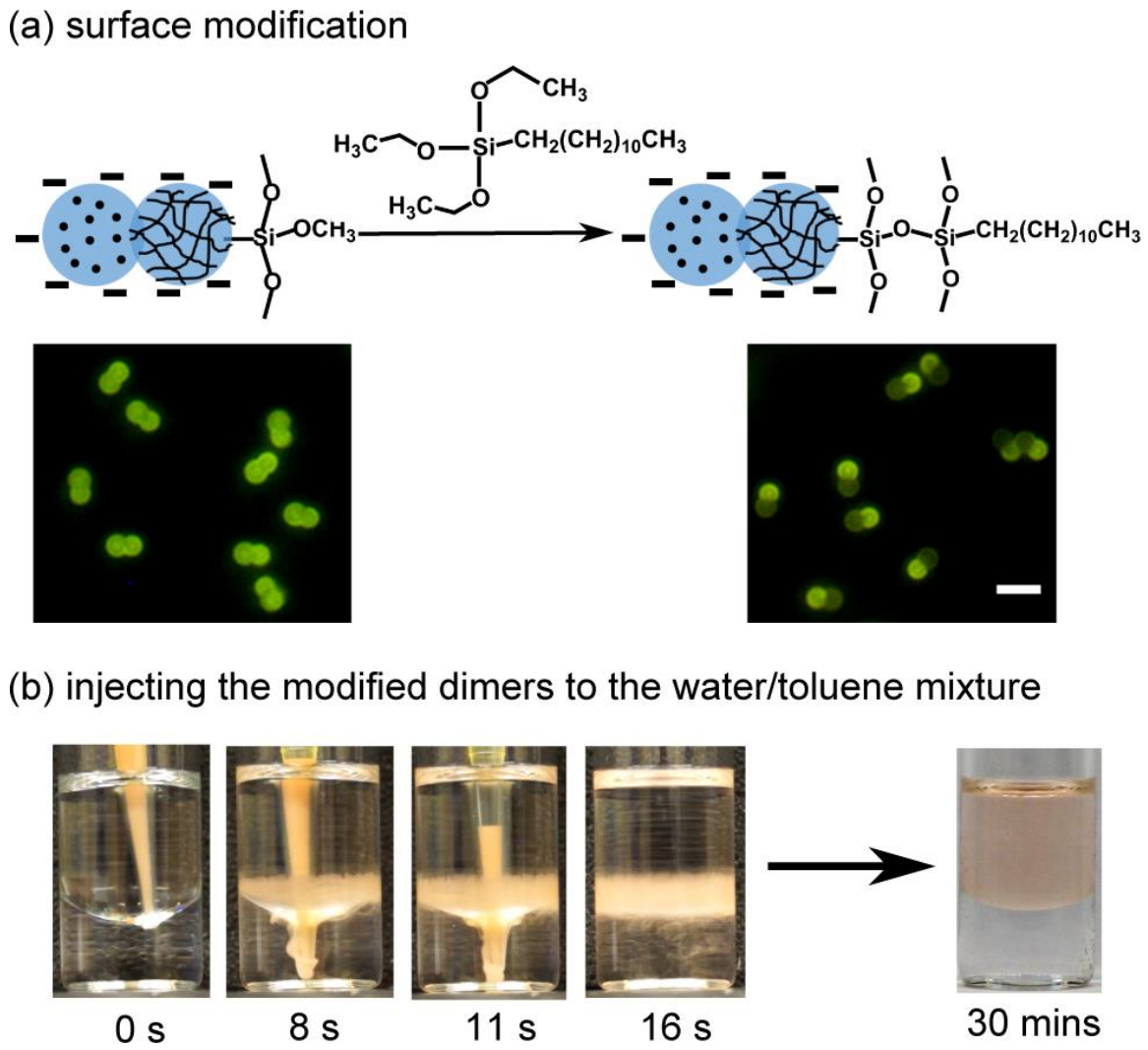

Figure 4.6 Adding amphiphilicity to polystyrene dimers to shorten the release time. (a) Selective attachment of n-dodecyltriethoxysilane on the crosslinked lobe renders the dimer amphiphilic. Fluorescent images show the absorption of Rhodamine 6G before and after surface modification. Scale bar is the same for both images: 5 µm. (b) Dye release from the amphiphilic dimers. The first four snapshots show that the amphiphilic dimers accumulate at the interface immediately after injection. All encapsulated dye release to the oil phase within 30 minutes.

We notice that, in our previous experiments, it takes at least several days for dimers to migrate towards the oil-water interface. The time depends on the diffusion of toluene through water phase towards the particles, which sediment at the bottom of the vial. Due to small solubility of toluene, its diffusivity D is ~ $9.1*10^{-6}$ cm^2/s in water. If the height of water phase H is ~1.5 cm, it will take $t \sim H^2 / D \sim$ 50 hours for toluene to diffuse through, which is consistent with our experimental observation. This time significantly delays the process for complete release of the encapsulated agents. Although we have shown that this process can be sped up by introducing agitation to mix toluene with water (Figure 4.5a-ii), a more efficient way is to modify the surface properties of the dimers, so that they are amphiphilic on surface property.

The bi-compartmental nature of dimers allows us to tune the interfacial hydrophobicity easily. As illustrated in Figure 4.6a, when making the crosslinked seeds, we purposely add a small amount of vinylsilane molecules, i.e., the 3-(trimethoxysily) propyl acrylate. This incorporation allows us to modify the surface properties of the crosslinked lobe after the encapsulation of active agents and dimer synthesis. For example, via the conventional sol-gel coupling reaction[47] we can attach n-dodecyltriethoxysilane molecules on the crosslinked lobe so that it becomes more hydrophobic. Since the non-crosslinked lobe remains hydrophilic because of the sulfonate functional groups (Figure 4.2a), the surface-modified dimers are amphiphilic. We further prove the amphiphilicity by absorbing positively charged fluorophores on dimers before and after the surface modification. As indicated by the images in Figure 4.6a, the modified dimers show a significant decrease in fluorescence intensity on the crosslinked lobe due to its hydrophobic surface. As Figure 4.6b shows, these amphiphilic dimers go to the oil-water interface immediately even when we inject the particle solution into the water phase. This also significantly reduces the amount of time for agent release, which takes place less than 30 minutes after the injection.

4.5 Conclusions

We develop a new type of bi-compartment and phase transfer vehicle for molecular catalysts based on colloidal dimers. The polymer in one lobe is crosslinked while the other one is not. Because of this structural anisotropy, we show that dimers can be surface active. Although they are initially dispersible in water, the dimers migrate to the oil-water interface upon contact with a trace amount of oil. This is because the uncrosslinked lobes can be swollen significantly by oil, rendering the dimers amphiphilic. By further encapsulating active species such as fluorescent dye and catalytic molecules in the uncrosslinked lobe selectively, we demonstrate that the dimers can be used as a delivery vehicle to transfer catalysts from water to oil. The successful release of catalysts is further confirmed by hydrogenation of unsaturated oil with high conversion efficiency. Moreover, the phase-transfer time can be significantly reduced when we combine both interfacial and structural anisotropy on the dimer vehicles. The advantages of this new type of colloidal emulsifier and delivery vehicle include: (1) the initial dispersity of particles in water ensures high particle stability and sufficient loading of catalysts or active molecules; (2) the particles do not release materials until they are located at the interface. The active molecules are fully protected until they reach the destination; (3) compared with isotropic particles, the surface properties of our delivery vehicles can be tuned anisotropically on two lobes. Our work demonstrates a new concept in making colloidal emulsifiers and phase-transfer vehicles. The bi-compartmental particles developed here could find applications for encapsulation and sequential release of small molecules across two different phases.

4.6 Acknowledgement

We thank Prof. Ryan M. Richards for his help in the hydrogenation experiments, Prof. James F. Ranville for ICP-OES characterization, and Prof. Edward A. Dempsey for using the GC-

mass spectrometry. Acknowledgment is also made to the Donors of the American Chemical Society Petroleum Research Fund (PRF No. 53638-DN110) for support of this research.

References

(1) McGorty, R.; Fung, J.; Kaz, D.; Manoharan, V. N. Colloidal Self-Assembly at an Interface. *Mater. Today* **2010**, *13*, 34–42.

(2) Sullivan, A. P.; Kilpatrick, P. K. The Effects of Inorganic Solid Particles on Water and Crude Oil Emulsion Stability. *Ind. Eng. Chem. Res.* **2002**, *41*, 3389–3404.

(3) Hunter, T. N.; Pugh, R. J.; Franks, G. V; Jameson, G. J. The Role of Particles in Stabilising Foams and Emulsions. *Adv. Colloid Interface Sci.* **2008**, *137*, 57–81.

(4) Gaaseidnes, K.; Turbeville, J. Separation of Oil and Water in Oil Spill Recovery Operations. *Pure Appl. Chem.* **1999**, *71*, 95–101.

(5) Hannisdal, A.; Ese, M.-H.; Hemmingsen, P. V.; Sjöblom, J. Particle-Stabilized Emulsions: Effect of Heavy Crude Oil Components Pre-Adsorbed onto Stabilizing Solids. *Colloids Surf., A* **2006**, *276*, 45–58.

(6) Al-Sahhaf, T.; Elsharkawy, a.; Fahim, M. Stability of Water-in-Crude Oil Emulsions: Effect of Oil Aromaticity, Resins to Asphaltene Ratio, and pH of Water. *Pet. Sci. Technol.* **2008**, *26*, 2009–2022.

(7) Kralova, I.; Sjöblom, J.; Øye, G.; Simon, S.; Grimes, B. a; Paso, K. Heavy Crude Oils/particle Stabilized Emulsions. *Adv. Colloid Interface Sci.* **2011**, *169*, 106–127.

(8) Drexler, S.; Faria, J.; Ruiz, M. P.; Harwell, J. H.; Resasco, D. E. Amphiphilic Nanohybrid Catalysts for Reactions at the Water/Oil Interface in Subsurface Reservoirs. *Energy Fuels* **2012**, *26*, 2231–2241.

(9) Aveyard, R.; Binks, B. P.; Clint, J. H. Emulsions Stabilised Solely by Colloidal Particles. *Adv. Colloid Interface Sci.* **2003**, *100-102*, 503–546.

(10) Zeng, C.; Bissig, H.; Dinsmore, a. D. Particles on Droplets: From Fundamental Physics to Novel Materials. *Solid State Commun.* **2006**, *139*, 547–556.

(11) Dickinson, E. Food Emulsions and Foams: Stabilization by Particles. *Curr. Opin. Colloid Interface Sci.* **2010**, *15*, 40–49.

(12) Binks, B. P. Particles as Surfactants—similarities and Differences. *Curr. Opin. Colloid Interface Sci.* **2002**, *7*, 21–41.

(13) Binks, B. P.; Fletcher, P. D. I. Particles Adsorbed at the Oil-Water Interface : A Theroretical Comparision between Spheres of Uniform Wettability and " Janus " Particles. *Langmuir* **2001**, *17*, 4708–4710.

(14) Adams, D. J.; Adams, S.; Melrose, J.; Weaver, A. C. Influence of Particle Surface Roughness on the Behaviour of Janus Particles at Interfaces. *Colloids Surf., A* **2008**, *317*, 360–365.

(15) Tanaka, T.; Okayama, M.; Minami, H.; Okubo, M. Dual Stimuli-Responsive "Mushroom-like" Janus Polymer Particles as Surfactants Particulate. *Langmuir* **2010**, *26*, 11732–11736.

(16) Jiang, S.; Chen, Q.; Tripathy, M.; Luijten, E.; Schweizer, K. S.; Granick, S. Janus Particle Synthesis and Assembly. *Adv. Mater.* **2010**, *22*, 1060–1071.

(17) Tu, F.; Lee, D. Shape-Changing and Amphiphilicity-Reversing Janus Particles with pH-Responsive Surfactant Properties. *J. Am. Chem. Soc.* **2014**, *136*, 9999–10006.

(18) Hong, L.; Cacciuto, A.; Luijten, E.; Granick, S. Clusters of Charged Janus Spheres. *Nano Lett.* **2006**, *6*, 2510–2514.

(19) Hong, L.; Cacciuto, A.; Luijten, E.; Granick, S. Clusters of Amphiphilic Colloidal Spheres. *Langmuir* **2008**, *24*, 621–625.

(20) Qiang, W.; Wang, Y.; He, P.; Xu, H.; Gu, H.; Shi, D. Synthesis of Asymmetric Inorganic/polymer Nanocomposite Particles via Localized Substrate Surface Modification and Miniemulsion Polymerization. *Langmuir* **2008**, *24*, 606–608.

(21) Israelachvili, J. N. *Intermolecular and Surface Forces Third Edition*; Academic Press, **2010**.

(22) Park, B. J.; Brugarolas, T.; Lee, D. Janus Particles at an Oil–water Interface. *Soft Matter* **2011**, *7*, 6413–6417.

(23) Park, B. J.; Lee, D. Equilibrium Orientation of Nonspherical Janus Particles at Fluid-Fluid Interfaces. *ACS Nano* **2012**, *6*, 782–790.

(24) Isa, L.; Samudrala, N.; Dufresne, E. R. Adsorption of Sub-Micron Amphiphilic Dumbbells to Fluid Interfaces. *Langmuir* **2014**, *30*, 5057–5063.

(25) De Folter, J. W. J.; Hutter, E. M.; Castillo, S. I. R.; Klop, K. E.; Philipse, A. P.; Kegel, W. K. Particle Shape Anisotropy in Pickering Emulsions: Cubes and Peanuts. *Langmuir* **2014**, *30*, 955–964.

(26) Yang, J.; Sargent, E. H.; Kelley, S. O.; Ying, J. Y. A General Phase-Transfer Protocol for Metal Ions and Its Application in Nanocrystal Synthesis. *Nat. Mater.* **2009**, *8*, 683–689.

(27) Li, D.; Zhao, B. Temperature-Induced Transport of Thermosensitive Hairy Hybrid Nanoparticles between Aqueous and Organic Phases. *Langmuir* **2007**, *23*, 2208–2217.

(28) Wu, Y.; Zhang, C.; Qu, X.; Liu, Z.; Yang, Z. Light-Triggered Reversible Phase Transfer of Composite Colloids. *Langmuir* **2010**, *26*, 9442–9448.

(29) Stocco, A.; Chanana, M.; Su, G.; Cernoch, P.; Binks, B. P.; Wang, D. Bidirectional Nanoparticle Crossing of Oil-Water Interfaces Induced by Different Stimuli: Insight into Phase Transfer. *Angew. Chem., Int. Ed.* **2012**, *51*, 9647–9651.

(30) Karanikas, J. M. Unconventional Resources : Cracking the Hydrocarbon Molecules In Situ. *J. Pet. Technol.* **2012**, 68–75.

(31) Judzis, A.; Felder, R.; Curry, D.; Seiller, B.; Pope, G. A.; Burnett, D.; Torp, T. A.; Neal, J.; Krohn, C.; Karanikas, J. M.; *et al.* The Five R & D Grand Challenges Plus One. *J. Pet. Technol.* **2011**, 34–35.

(32) Liu, S.; Bai, S. Q.; Zheng, Y.; Shah, K. W.; Han, M. Y. Composite Metal-Oxide Nanocatalysts. *ChemCatChem* **2012**, *4*, 1462–1484.

(33) Wang, S.; Ma, F.; Zhao, H.; Wu, N. Bulk Synthesis of Metal–Organic Hybrid Dimers and Their Propulsion under Electric Fields. *ACS Appl. Mater. Interfaces* **2014**, *6*, 4560–4569.

(34) Zhang, F.; Cao, L.; Yang, W. Preparation of Monodisperse and Anion-Charged Polystyrene Microspheres Stabilized with Polymerizable Sodium Styrene Sulfonate by Dispersion Polymerization. *Macromol. Chem. Phys.* **2010**, *211*, 744–751.

(35) Sheu, H. R.; El-Aasser, M. S.; Vanderhoff, J. W. Phase Separation in Polystyrene Latex Interpenetrating Polymer Networks. *J. Polym. Sci., Part A: Polym. Chem.* **1990**, *28*, 629–651.

(36) Kim, J.-W.; Larsen, R. J.; Weitz, D. A. Synthesis of Nonspherical Colloidal Particles with Anisotropic Properties. *J. Am. Chem. Soc.* **2006**, *128*, 14374–14377.

(37) Mock, E. B.; De Bruyn, H.; Hawkett, B. S.; Gilbert, R. G.; Zukoski, C. F. Synthesis of Anisotropic Nanoparticles by Seeded Emulsion Polymerization. *Langmuir* **2006**, *22*, 4037–4043.

(38) Kim, J.-W.; Lee, D.; Shum, H. C.; Weitz, D. A. Colloid Surfactants for Emulsion Stabilization. *Adv. Mater.* **2008**, *20*, 3239–3243.

(39) Park, J.-G.; Forster, J. D.; Dufresne, E. R. High-Yield Synthesis of Monodisperse Dumbbell-Shaped Polymer Nanoparticles. *J. Am. Chem. Soc.* **2010**, *132*, 5960–5961.

(40) Sherrington, D. C. Preparation, Structure and Morphology of Polymer Supports. *Chem. Commun.* **1998**, 2275–2286.

(41) Kim, J. W.; Larsen, R. J.; Weitz, D. a. Uniform Nonspherical Colloidal Particles with Tunable Shapes. *Adv. Mater.* **2007**, *19*, 2005.

(42) Sheu, H. R.; El-Aasser, M. S.; Vanderhoff, J. W. Uniform Nonspherical Latex Particles as Model Interpenetrating Polymer Networks. *J. Polym. Sci., Part A: Polym. Chem.* **1990**, *28*, 653–667.

(43) Qiang, W.; Wang, Y.; He, P.; Xu, H.; Gu, H.; Shi, D. Synthesis of Asymmetric Inorganic/polymer Nanocomposite Particles via Localized Substrate Surface Modification and Miniemulsion Polymerization. *Langmuir* **2008**, *24*, 606–608.

(44) Wang, Y.; Zhang, C.; Tang, C.; Li, J.; Shen, K.; Liu, J.; Qu, X.; Li, J.; Wang, Q.; Yang, Z. Emulsion Interfacial Synthesis of Asymmetric Janus Particles. *Macromolecules* **2011**, *44*, 3787–3794.

(45) Speight, J. G. *The Chemistry and Technology of Petroleum*; 5th ed.; CRC press: Boca Raton, FL, **2014**.

(46) Hyne, N. *Nontechnical Guide to Petroleum Geology, Exploration, Drilling, and Production*; 2nd ed.; PennWell Books: Tulsa, OK, **2001**.

(47) Plueddemann, E. P. *Silane Coupling Agents*; 2nd ed.; Springer: New York, **1991**.

CHAPTER 5

THE IMPACT OF SWELLING AGENT ON THE SYNTHESIS OF ANISOTROPIC PARTICLES AND THEIR APPLICATIONS

We investigate the effect of two non-polymerizable swelling agents on anisotropic particle synthesis and expand the capabilities of seeded emulsion polymerization to prepare anisotropic dumbbells with either interfacial or compositional anisotropies.

5.1 Introduction

Synthesis of anisotropic particles has been an active pursuit for the past decade.[1] Particles with either non-spherical shapes or non-uniform surface properties have shown unprecedented assembly structures and phase behavior driven by different kinds of directional interactions.[2,3] However, facile and scalable synthetic approaches that can produce anisotropic particles with high quality are still limited.[4–7] The seeded emulsion polymerization is one of the most promising strategy for making monodisperse colloidal dimers in high throughput.[7–13] This method is based on swelling crosslinked polymer spheres (CPS) with its own monomer such as styrene. Although the enthalpy of mixing is negative, the increase in elastic energy of the crosslinked polymer prevents the seed particles from swelling isotropically. Instead, the monomer is squeezed out of the seed and forms a second lobe, which can be solidified through an additional step of polymerization. Since this is a bulk synthesis in liquid phase, the output can be very high. In addition, the size of the second lobe can be easily tuned by controlling the amount of swelling monomer. Geometric anisotropy in terms of both size ratio and bond length between two lobes can be controlled precisely.[14,15]

However, the above swelling-polymerization method has a number of limitations. First, it can only be applied to certain types of monomers, which need to be compatible with the

crosslinked seeds (the most common one is polystyrene). Therefore, most dimers typically consist of polymers on both lobes.[16–20] Organic-inorganic hybrid dimers with compositional anisotropy have only been fabricated with limited size range or monodispersity.[21–23] Second, most work reported so far for creating interfacial anisotropy involves modifying the surface of the original lobe by adding functional monomers in CPS. For example, Kim *et. al*. added glycidyl methacrylate and showed that the epoxy groups can be reacted with poly(ethyleneimine) selectively on the original lobe.[10] Tang *et. al.* performed a more sophisticated study by first making polyacrylonitrile (PAN) hollow spheres and then using them as seeds to swell with styrene and divinylbenzene (DVB) mixture to make PAN-polystyrene dimers.[17] PAN can be further hydrolyzed and modified to attain more functionalities. Our previous work utilized silane chemistry to coat different types of metallic nanoparticles on the original lobe, making metal-organic hybrid particles in high quality.[14] There is, however, no concrete evidence showing the successful functionalization of the second lobe, which might be inherently related to the monomer swelling process. Although a functional monomer as the swelling agent would mostly form into the second lobe, it can still swell the original lobe slightly. Once polymerized, both lobes can contain the same functional polymer, hence reducing the degree of interfacial anisotropy.[7,10] Last but not least, as can be inferred from literature and the above examples, the surface modification based on the seeded emulsion polymerization typically involves multiple steps, which is both time consuming and hard to control.[14,23]

In this work, we explore the possibility to use non-polymerizable swelling agents such as toluene and tetraethyl orthosilicate (TEOS), and investigate their impacts on making dimers with combined geometric, interfacial, or compositional anisotropy. Both the simple solvent toluene and sol-gel precursor TEOS can swell CPS into dimers. Surprisingly, by quickly extracting the excess

toluene, we can obtain dimers with novel properties such as the asymmetric distribution in both interfacial charges and surface roughness. We also utilize the hydrolysis/condensation reaction to convert the TEOS lobes into silica, making polystyrene-silica hybrid particles with compositional anisotropy. These particles exhibit novel propelling behavior under a perpendicular applied AC electric field. Our method not only simplifies the procedure for making dimers but also can be potentially extended to other types of non-polymerizable swelling agents for expanding the existing catalogue of anisotropic particles.

5.2 Materials and Experimental Methods

The following sections first introduce the materials we used in this Chapter, and afterwards describe the detailed experimental procedures and characterization methods.

Materials

Styrene, divinylbenzene (DVB), sodium 4-vinylbenzenesulfonate, polyvinylpyrrolidone (PVP, M_w: ~40,000 and ~10,000), sodium dodecyl sulfate (SDS), 3-aminopropyltriethoxysilane (APS), potassium chloride (KCl), trisodium citrate, cetrimonium bromide (CTAB), ascorbic acid, N-Isopropylacrylamide (NIPAm), ethidium bromide-N, N' bisacrylamide, Pluronic F127, Rhodamine 6G, tert-butyl acrylate, trifluoroacetic acid, formic acid, tetraethyl orthosilicate, polyvinyl alcohol (PVA, M_w: ~13,000-23,000), and n-octylamine are purchased from Sigma-Aldrich. Toluene, and 3-(trimethoxysily) propyl acrylate (TMSPA) is purchased from TCI. The thermal initiator V65 is bought from Wako Chemicals. Hydrogen tetrachlororaurate (III) trihydrate ($HAuCl_4 \cdot 3H_2O$, 99.9+%), and potassium tetrachloroplatinate (II)(K_2PtCl_4, 99.9%) are bought from Alfa Aesar. All chemicals are used as received except that styrene, divinylbenzene and tert-butyl acrylate are purified to remove the inhibitors by aluminum oxide before usage.

Dimer formation by swelling with toluene

Spherical polystyrene (PS) seed particles are first prepared by dispersion polymerization in methanol and are cleaned four times via centrifugation (4000 rpm, 30 mins, IEC HT Centrifuge).[24] After that, a mixture of 4 ml 5 wt% PVP aqueous solution, 0.5 ml 2wt% SDS, 1 ml styrene, 0.02 g V65, varying amount of DVB, and 3-trimethoxysily propylacrylate are emulsified using ultrasonication (Branson digital sonifier 450). The emulsion is then used to swell 1 ml polystyrene seed particles (10 wt% in deionized water) for 24 hours. The swollen seeds are then polymerized and crosslinked in the reactor at 70°C for another 24 hours. Polystyrene dimers are formed from the crosslinked polystyrene seeds (CPS) via a second swelling stage. We use 0.7 ml toluene to swell 1 ml CPS (1 wt%) with 4 ml 5 wt% PVP, and 0.5 ml 2 wt% SDS for 3 hours at different temperatures. Once dimers are formed during swelling, we then remove the excess toluene via two different methods. The slower way is to evaporate toluene in an open vial overnight while the faster one is through centrifugation with ethanol. To stabilize the dimers, we add 5 ml Pluronic F127 (2 wt%) in the original PVP and SDS solution.

Functionalization of the second lobe with PNIPAm

We dissolve 0.1 g NIPAm and V65 (0.01 g/ml) in 0.7 ml toluene and emulsify them in 4ml 5 wt% PVP and 0.5ml 2 wt% SDS solution. The emulsion is then used to swell CPS for 3 hrs. Subsequent polymerization is then carried out at 70 ºC overnight.

pH responsive dimers

The procedures are similar to those for PNIPAm functionalization. We replace NIPAm with 50-100 µl methacrylic acid. After polymerization, centrifugation is performed four times at 2000 rpm for 20 mins each.

Synthesis of PS-SiO_2 hybrid particles

We emulsify 300 µl tetraethyl orthosilicate (TEOS) in 4 ml 5 wt% PVA solution and mix it with 1 ml CPS (2 wt%) solution. Within 30 minutes, the additional TEOS lobe appears on CPS. We then add 100 µl n-octylamine to catalyze the sol-gel reaction for hydrolysis and condensation of TEOS into silicon dioxide. After one hour, the reaction is stopped and particles are cleaned via centrifugation in a water/ethanol mixture for four times at 2000 rpm. To further grow a thin silica layer selectively on the silica lobe, we disperse 1 ml of PS-SiO_2 particle solution (~5 mg/ml) into 10 ml of ethanol/ water mixture (95/5 v/v) containing 200 µl NH4OH (30%) with ultra-sonication. A mixture of 1 ml TEOS and 1 ml ethanol was then added dropwise to the above solution under magnetic stirring at 20 °C with a rate of 1 mL/h.[25]

Synthesis of metallic nanoparticles

We follow previously reported methods to make CTAB[26] and citrate stabilized[27] gold nanoparticles, respectively. We also synthesize citrate[28] and PVP[29] functionalized Pt nanoparticles based on wet chemical methods.

Characterization

The size and morphology of all synthesized particles are characterized by scanning electron microscopy (JEOL JSM-7000F). Both bright-field and fluorescent images are taken by a color camera (Retiga 2000R) connected to an inverted microscope (Olympus IX71). Zeta sizer (Brookhaven 90Plus PALS) is used to measure the zeta potential of particles.

Electric-field induced propulsion

We inject 10 µl PS-silica dimer solution between two indium tin oxide (ITO) glass slides separated by a ~100 µm polyester spacer. Subsequently, we apply an AC electric field (Rigol DG 1022) and use a high speed camera (SILICON VIDEO monochrome SV642) to record the particle

motion at 30 frames/sec. We follow our previously reported methods to calculate the propulsion speed.[14]

5.3 Results and Discussion

We first employ toluene as a swelling agent, and systematically study different synthetic parameters that would affect the formation of polystyrene dimers with various interfacial anisotropies. We successfully incorporate pH responsiveness into our polystyrene dimer system as well. In the meantime, we also try an inorganic precursor-tetraethyl orthosilicate as the swelling agent and find polystyrene-silica hybrid particles can be easily obtained at the right synthetic conditions. We also observe quite rich and interesting phenomena of the hybrid particles under AC electric fields.

5.3.1 Using toluene as a swelling agent for making dimers

Formation mechanism

The conventional method for making dimers is based on swelling of the crosslinked polystyrene spheres (CPS) with styrene.[8–10] Because of its negative mixing enthalpy with polystyrene, styrene has a tendency to enter CPS and to swell them into larger spheres. However, the polymer matrix inside CPS is mostly crosslinked, there will be an increase in elastic energy if CPS expands uniformly. As a compromise, the excess amount of styrene will be expelled and form a second lobe attaching to the original CPS. This second lobe needs to be solidified by another step of polymerization. More details about this conventional styrene-swelling method has been discussed previously.[14]

Styrene is not the only swelling agent to make dimers. For example, other monomers such as methyl methacrylate and n-butyl acrylate have been used to synthesize heterogeneous PS-PMMA and PS-PBA dimers.[16,30] In principle, one does not need to use monomer either. As long

as the swelling agent has enough miscibility with polystyrene, it should be able to swell the CPS and form a second lobe. We have tried a series of simple liquid with different Hildebrand solubility parameters[31] including dodecane (δ=16.2), cyclohexane (δ=16.8), α-methylstyrene (δ=17.4), and toluene (δ=18.2). We find that when the liquid has a solubility parameter close to styrene (δ=19), it can swell CPS and form a second lobe. Linear hydrocarbons, such as decane and dodecane, cannot swell CPS at all due to their poor miscibility with styrene. Among the liquids mentioned above, toluene is most effective to swell a wide range of CPS with different crosslinking densities probably due to its very similar chemical structure to styrene. However, previous work does not use toluene to make dimers because the toluene lobe cannot be polymerized or solidified. In this work, we demonstrate our surprising results that one can conveniently make dimers with novel anisotropic properties simply by removing the excess toluene in a proper way.

Figure 5.1a shows the schematic route we have followed. We first crosslink pre-synthesized polystyrene spheres (with sulfonate groups) based on seeded emulsion polymerization.[14] The CPS are then swollen by toluene droplets which are pre-emulsified in water, forming a second lobe. Under the optical microscopy (Inset of Figure 5.1b), we observe dumbbell shape particles on which the second lobe is much larger than the original one and appears to be filled with toluene. In the final step, we remove the excess amount of toluene by centrifuging the dumbbells in ethanol. What surprises us is that the dumbbells do not change back to the spherical shape of CPS as the toluene lobe is removed completely and we obtain monodisperse polystyrene dimers (Figure 5.1b). Moreover, these new dimers look very differently from conventional dimers where both lobe surfaces are smooth. Instead, Figure 5.1b shows that one of the two lobes is consistently buckled, while the other surface is smooth, i.e., the rough-smooth dimers.

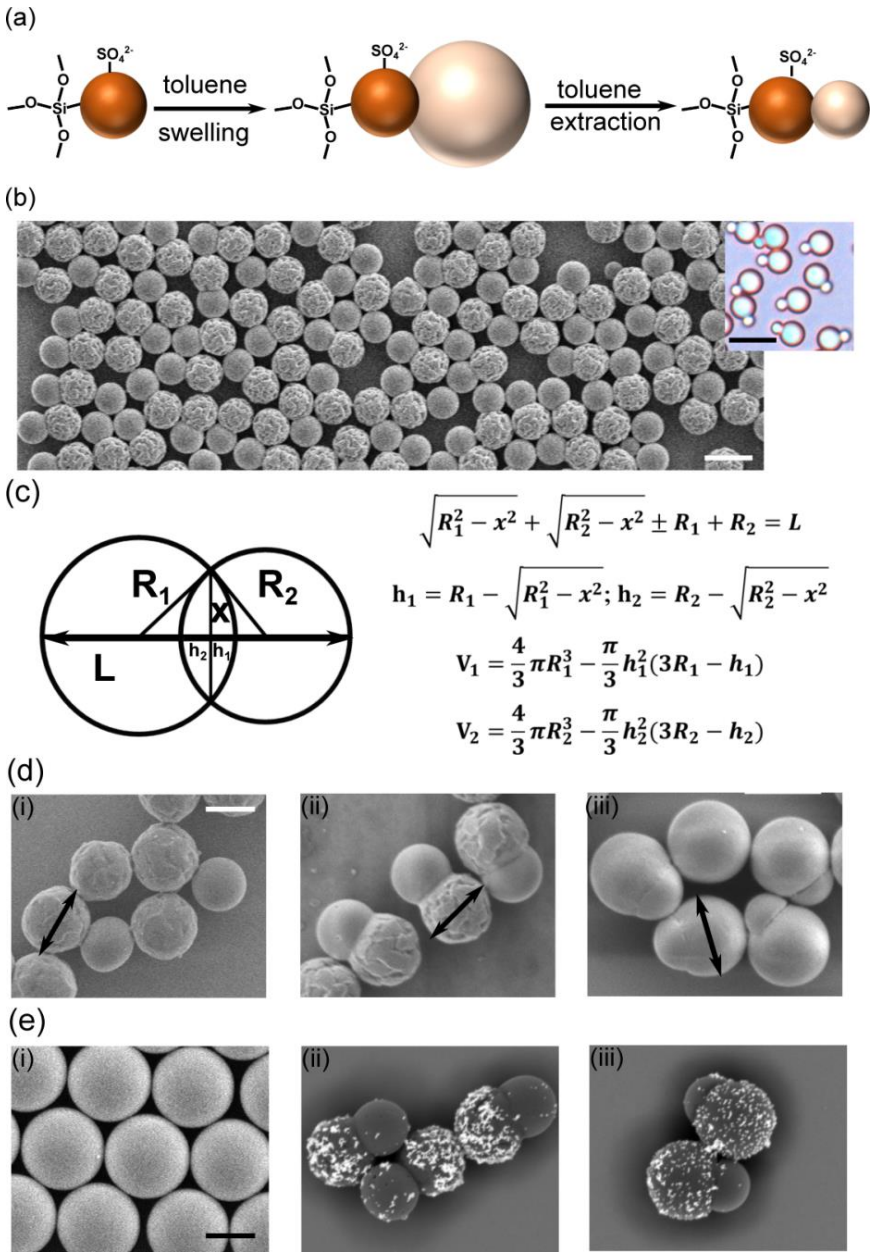

Figure 5.1 Dimers formed by swelling CPS with toluene. (a) The schematics for our toluene swelling-extraction method. (b) A large field view of monodisperse rough-smooth dimers after toluene extraction. Scale bar: 2 µm. Inset: An optical image of the CPS after swelling with toluene but before the extraction. Scale bar: 5 µm. (c) Equations showing the volume of two intersecting spheres. (d) Both swelling temperature and toluene removal speed affect the dimer morphology. Scale bar: 1 µm. (i) 20 °C and fast centrifugation; (ii) 70 °C and fast centrifugation; (iii) 70 °C and slow evaporation. (e) SEM of (i) the CPS of dimers shown in Figure 5.1d; citrate-gold nanoparticles coated (ii) APS modified corresponding dimers in Figure 5.1d-ii; (iii) APS modified corresponding dimers in Figure 5.1d-iii. Scale bar: 1 µm.

Equations in Figure 5.1c show the volume of dimers that are made of two intersecting spheres. Based on which, we can compare the volumes of the initial CPS particles and the resulting rough-smooth dimers. It is interesting to note that the dimer volume V_d is 10-20% less than the volume of CPS V_C, which indicates that some polymers are lost during the centrifugation step. This can be understood since toluene is a good solvent of uncrosslinked polystyrene. Potentially some polymer chains can be dissolved in toluene which are then removed by centrifugation. We also find that the speed of removing toluene can affect the particle morphologies significantly. In addition to using centrifugation to remove toluene quickly, we have also tried to evaporate toluene naturally in an open vial at room temperature overnight. This slow process can only produce tiny protrusions on CPS and the particle shape is close to a "snowman" (Figure 5.1d-iii), while its volume is equal to the volume of initial CPS. Interestingly, the particle surface is smooth too. Another interesting observation is that the dimer morphology depends on the swelling temperature too. For example, if we swell CPS with toluene at room temperature and directly wash (centrifuge) them with ethanol, we obtain a mixture of spheres and dimers (Figure 5.1d-i). It is clear that the contact between two lobes on those surviving dimers is very little, making them easily separated under weak sonication between sequential centrifugation steps. When the swelling temperature is increased to 70 °C, the bonding between two lobes is much stronger and no single sphere is observed (Figure 5.1d-ii). Hence the ideal conditions for making dimers with distinct lobes are at a high swelling temperature and with fast toluene removal speed.

One notable morphology of our dimers is that one lobe is rough but the other is smooth. It is therefore important to find out which lobe is from the original CPS sphere. Since silane molecules (TMSPA) are incorporated during the synthesis of the original CPS spheres (Figure 5.1e-i), we can detect their positions following our previously reported method.[14] In brief, we first

attach 3-aminopropyltriethoxysilane to the dimers based on silane chemistry, and then mix the modified particles with gold nanoparticles. Clearly, gold nanoparticles mainly coat on the rough lobe surface due to amine-metal complexation (Figure 5.1e-ii), which indicates the location of TMSPA. Therefore, the rough lobe comes from the original CPS sphere. As for the dimers generated with slow evaporation, the bigger lobe have majority of the gold nanoparticles. This is also consistent with our observation that the newly formed lobe is always smaller than the original lobe. Based on our findings, we propose that some of the uncrosslinked polymer chains (typically located in the core of CPS) migrate to the toluene-swollen lobe. When the toluene removal speed is slow, e.g., through natural evaporation, most of the chains can migrate back to CPS and only a small protrusion is left when toluene is evaporated completely. In contrast, when the toluene removal speed is fast through centrifugation, there is little time for the polymer chains in the second lobe to migrate back and a significant second lobe is preserved. On the CPS lobe, there is a mismatch in terms of elastic moduli between the shell which is primarily composed of crosslinked polystyrene and the core (less crosslinked). Therefore, a mechanical buckling develops during the fast removal of toluene, leaving rough surfaces on the original lobe. The similar mechanism has also been employed to create highly-folded microspheres.[32]

The effect of CPS composition

We also systematically study other parameters that can influence the morphologies of dimers for optimization. The first critical parameter is the CPS composition. Figure 5.2a shows the swelling stage of a series of CPS with different crosslinking densities (amount of DVB) and amounts of functional silane (trimethoxysilylpropylacrylate, TMSPA). Figure 5.2b represents the same particles after the removal of toluene through slow evaporation. Crosslinked polymer

network is necessary for creating elastic stress during swelling,[9] while the hydrophilic silane also promotes dewetting of toluene on CPS, maintaining itself a distinct lobe.[33]

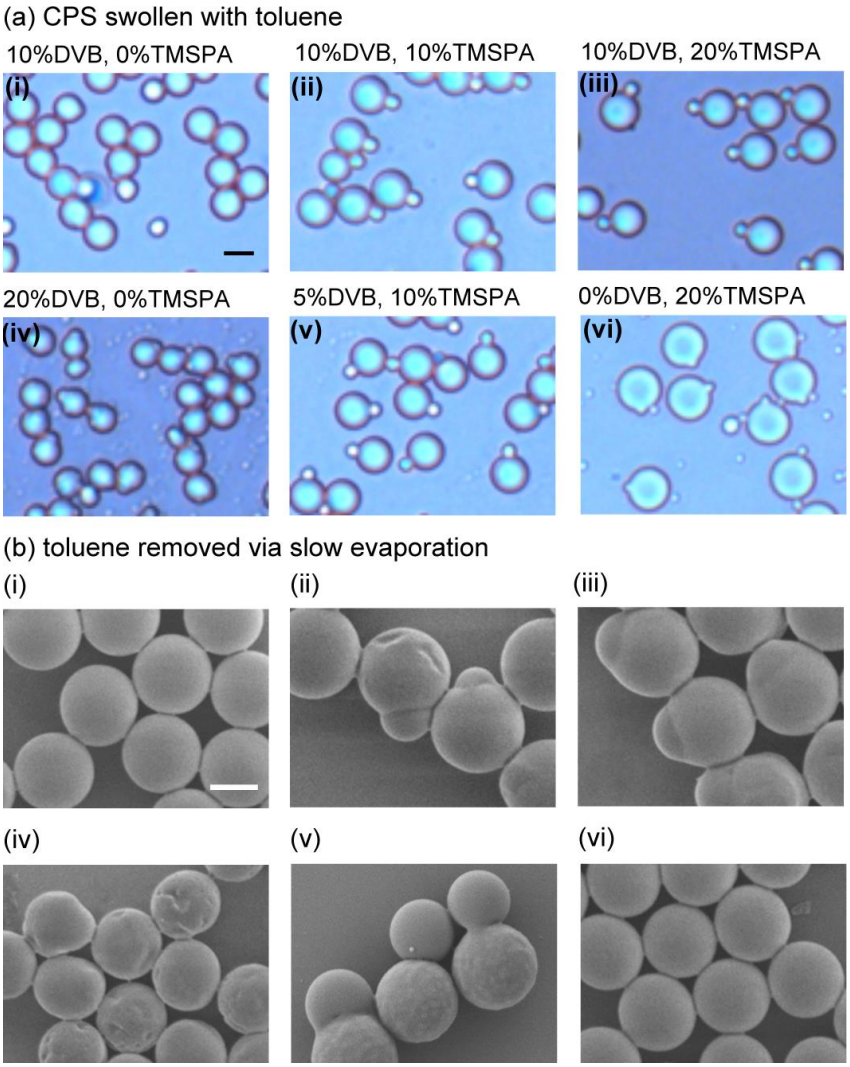

Figure 5.2 The impact of CPS compositions on dimer morphologies. (a) The morphology of CPS swollen by toluene depends on both the crosslinking density (%DVB) and the amount of TMSPA in CPS. Scale bar: 5 µm. (b) SEM images of the corresponding particles after slow evaporation of toluene. Scale bar: 1 µm.

The first row in Figure 5.2a lists all toluene swollen CPS that have 10 vol % crosslinking densities but with an increasing amount of silane. When there is no TMSPA in CPS, we do not observe the formation of second lobe (Figure 5.2a-i). When the CPS crosslinking density is increased to 20 vol% (Figure 5.2a-iv), a small lobe shows up during swelling but disappears after

toluene evaporation. Therefore, the incorporation of silane is essential to form dimers, which is different compared with the conventional (styrene) swelling method, where CPS without silane is still able to form "snowman" shaped particles.[14] However, CPS with silane only is not sufficient either. As shown in (Figure 5.2a-vi and 2b-vi), although a small protrusion shows up during swelling, it disappears after toluene evaporation. Overall, Figure 5.2 reveals that the optimal composition of CPS for making dimers with distinct lobes should have sufficient amounts of DVB (≥5 vol %) and TMSPA (≥10 vol %) to create a high elastic modulus for the polymer matrix inside of the CPS. However, too much DVB will lead to a highly crosslinked polymer matrix, which makes the migration of the un-crosslinked polymer chains to the second lobe difficult. Therefore, only relatively small second lobe can be obtained (particles ii and iii). So far, CPS in Figure 5.2a-v shows the best morphology of the dimer after toluene evaporation, which have 5 vol % DVB and 10 vol % TMSPA. For rest of the studies, we use CPS that has the same composition as the one in Figure 5.2a-v.

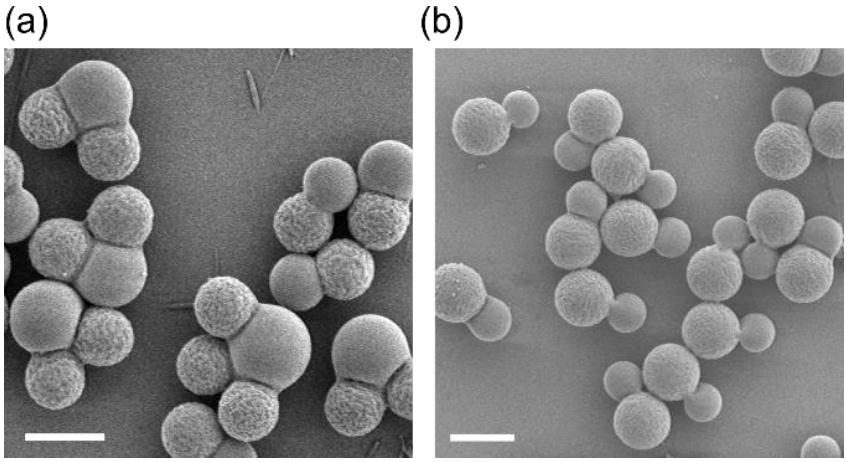

Figure 5.3 Stabilization of dimers. (a) Fusion between toluene lobes making triangular colloids but reducing the monodispersity of dimers. (b) The addition of pluronic F127 during swelling enhance particle stability dramatically. Scale bars: 2 µm.

When pure toluene is used as the swelling agent, the smooth second lobe can be easily fused to another under centrifugation, forming triangular particles shown in Figure 5.3a. To

enhance the stability, a triblock copolymer, Pluronic F127, can be added as a costabilizer in the toluene-in-water emulsion. During swelling, the hydrophobic segment - poly(propylene glycol) of Pluronic F127 embeds inside the toluene droplet, while the hydrophilic part - poly(ethylene glycol) lies at the interface as a steric stabilizer. This strategy was first developed for stabilizing polystyrene spheres[34] and it works well for our dimers too (Figure 5.3b).

Anisotropy in surface charge distribution

We are also interested in examining the surface charge distribution on our newly formed polystyrene dimers. Our original CPS particles are negatively charged because of the added sodium 4-styrene sulfonate monomer during the synthesis of seed polystyrene spheres, which is intended to enhance their stabilities in water. Therefore, we mix our dimers with a positively charged dye - Rhodamine 6G.[14]

As shown in Figure 5.4a, the much stronger fluorescence intensity on the larger lobe indicates that negative charges remain on the original lobe and they do not migrate to the second lobe. In contrast, we find that the dimers produced via the conventional method, i.e., swelling with styrene and subsequent polymerization, have symmetric charge distribution on both lobes. As shown in Figure 5.4b, this uniform charge distribution is consistently observed for both symmetric and asymmetric dimers regardless of the relative size ratio between two lobes. This indicates that the charged polymer chains (i.e., poly(sodium 4-styrenesulfonate)) in CPS do migrate to second lobe possibly during the polymerization stage. By avoiding the additional step of polymerization with toluene swelling, we make dimer particles with a new type of interfacial anisotropy, i.e., the anisotropy in surface charges. This is an exciting result because particles with asymmetric charge distributions are considered important building blocks for directed-assembly that can behave very differently from isotropic particles under external electric fields.

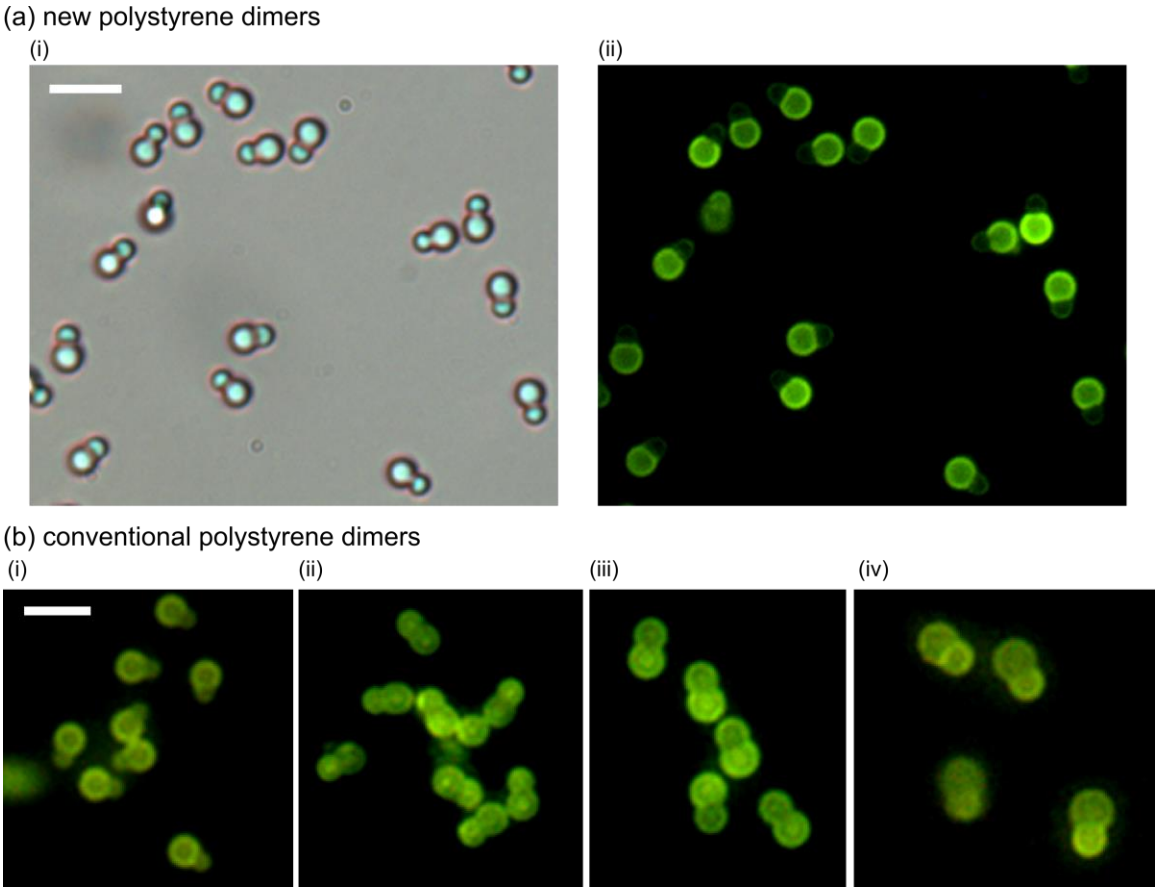

Figure 5.4 Surface charge characterization on dimers. (a) Bright-field and corresponding fluorescent images of new polystyrene dimers (based on the toluene-swelling-extraction method) coated with Rhodamine 6G; (b) Fluorescent images of conventional polystyrene dimers (based on the styrene-swelling-polymerization method) coated with Rhodamine 6G. Images i-iv are dimers with increasing size of the second lobe, from (i) smaller than the orginal lobe to (iv) larger than the original lobe. Scale bar: 5 μm.

This anisotropy in surface charge distribution can also be utilized for further surface modification based on charge-charge interactions. For example, we can coat positively charged CTAB-gold NPs[26] (zeta potential ξ ~64 mV) selectively on one lobe (the original lobe) of the dimers, as shown in Figure 5.5a-i. Following the same principle, other types of positively charged nanoparticles or molecules can also be selectively coated on one lobes. In comparison, the CTAB-gold NPs are coated uniformly on the conventional dimers with both symmetric and asymmetric geometries (Figure 5.5a-ii and iii). This demonstrates a significant advantage of new dimers

because our previous strategy to make anisotropic metal-organic hybrid dimers relied on surface modification of TMSPA on the conventional dimers,[14] which requires multiple and tedious steps.

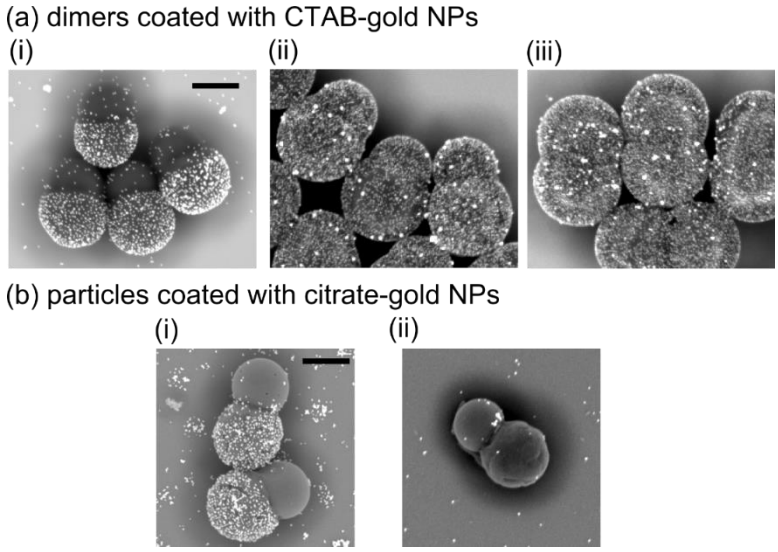

Figure 5.5 Metallic nanoparticles coating on dimers. (a) Coating of positively charged CTAB-gold NPs on (i) new dimers, (ii) conventional asymmetric dimers, and (iii) conventional symmetric dimers. (b) (i) New dimers with negatively charged citrate-gold NPs coating. (ii) Same particles in (i), but after one time centrifugation by water. Scale bar: 1 µm.

In fact, even negatively charged metallic nanoparticles (e.g., citrate-gold NPs[27] and citrate-Pt NPs[28]) can be selectively coated on the original lobe of our dimers (Figure 5.5b-i). The interaction between dimers and citrate-gold NPs is, however, weak. The metal nanoparticles coating can be easily washed off after one time centrifugation (Figure 5.5b-ii), different from the strong electrostatic interaction between CTAB-capped gold NPs and our dimers. To find out the origin of the weak interaction, we have tried to coat the citrate-gold NPs on both smooth and rough PS spheres synthesized with silane groups. Both can be coated with nanoparticles successfully. Thus we can rule out the possibility of the surface roughness on the original lobe might cause nanoparticle adsorption. And we mix PVP-capped platinum NPs[29] with our dimers and find that no nanoparticle coats on the dimers. We also find that no gold NPs can be coated on particles without silane functionalization. Therefore, we conclude that the weak interaction is from citrate

and silane functional groups, which helps the adsorption of citrate-gold nanoparticles on the original lobe selectively, since the second lobe does not have silane functional groups as proved by our previous method.[14] In summary, using toluene as a swelling agent can not only simplify the synthetic procedures for making dimers, but also simultaneously create asymmetric distribution of surface charges and other functional molecules on the same dimer. This approach also presents a significant advantage for further attaching metallic nanoparticles to make inorganic-organic hybrid dimers.

Functionalization of the second lobe

Although our dimers exhibit various unique properties compared with the conventional dimers, the tunability in terms of the size and surface functionality of the second lobe is still limited, which can be overcome by dissolving functional monomers in toluene and polymerizing the second lobe in presence of toluene. For example, by increasing the concentration of methyl methacrylate in toluene, the size of the second lobe gradually increases while the CPS lobe maintains its size. Monomers, such as styrene, methyl methacrylate, methyl acrylate, methacrylic acid (MAA), and tert-butyl acrylate can all be polymerized in the second lobe with the coexistence of toluene.

However, depending on the compatibility between monomer and toluene, the amount of the monomer can be polymerized into dimers varies. Figure 5.6a shows dimers incorporated with a small amount of hydrophilic monomer, n-isopropylacrylamide (NIPAm). The addition of NIPAm not only improves the stability of the particles, but also enhances the roughness of the original lobe (Figure 5.6a-i). Moreover, the surface charge contrast is still preserved (Figure 5.6a-iii). We suspect that the enhanced roughness arises from the mechanical buckling induced by the

polymerization of NIPAm. It most likely takes place at the particle-water interface due to its hydrophilic nature.

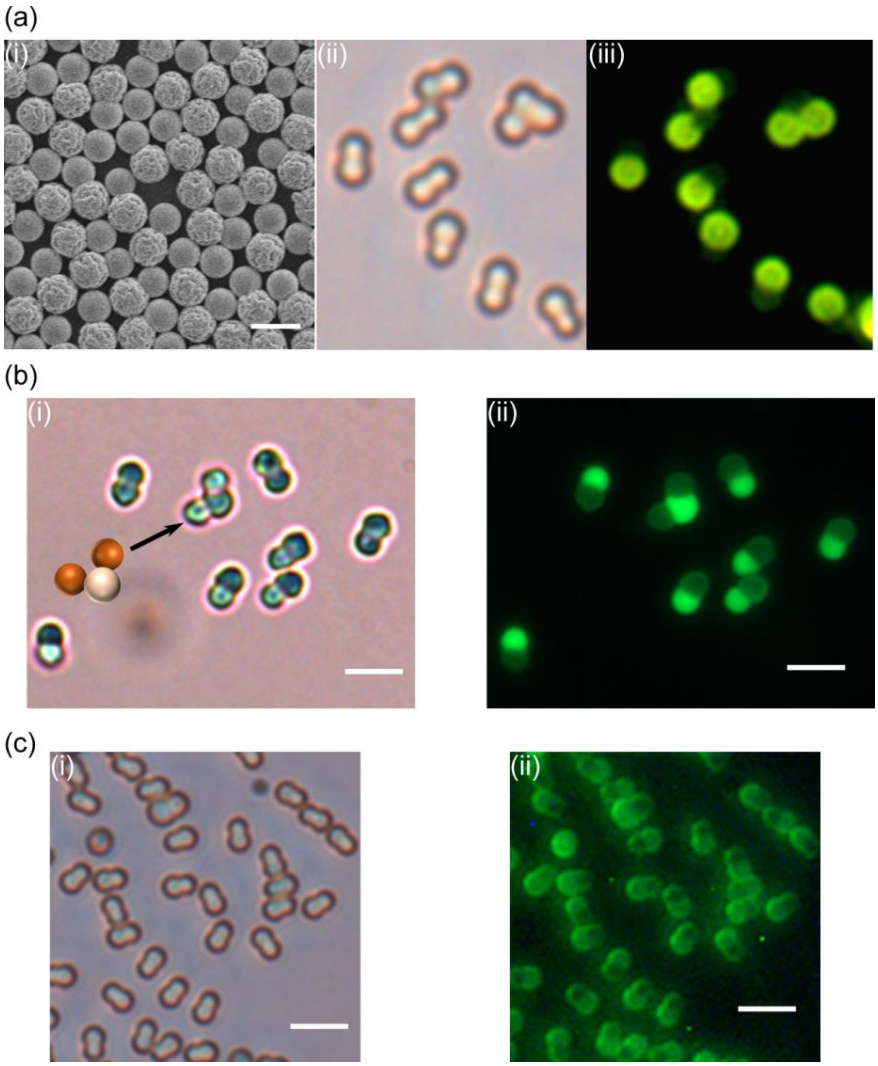

Figure 5.6 Functionalization of the second lobe. (a) (i) SEM; and (ii) bright-field optical image of dimers with NIPAm incorporated via toluene-swelling-polymerization-extraction method. (iii) Fluorescent image of the same dimers coated with Rhodamine 6G. Scale bar: 2 µm. (b) Dimers with both NIPAm and a fluorescent monomer (ethidium bromide-N, N' bisacrylamide) incorporated via toluene-swelling-polymerization-extraction method. (i) Optical image; and (ii) the corresponding fluorescent image. Scale bar: 5 µm. (c) Dimers with both NIPAm and ethidium bromide-N, N' bisacrylamide incorporated via styrene-swelling-polymerization method. (i) optical image; and (ii) corresponding florescent image. Scale bar: 5 µm.

Since the amount of NIPAm added is small, it is difficult to directly probe the location of PNIPAm based on the size change of dimers with temperature. Thus we use an indirect method.

Ethidium bromide-N, N' bisacrylamide is a fluorescent monomer that shares a similar chemical structure with NIPAm. We dissolve a trace amount of ethidium bromide-N, N' bisacrylamide in NIPAm and mix them with toluene. After polymerization, we find that most of the fluorescent monomers are located on the smaller second lobe (Figure 5.6b). For better clarity, we purposely show the area where a trimer is formed by the fusion of two dimers. As Figure 5.6b displays, the fused second lobe shows much brighter fluorescence. Accordingly, NIPAm should also be polymerized at the surface of the second lobe to increase hydrophilicity of the dimer, which also explains the improved stability of the particles. Considering the previously mentioned stabilization strategy - incorporation of Pluronic F127, we conclude that these two approaches employ the same concept to enhance the particle stability in aqueous phase: adding hydrophilic functional groups on the particle surface. If we substitute the swelling agent toluene for styrene, both the fluorescent intensity and its contrast between two lobes are much weaker (Figure 5.6c), indicating little incorporation of the hydrophilic PNIPAm on particles. The comparison between Figure 5.6b and Figure 5.6c reveals that our toluene swelling method can promote the surface modification of the second lobe with hydrophilic and potentially stimuli-responsive polymers, which is a significant challenge in dimer synthesis.

Encouraged by the above success, we have also tried to incorporate pH-responsive polymers such as poly(methacrylic acid) (PMAA) into dimers with the goal to create anisotropy in hydrophobicity. We first mix different amounts of monomer MAA with toluene, which is then used to swell CPS particles. Figure 5.7a shows the SEM images of dimers after polymerization. It is clear that the polymerization of MAA in toluene induces significant mechanical buckling and the second lobe morphology (i.e., collapsed shell) is dramatically different from conventional dimers when the MAA concentration is relatively high (≥10 vol%). This is reasonable since MAA

polymerization might only take place at the interface between toluene and water due to the hydrophilic nature of PMAA.

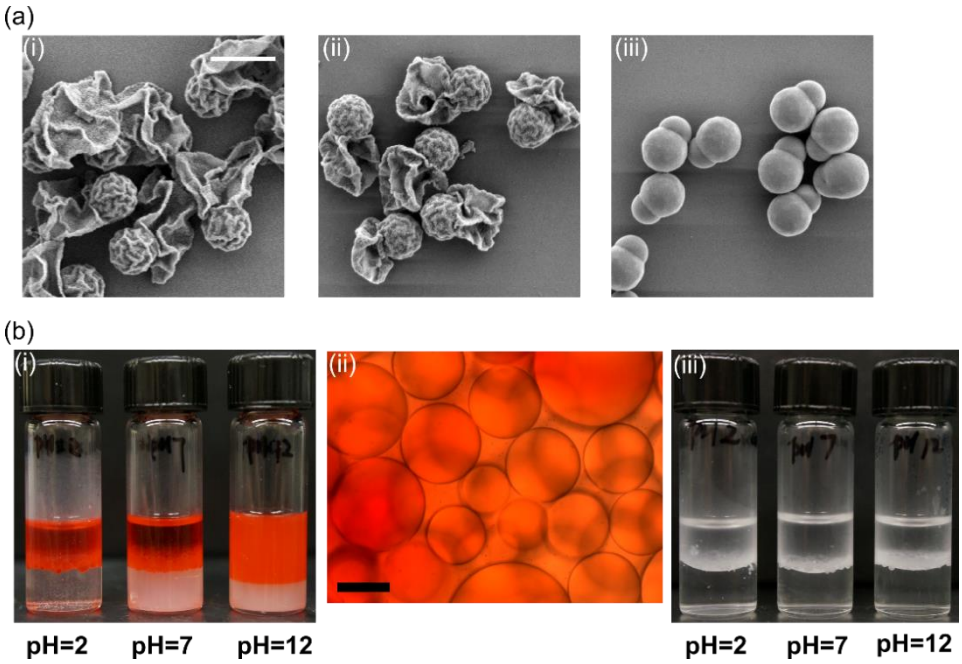

Figure 5.7 Synthesis and interfacial activity of pH responsive dimers. (a) Dimers with different amount MAA incorporated during swelling. (i) 12.5 vol% MAA in toluene; (ii) 10 vol% MAA in toluene; and (iii) 6.7 vol% MAA in toluene. Scale bar: 2 µm. (b) Interfacial activity of dimers at different pH. (i) PMAA (12.5 vol%) incorporated dimers in hexane-water mixture. The dye Oil Red O is added in the hexane phase. (ii) Optical image of oil-in-water emulsions formed at pH 12. Scale bar: 100 µm. (iii) Dimers without MAA incorporated in a hexane-water mixture.

The morphology difference between the original and second lobes in Figure 5.7a-i indicates the possible interfacial anisotropy where the buckled lobe consists of primarily PMAA and the original (spherical) lobe is made of polystyrene. To test this possibility, we add the particles in a mixture of (50:50 vol%) hexane (with dye Oil Red O) and water at different pH by vortexing them for 5 minutes. After that, the vials are kept still on bench. And the emulsion stabilities are examined. As shown in Figure 5.7b-i, at pH 2, the carboxylic groups in PMAA are protonated. Therefore, both lobes of the dimers are more hydrophobic and they prefer to leave the aqueous phase. At pH 7, some of the carboxyl groups on dimer surfaces are partially deprotonated since

the pKa of PMAA is ~5.5.[35] Therefore, more particles can be suspended in the water phase. But they cannot stabilize emulsions. After vortexing, oil and water are phase-separated. At pH 12, essentially all carboxylic groups are deprotonated and the PMAA lobes are hydrophilic. The contrast in hydrophobicity between the polystyrene and PMAA lobes becomes significant enough so that oil-in-water emulsions (Figure 5.7b-ii) can be stabilized over a period of at least one month. In comparison, the dimers without PMAA incorporated in the second lobe do not show any pH responsiveness and cannot stabilize emulsions either.

5.3.2 Synthesis of polystyrene-silica hybrid particles

Inspired by our work using toluene as the swelling agent, we have also tried another type of swelling agent, the tetraethyl orthosilicate (TEOS), with the aim to make hybrid particles composed of polystyrene and silica. We choose TEOS because of its compatibility with styrene and it is a commonly used precursor for silica synthesis via sol-gel reactions.[36,37] As shown schematically in Figure 5.8a, we first prepare emulsions of TEOS in polyvinyl alcohol solution, which are then used to swell CPS. The TEOS lobe shows up shortly after swelling. After swelling for thirty minutes, we add an organic base (octylamine) to initiate and catalyze the sol-gel reaction of TEOS, which eventually converts into solid silica via hydrolysis and condensation. We have tried several different types of base including ammonium hydroxide, triethylamine, and octylamine. We find that both the property and amount of base are vital. A hydrophilic base such as ammonia hydroxide typically leads to dissolution of the TEOS lobe in water. Therefore, a relatively weak organic base such as octylamine, is necessary so that the TEOS condensation can take place at the TEOS/water interface. High amount of base or base with high strength (triethylamine) causes particle aggregation due to fast TEOS hydrolysis. Meanwhile, insufficient

amount of base leads to incomplete hollow silica shells, which are fragile and cannot survive during the separation (e.g., centrifugation and sonication) stage.

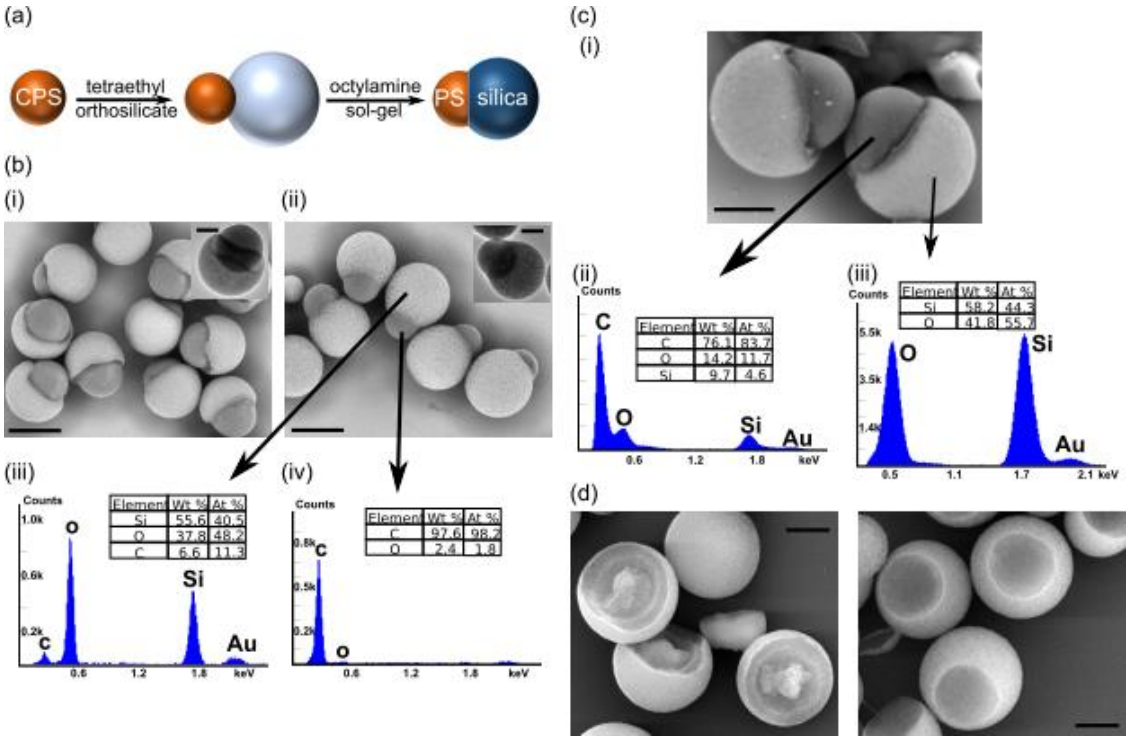

Figure 5.8 PS-silica dimer synthesis and characterization. (a) Schematic of the synthetic route for making PS-silica hybrid particles. (b) Large field scale of hybrid particles. Particles with (i) acorn and (ii) dumbbell shapes. Scale bar: 2 µm. Insets are corresponding TEM images. Scale bar: 1 µm. EDX analysis of (iii) silica and (iv) PS lobes. (c) SEM of the hybrid particles (b-i) with additional growth of thin silica film. Scale bar: 1 µm. EDX analysis of the (ii) PS and (iii) silica lobes. (d) SEM of the remaining silica lobes after annealing at 200 ºC. Scale bar: 1 µm.

Under the appropriate conditions (see experimental for details), PS-silica hybrid particles with different shapes such as acorn and dumbbell can be formed (Figure 5.8b). The energy-dispersive X-ray spectroscopy (EDX) in Figure 5.8b-iii further confirms that the brighter and porous compartment is rich in both silicon and oxygen signals (the signal of gold comes from the sputtering for SEM sample preparation and has been subtracted as background in elemental analysis). In contrast, the darker part is primarily polystyrene (the oxygen signal might come from sulfonate groups added during the synthesis of polystyrene seeds). The TEM images (insets in Figure 5.8b-i, ii) also show that the silica part is brighter than polystyrene, which is opposite to

previous reports.[38] This could be attributed to two reasons: (1) the silica lobe is porous and (2) the polystyrene lobe is crosslinked. In fact, the distinct polystyrene and silica compartments can also be clearly observed in bright-field optical microscopy. Shown in Figure 5.10b or Figure 5.12b, the silica lobe is much more transparent than the polystyrene lobe because its refractive index (1.45) is closer to water (1.38). We also note that the silica lobe shows a high percentage of carbon (~11.3 at%). It is possible that some polystyrene chains have migrated from CPS to the silica lobe. In addition, considering the amount of octylamine (C/Si~3.6 in mole) added, we also suspect that some residual organic base are trapped in the amorphous silica pores during sol-gel reaction. We also notice that it is crucial to minimize the swelling time of TEOS, which helps create an asymmetric distribution of silica. When the swelling time is three hours, the silicon signal on the polystyrene lobe can be as high as 24 at%.

To further enhance the compositional anisotropy, we have also tried to grow an additional thin layer of silica on hybrid dimers. We use the particles shown in Figure 5.8b-i as seeds and ammonium hydroxide as the catalyst. The transformation of particle morphology is noticeable since the silica lobe becomes less porous (Figure 5.8c-i). Moreover, the carbon signal on the silica lobe disappears (Figure 5.8c-iii); while the silicon signal on the PS compartment is below 5 at% (Figure 5.8c-ii). We also anneal the hybrid particles (Figure 5.8b) at 200 °C to remove the polystyrene compartment. Under SEM images (Figure 5.8d), the remaining silica lobes are in the form of dimpled spheres, which are consistent with the TEM images shown in Figure 5.8b. Therefore our method can make not only hybrid PS-silica particles but also dimpled silica particles which are important building blocks in the study of “lock and key” interactions.[2]

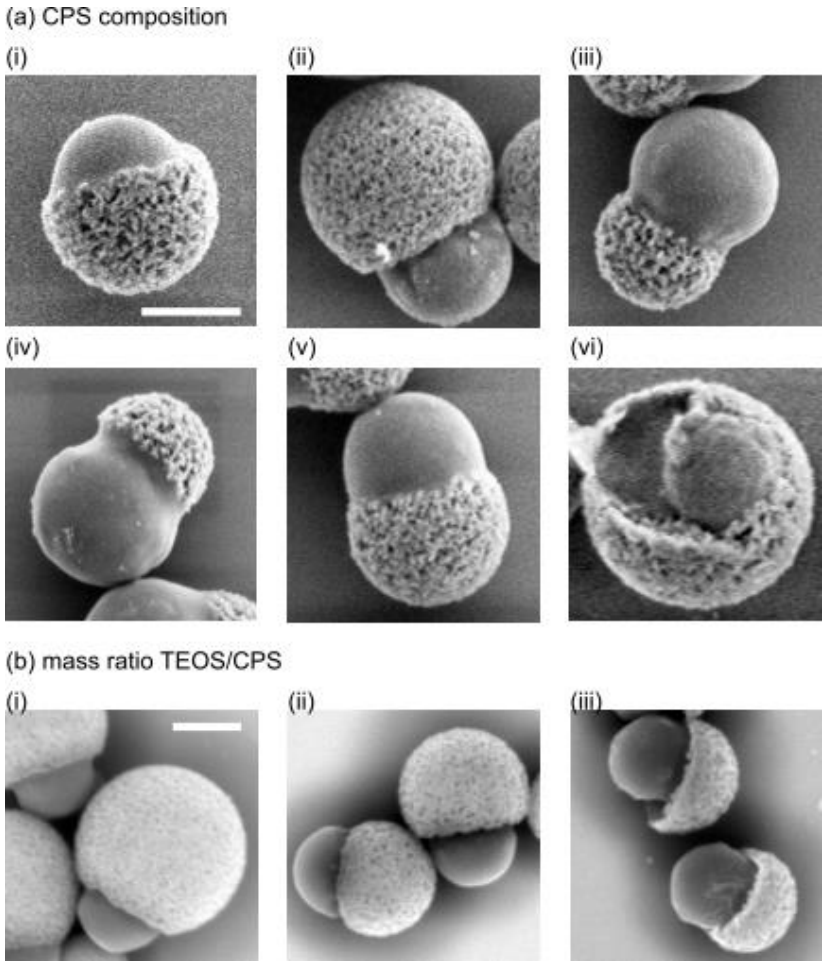

Figure 5.9 Morphology study of PS-silica dimers. (a) The impact of CPS composition on the formation of PS-silica hybrid dimers. (i) – (iv) CPS with increasing DVB concentration (5, 10, 15, and 18 vol%); CPS incorporated with (v) 10 vol% DVB and 10 vol% MMA; and (vi) 10 vol% DVB and 10 vol% MAA. Scale bar is the same for all images: 1 µm. (b) The impact of TEOS/CPS mass ratio (CPS are synthesized with 10 vol% DVB): (i) 28:1, (ii) 14:1, and (iii) 7:1. Scale bar is the same for all images: 1 µm.

The morphology of PS-silica particles can be tuned by controlling either the CPS composition or the relative amount of TEOS to CPS. Figure 5.9a (i-iv) show the impact of increasing the crosslinking density of CPS from 5 to 18 vol%. Clearly, a higher crosslinking density yields a larger elastic modulus in CPS and creates more distinct lobes (from acorn to dumbbell). The surface hydrophilicity of CPS is important, too. Because it determines the wettability of TEOS on CPS. For example, mixing TEOS with CPS that having a hydrophobic

monomer methyl methacrylate (MMA) incorporated yields distinct lobes of silica and polystyrene (Figure 5.9a-v) since the hydrolyzed TEOS wets poorly on hydrophobic surfaces.[33] In comparison, when we add a hydrophilic monomer methacrylic acid (MAA) into CPS synthesis, the silica shell almost encapsulates the polystyrene lobe (Figure 5.9a-vi). We have also varied the relative amount of TEOS to CPS. As shown in Figure 5.9b, higher TEOS/CPS mass ratio leads to a larger silica lobe. We note that the absolute amount of TEOS used for swelling should be kept relatively high (300 µl), since it also diffuses into water during hydrolysis. Therefore, by adjusting the CPS composition and TEOS/CPS mass ratio, our seeded swelling-condensation synthetic route allows convenient control for both the morphology and size ratio between polystyrene and silica compartments.

5.3.3 Propulsion and assembly of PS-silica hybrid particles under AC electric fields

The synthesized PS-silica particles possess combined geometric and compositional anisotropy. They are excellent model systems to study both the propulsion and assembly of asymmetric particles under electric fields. We use the same experimental setup as we have described in Chapter 2. A thin film (~100 µm) of particle suspension is sandwiched between two ITO glasses, where an AC bias is applied. Under sufficient field strength (>5 V), we find that the particles propel vigorously on substrate (Figure 5.10d). We emphasize that the observed propulsion is different from conventional electrophoresis and dielectrophoresis, where the electric field usually dictates particles' trajectories either along the field line (electrophoresis) or toward the field gradient (dielectrophoresis). Our asymmetric particles, influenced by a uniform AC electric field, move in a direction perpendicular to the applied field. Such a feature allows them to potentially perform other intelligent tasks (e.g., sensing and cargo delivery) independently. As shown in Figure 5.10a, the propulsion velocity is proportional to the square of the applied field

strength in low frequency (500 Hz) regardless of the particle morphology. Such a relationship is a characteristic of the electrohydrodynamic-driven propulsion, as we have discovered in Chapter 2 for metal-organic hybrid dimers. When the particles are close to the conducting substrate, the induced dipole distorts the vertically applied electric field and creates a tangential field, which acts on the induced charges near the substrate and drives solvent flow. Because both the amount of induced charges q and the tangential electric field E_t are proportional to applied electric field E_0, the particle velocity $U \propto qE_t$ is proportional to E_0^2.[39]

The frequency dependence of the particle propulsion is more interesting. We find that in the low frequency regime (500-5000 Hz), particles always move with the PS lobe facing forward (Figure 5.10b). However, at higher frequencies (5k-500k Hz), the motion direction is reversed, i.e., the silica lobe orients forward. We hypothesize that the propulsion of the PS-silica dimers is caused by an unbalanced electrohydrodynamic (EHD) flow surrounding the particles. The fact that PS spheres, SiO_2 spheres, and symmetric PS or SiO_2 dimers do not propel under the same experimental conditions is consistent with our hypothesis since the EHD flow surrounding those particles are expected to be symmetric. Moreover, the propulsion velocity scales with the field strength squared and decreases with increasing frequency. Both are characteristic features of the EHD flow, based on previous experiments and modeling for spheres.[40] To probe the EHD flow surrounding our dimers, we purposely immobilize them on the substrate and use small fluorescent polystyrene spheres (~500 nm) as tracers. At low frequencies, we find that tracers are attracted towards the polystyrene lobe and ejected away from the silica lobe. As a result, they are surrounded by a concentration and a depletion zone, respectively (Figure 5.10c-i). The similar phenomenon is observed for acorn-shape particles too. Based on which, the EHD flow profile can be depicted in Figure 5.10c-ii.

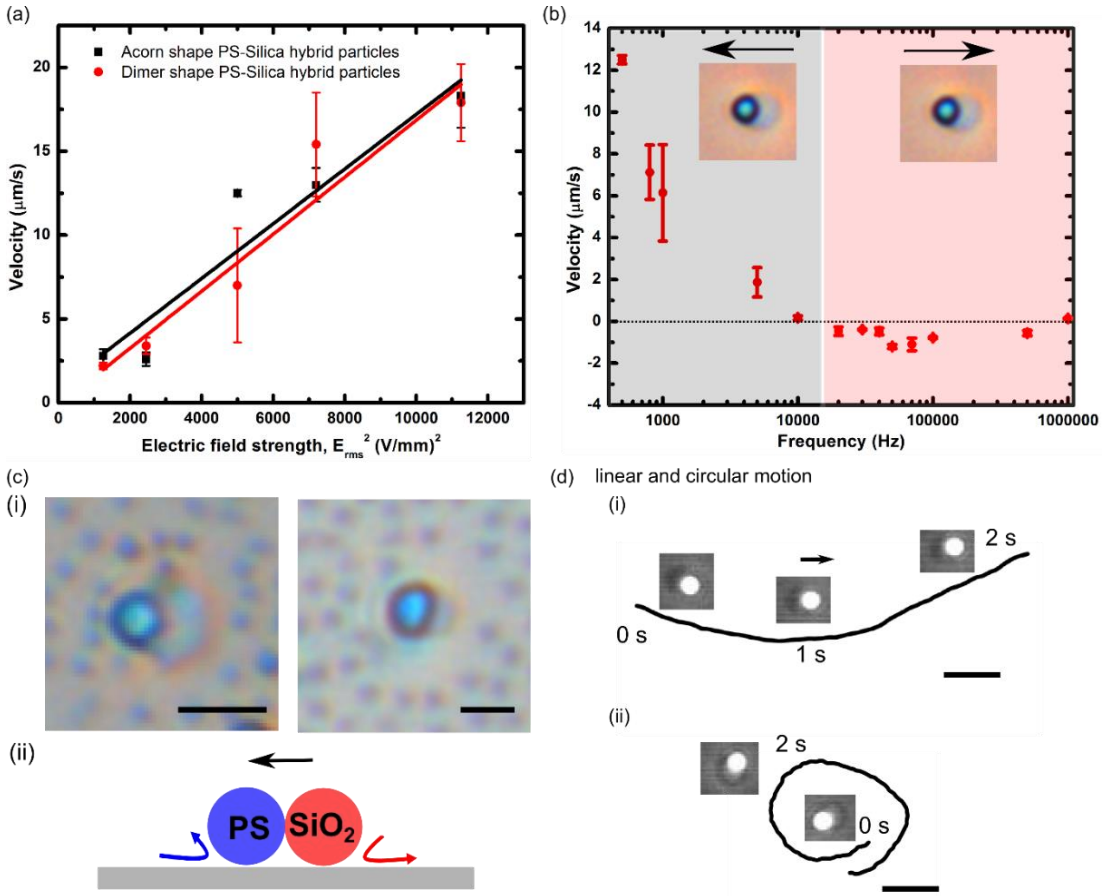

Figure 5.10 Propulsion of PS-silica dimers under AC electric field. (a) Velocity of the PS-silica hybrid particles with different shapes at different field strengths (500 Hz, in DI water). (b) Frequency dependence of the particle velocity (10 V). In low frequency, the hybrid particles move with its PS lobe facing forward; while at high frequency, the particles reverse its moving direction. (c) (i) The distribution of small tracer particles surrounding an immobilized PS-silica dimer and a PS-silica acorn shape particle at low frequency. Scale bar: 3 μm. (ii) Schemes indicating the surrounding electrohydrodynamic (EHD) flow. The black arrow indicates the dimer propulsion direction. (d) Linear and circular trajectories of PS-silica dimer (12 V and 500 Hz). Insets are the phase contrast optical images of the particles at different time. Scale bar: 5 μm.

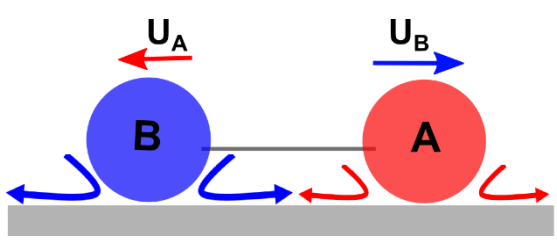

Figure 5.11 A simple dumbbell model to explain the propulsion of polystyrene-silica dimers. The red sphere A represents silica, the blue sphere B represents polystyrene, and the positive moving direction is towards right.

We attempt to explain the complex propulsion phenomenon for our synthesized dimers semi-quantitatively by using a dumbbell model shown in Figure 5.11. We consider two spheres of types A and B, which are connected by a long but negligibly thin rod. If two spheres are not connected, under an AC electric field each will move due to convective entrainment in the EHD flow initiated from the other. For example, the repulsive (attractive) EHD flow surrounding sphere B will push (draw) sphere A away from (towards) it with a lateral velocity U_B. Similarly, sphere B experiences an EHD flow initiated from sphere A and acquires a lateral velocity U_A. Both U_A and U_B depend sensitively on the sphere diameter, zeta potential, material property, as well as field conditions (strength and frequency). When two spheres are connected, however, equal and opposite forces $\pm F$ on two ends of the rod keep them from moving relative to each other, so that the rigid dumbbell moves with a velocity U.

$$U = U_B - F / 6\pi\mu R_A = U_A + F / 6\pi\mu R_B \tag{5.1}$$

where R_A and R_B are radii of sphere A and B, respectively and μ is the solvent viscosity. Solving F from Eq. (5.1), we obtain

$$U = \left(U_B R_A + U_A R_B\right) / (R_A + R_B) \tag{5.2}$$

Although the dumbbell shown in Fig. 11 is different from our synthesized dimers, their propulsion behavior should be perturbatively similar. This simple model allows us to explain the propulsion direction of PS-silica dimers based on the EHD flow surrounding individual lobes. For example, based on the flow tracing results in Figure 5.10c, $U_A < 0$ for polystyrene and $U_B < 0$ for silica. Therefore, the overall propulsion direction should be towards the left following Eq. (5.2), i.e., the silica lobe pushes the polystyrene lobe. This propulsion direction is consistent with our experimental observation. At higher frequencies, the propulsion direction is reversed. This can be

explained by the change of either magnitude or sign of U_A and U_B as frequency changes. Although quantitative validation of Eq. (5.2) for our synthesized dimers needs further experimental investigation, it has been tested and proved on a series of other types of dimers performed by one of our lab members F. Ma.[41]

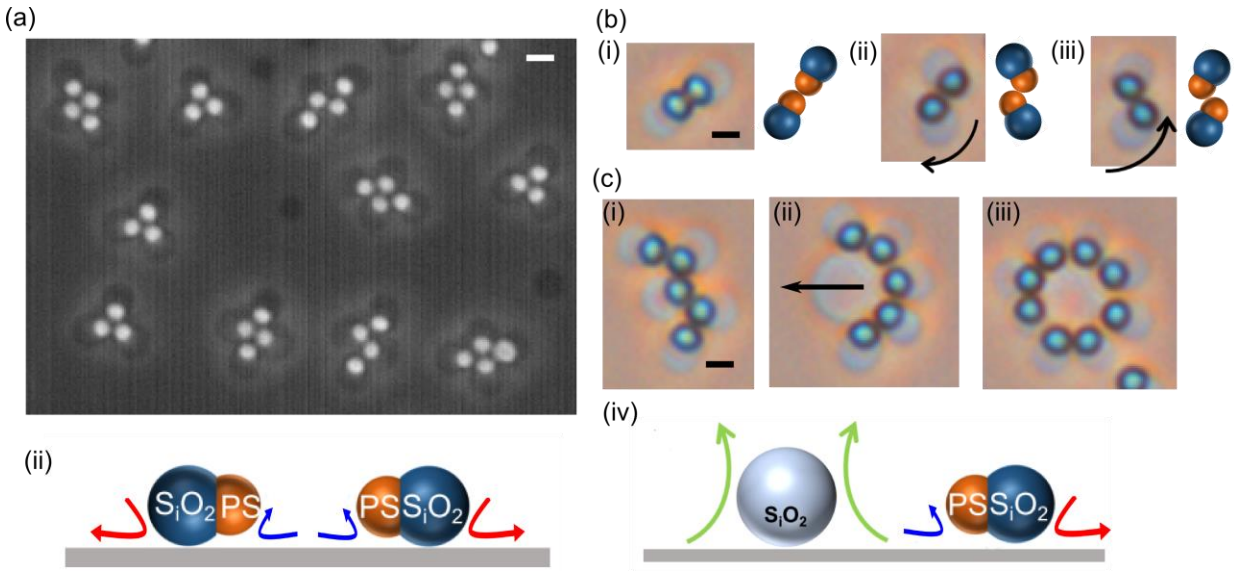

Figure 5.12 Assembly of PS-silica hybrid dimers under low frequency. Images (a), (b), and (c) are the structures formed at low frequencies (8V and 800 Hz). (a) (i) A phase contrast optical image of the clusters formed by three or four PS-silica hybrid dimers. The brighter lobe is polystyrene and the darker one is silica. (ii) The schematic illustrating the unbalanced flow surrounding two dimers, which leads to the aggregation of dimers. (b) Bright-field images of the symmetric and chiral doublets of dimers. The more transparent lobe is silica. Scale bar is same for all images: 2μm. (c) Large clusters formed by multiple dimers. (i) A short staggered chain. (ii) A large silica sphere is pushed by several surrounding dimers. (iii) A static cluster where a large silica sphere was encircled uniformly by dimers. (iv) A schematic reveals the flows around silica and hybrid particles.

The unbalanced electrohydrodynamic flow surrounding asymmetric PS-silica dimers can also induce assembly of multiple particles into novel structures. Figure 5.12a-i shows symmetric clusters formed by three or four dimers. Interestingly, all silica lobes on the dimers are located in the peripheral regime of the clusters. This is can be understood by the schematic shown in Figure 5.12a-ii. The attractive flow surrounding the polystyrene lobes draws all hybrid particles together, while the repulsive flow on the silica side prevents the contact of silica lobes with others. We also

found clusters only consist of two dimers but with different orientations in regions having less particle densities. Both symmetric (head-to-head) and chiral clusters (side-by-side) have been observed (Figure 5.12b). More intriguingly, the symmetric cluster does not move while the chiral clusters rotate continuously under electric field. The cluster shown in Figure 5.12b-ii rotates clockwise while the oppositely-handed cluster (Figure 5.12b-iii) rotates counterclockwise. The size ratio between polystyrene and silica lobes can affect the maximum number of particles in a stable cluster.[42] For example, we observed two dimensional structures, such as staggered chains and hexagonal arrays on assembly of PS-silica acorn shape particles, possibly due to the decreased repulsion from silica. Similar phenomena are also observed when salt was added into the system.

Figure 5.12c-i represents a short staggered chain formed by five dimers. In fact, this is a meta-stable structure which is often observed during the dynamic formation of tetramers. When an additional dimer approaches a pre-formed tetramer, the cluster will first transform into the structure shown in Figure 5.12c-i. After a while, a less stable dimer will leave and a new but more stable tetramer is formed. When the hybrid dimers are mixed with large size silica spheres, we observe some additional structures. For example, as shown in Figure 5.12c-ii, the large silica sphere is surrounded by a few PS-silica dimers into an asymmetric configuration. The electrohydrodynamic flow surrounding silica sphere is no longer balanced. As a result, it is pushed toward the left with a speed ~2 μm/s, mimicking cargo transport by propelling motors. However, when the silica sphere is encircled uniformly by the hybrid dimers (Figure 5.12c-iii), it, however, stops propulsion simply because the electrohydrodynamic force is balanced now.

In the high frequency regime (e.g., 20 kHz), dipolar interaction is dominant. We find three-dimensional assembly between dimers. As shown in Figure 5.13a, when two dimers approach each other, one dimer lifts away from the substrate since one of the PS lobes appears out of focus at

$t = 0.3\,\text{sec}$. The (larger) silica lobes from both dimers are aligned parallel to the applied field direction, i.e., perpendicular to the substrate. This is because the dipolar force between silica lobes is attractive when they are aligned parallel with the electric field. However, what surprises us is that each dimer itself does not align parallel to the electric field. This is probably due to the fact that the silica and polystyrene lobes have opposite polarizabilities (hence dipoles) within the frequency regimes that we are investigating. As depicted in Figure 5.13c, this configuration represents a minimum energy state for the doublet.

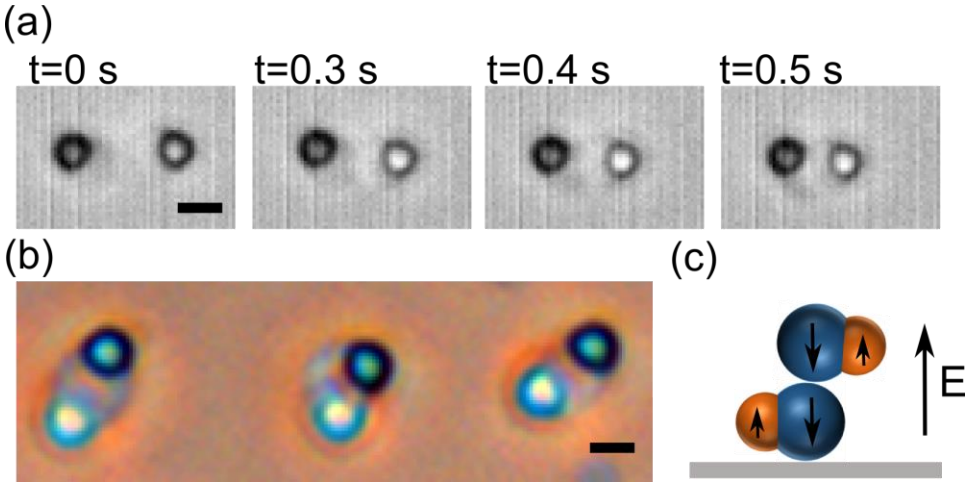

Figure 5.13 Assembly of PS-silica dimers under high frequency. (a) Bright-field snapshots showing the dynamic formation of three-dimensional doublets at high frequencies (5V and 20 kHz). (b) Representative bright-field images of the doublets. (c) Schematic depicts the orientation and possible dipoles of two dimers in the doublet. Scale bar is the same for all images: 2μm.

5.4 Conclusions

We have adopted two different types of swelling agents to fabricate anisotropic particles in a bulk synthetic manner. One swelling agent is toluene. The benefits of replacing the conventional swelling agent styrene with toluene are surprisingly rich. Although toluene is not polymerizable, the dimer shape formed during swelling can still be preserved if we remove toluene properly later on, which indicates the migration of uncrosslinked polymer chains in the seed

spheres towards the second lobe during toluene swelling. Such a method can not only simplify the synthetic procedures compared with the conventional method, but also produce dimers with new types of interfacial anisotropy. For example, we demonstrate that the surface charges are asymmetrically distributed between two lobes. Such an anisotropy allows us to further modify part of the dimers selectively based on strong electrostatic interactions, making metal-organic hybrid dimers conveniently. Geometrically, our dimers also exhibit anisotropy in terms of surface roughness, which can be potentially utilized for making colloidal micelles based on depletion interactions. Furthermore, by mixing toluene with a small amount of hydrophilic monomers, we also find that our toluene-swelling-extraction method can selectively modify one lobe with hydrophilic polymers. Hence, we utilize this property to incorporate pH responsive polymers into dimers and they exhibit different interfacial activities with the change of pH.

The other swelling agent is an alkoxide sol-gel precursor, i.e., TEOS. By using TEOS to swell CPS, we create dimers with compositional anisotropy, i.e., the polystyrene-silica hybrid dimers. The TEOS lobe can be reliably converted into silica via the well-developed sol-gel reaction. By controlling the composition of polystyrene seeds, we can tune the dimer morphology from acorn to dumbbell shapes. These synthesized particles exhibit intriguing propulsion in a direction that is perpendicular to the applied AC electric field. We prove that the propulsion is a result of an unbalanced electrohydrodynamic flow surrounding the compositionally asymmetric particles. Both the propulsion speed and moving direction can be controlled by the frequency of the applied field. The unbalanced electrohydrodynamic interactions between multiple particles also induce diversified assembly structures. In the low frequency regime (<5k Hz), the attraction between PS lobes generates self-regulated two-dimensional symmetric and chiral structures. While

at high frequencies (>20 kHz), the attraction between silica compartments generates three-dimensional structures that minimize the electrostatic energy of the whole cluster.

References

(1) Walther, A.; Müller, A. H. E. Janus Particles: Synthesis, Self-Assembly, Physical Properties, and Applications. *Chem. Rev.* **2013**, *113*, 5194–5261.

(2) Sacanna, S.; Irvine, W. T. M.; Chaikin, P. M.; Pine, D. J. Lock and Key Colloids. *Nature* **2010**, *464*, 575–578.

(3) Chen, Q.; Whitmer, J. K.; Jiang, S.; Bae, S. C.; Luijten, E.; Granick, S. Supracolloidal Reaction Kinetics of Janus Spheres. *Science* **2011**, *331*, 199–202.

(4) Cayre, O.; Paunov, V. N.; Velev, O. D. Fabrication of Asymmetrically Coated Colloid Particles by Microcontact Printing Techniques. *Journal of Materials Chemistry*, **2003**, *13*, 2445–2450.

(5) Liang, H.; Cacciuto, A.; Luijter, E.; Granick, S. Clusters of Charged Janus Spheres. *Nano Lett.* **2006**, *6*, 2510–2514.

(6) Mock, E. B.; Zukoski, C. F. Emulsion Polymerization Routes to Chemically Anisotropic Particles. *Langmuir* **2010**, *26*, 13747–13750.

(7) Jiang, T.; Zukoski, C. F. Synthesis of pH-Responsive Particles with Shape Anisotropy. *Langmuir* **2012**, *28*, 6760–6768.

(8) Sheu, H. R.; El-Aasser, M. S.; Vanderhoff, J. W. Uniform Nonspherical Latex Particles as Model Interpenetrating Polymer Networks. *J. Polym. Sci., Part A: Polym. Chem.* **1990**, *28*, 653–667.

(9) Sheu, H. R.; El-Aasser, M. S.; Vanderhoff, J. W. Phase Separation in Polystyrene Latex Interpenetrating Polymer Networks. *J. Polym. Sci., Part A: Polym. Chem.* **1990**, *28*, 629–651.

(10) Kim, J.-W.; Larsen, R. J.; Weitz, D. A. Synthesis of Nonspherical Colloidal Particles with Anisotropic Properties. *J. Am. Chem. Soc.* **2006**, *128*, 14374–14377.

(11) Mock, E. B.; De Bruyn, H.; Hawkett, B. S.; Gilbert, R. G.; Zukoski, C. F. Synthesis of Anisotropic Nanoparticles by Seeded Emulsion Polymerization. *Langmuir* **2006**, *22*, 4037–4043.

(12) Mock, E. B.; Zukoski, C. F. Emulsion Polymerization Routes to Chemically Anisotropic Particles. **2010**, *26*, 13747–13750.

(13) Van Ravensteijn, B. G. P.; Kamp, M.; van Blaaderen, A.; Kegel, W. K. General Route toward Chemically Anisotropic Colloids. *Chem. Mater.* **2013**, *25*, 4348–4353.

(14) Wang, S.; Ma, F.; Zhao, H.; Wu, N. Bulk Synthesis of Metal–Organic Hybrid Dimers and Their Propulsion under Electric Fields. *ACS Appl. Mater. Interfaces* **2014**, *6*, 4560–4569.

(15) Ma, F.; Wang, S.; Wu, D. T.; Wu, N. Electric-Field Induced Assembly and Propulsion of Chiral Colloidal Clusters. *Proc. Natl. Acad. Sci.* **2015**, under review.

(16) Hoffmann, M.; Lu, Y.; Schrinner, M.; Ballauff, M.; Harnau, L. Dumbbell-Shaped Polyelectrolyte Brushes Studied by Depolarized Dynamic Light Scattering. *J. Phys. Chem. B* **2008**, *112*, 14843–14850.

(17) Tang, C.; Zhang, C.; Liu, J.; Qu, X.; Li, J.; Yang, Z. Large Scale Synthesis of Janus Submicrometer Sized Colloids by Seeded Emulsion Polymerization. *Macromolecules* **2010**, *43*, 5114–5120.

(18) Peng, B.; Vutukuri, H. R.; van Blaaderen, A.; Imhof, A. Synthesis of Fluorescent Monodisperse Non-Spherical Dumbbell-like Model Colloids. *Journal of Materials Chemistry*, **2012**, *22*, 21893–21900.

(19) Shin, K.; Kim, D.; Cho, J.-C.; Lim, H.-S.; Kim, J. W.; Suh, K.-D. Monodisperse Conducting Colloidal Dipoles with Symmetric Dimer Structure for Enhancing Electrorheology Properties. *J. Colloid Interface Sci.* **2012**, *374*, 18–24.

(20) Yu, H. K.; Mao, Z.; Wang, D. Genesis of Anisotropic Colloidal Particles via Protrusion of Polystyrene from Polyelectrolyte Multilayer Encapsulation. *J. Am. Chem. Soc.* **2009**, *131*, 6366–6367.

(21) Qiang, W.; Wang, Y.; He, P.; Xu, H.; Gu, H.; Shi, D. Synthesis of Asymmetric Inorganic/polymer Nanocomposite Particles via Localized Substrate Surface Modification and Miniemulsion Polymerization. *Langmuir* **2008**, *24*, 606–608.

(22) Lu, W.; Chen, M.; Wu, L. One-Step Synthesis of Organic-Inorganic Hybrid Asymmetric Dimer Particles via Miniemulsion Polymerization and Functionalization with Silver. *J. Colloid Interface Sci.* **2008**, *328*, 98–102.

(23) Liu, B.; Liu, J.; Liang, F.; Wang, Q.; Zhang, C.; Qu, X.; Li, J.; Qiu, D.; Yang, Z. Robust Anisotropic Composite Particles with Tunable Janus Balance. *Macromolecules* **2012**, *45*, 5176–5184.

(24) Zhang, F.; Cao, L.; Yang, W. Preparation of Monodisperse and Anion-Charged Polystyrene Microspheres Stabilized with Polymerizable Sodium Styrene Sulfonate by Dispersion Polymerization. *Macromol. Chem. Phys.* **2010**, *211*, 744–751.

(25) Zhang, S. W.; Zhou, S. X.; Weng, Y. M.; Wu, L. M. Synthesis of Silanol-Functionalized Latex Nanoparticles through Miniemulsion Copolymerization of Styrene and ??-Methacryloxypropyltrimethoxysilane. *Langmuir* **2006**, *22*, 4674–4679.

(26) Narayanan, R.; Lipert, R. J.; Porter, M. D. Cetyltrimethylammonium Bromide-Modified Spherical and Cube-like Gold Nanoparticles as Extrinsic Raman Labels in Surface-Enhanced Raman Spectroscopy Based Heterogeneous Immunoassays. *Anal. Chem.* **2008**, *80*, 2265–2271.

(27) Turkevich, J.; Stevenson, P. C.; Hillier, J. A Study of the Nucleation and Growth Processes in the Synthesis of Colloidal Gold. *Discuss. Faraday Soc.* **1951**, *11*, 55–75.

(28) Bigall, N. C.; Härtling, T.; Klose, M.; Simon, P.; Eng, L. M.; Eychmüller, A. Monodisperse Platinum Nanospheres with Adjustable Diameters from 10 to 100 Nm: Synthesis and Distinct Optical Properties. *Nano Lett.* **2008**, *8*, 4588–4592.

(29) Wilson, D. A.; Nolte, R. J. M.; Hest, J. C. M. Van. Autonomous Movement of Platinum-Loaded Stomatocytes. *Nat. Chem.* **2012**, *4*, 268–274.

(30) Skelhon, T. S.; Chen, Y.; Bon, S. A. F. Synthesis of "Hard–Soft" Janus Particles by Seeded Dispersion Polymerization. *Langmuir* **2014**, *30*, 13525–13532.

(31) Barton, A. F. M. *CRC Handbook of Solubility Parameters and Other Cohesion Parameters, Second Edition*; Taylor & Francis, **1991**.

(32) Zhao, T.; Qiu, D. One-Pot Synthesis of Highly Folded Microparticles by Suspension Polymerization. *Langmuir* **2011**, *27*, 12771–12774.

(33) Mock, E. B.; De Bruyn, H.; Hawkett, B. S.; Gilbert, R. G.; Zukoski, C. F. Synthesis of Anisotropic Nanoparticles by Seeded Emulsion Polymerization. *Langmuir* **2006**, *22*, 4037–4043.

(34) Kim, A. J.; Manoharan, V. N.; Crocker, J. C. Swelling-Based Method for Preparing Stable, Functionalized Polymer Colloids. *J. Am. Chem. Soc.* **2005**, *127*, 1592–1593.

(35) Zhang, J.; Peppas, N. A. Synthesis and Characterization of pH- and Temperature-Sensitive Poly(methacrylic acid)/Poly(N-Isopropylacrylamide) Interpenetrating Polymeric Networks. *Macromolecules* **2000**, *33*, 102–107.

(36) Stöber, W.; Fink, A.; Bohn, E. Controlled Growth of Monodisperse Silica Spheres in the Micron Size Range. *Journal of Colloid and Interface Science*, **1968**, *26*, 62–69.

(37) Hench, L. L.; West, J. K. The Sol-Gel Process. *Chem. Rev.* **1990**, *90*, 33–72.

(38) Yin, Y.; Zhou, S.; You, B. O.; Wu, L. Facile Fabrication and Self-Assembly of Polystyrene – Silica Asymmetric Colloid Spheres. **2011**, *49*, 3272–3279.

(39) Ma, F.; Wang, S.; Zhao, H.; Wu, D. T.; Wu, N. Colloidal Structures of Asymmetric Dimers via Orientation-Dependent Interactions. *Soft Matter* **2014**, *10*, 8349–8357.

(40) Ristenpart, W. D.; Aksay, I. A.; Saville, D. A. Electrohydrodynamic Flow around a Colloidal Particle near an Electrode with an Oscillating Potential. *Journal of Fluid Mechanics*, **2007**, *575*, 83–109.

(41) Ma, F.; Yang, X.; Zhao, H.; Wu, N. Electric-Field Driven Propulsion of Particles by Breaking the Symmetry in Electrokinetic Flow. **2015**, in preparation.

(42) Sacanna, S.; Rossi, L.; Pine, D. J. Magnetic Click Colloidal Assembly. *J. Am. Chem. Soc.* **2012**, *134*, 6112–6115.

CHAPTER 6

SUMMARY AND OUTLOOK

6.1 Summary

Overall, previously reported methods for synthesizing anisotropic particles typically suffer from low throughput, poor monodispersity, high cost, or tedious steps. We choose the seeded emulsion polymerization technique as our synthetic basis, which first guarantee the throughput and monodispersity of particles. Subsequently we modified the method in several manners, such as simplify the procedures, and broaden its capability to obtain particles with anisotropic properties in geometric, interfacial and compositional properties. For instance, by using toluene to swell crosslinked polystyrene spheres, we make particles with combined anisotropy in both surface roughness and charge distribution. Positively charged dye or nanoparticles can be directly coated only on one of the lobes. We have also established a more flexible surface modification method to make a series of metal-organic hybrid dimers by employing amine-metal complexation and heterogeneous nucleation. The metal-organic (e.g., platinum-polystyrene) dimers not only show complex propulsion behavior under AC electric field due to the competition between induced charge electro-osmosis and electrohydrodynamic flow, but also exhibit rich swimming phenomena in hydrogen peroxide solutions depend on different platinum deposition processes. Moreover, the combined geometric and interfacial anisotropy in these dimers are responsible to a variety of novel behavior compared with previous studies using Janus spheres (such as circular motion and bubble propulsion).

As for particles with compositional anisotropy, we have synthesized three different types: (1) polystyrene dimers where two lobes have different crosslinking densities and the non-crosslinked lobe encapsulates active molecules, such as catalysts. We have successfully

demonstrated that these dimers can be used for bicompartmental phase transfer vehicles for hydrogenation reactions in oil phase; (2) colloidal emulsifiers which is responsive to pH by dissolving functional monomers in a swelling solvent - toluene; (3) polystyrene-silica hybrid dimers using inorganic precursor as a swelling agent. We have also discovered their novel propulsion behavior due to unbalanced electro-hydrodynamic flow and intriguing self-assembly structures. The first two composite particles are both interfacial active, although arising from different mechanisms (e.g. swellability and amphiphlicity), and they can be applied into different fields.

6.2 Outlook

This section discusses our outlook of research on anisotropic colloidal particles in two aspects: synthesis and applications.

6.2.1 Synthesis of anisotropic particles

So far the most successful bulk synthesis of monodisperse anisotropic particles is based on seeded emulsion polymerization. It has limitation too. Most of the particles synthesized so far have crosslinked polystyrene spheres as the seeds. Few groups have tried to adopt other crosslinked seeds such as PAN,[1] PMMA,[2] and poly(NiPAM).[3] Although PAN and PMAA systems generate reasonably good particles, the results based on poly (NiPAM) is unsatisfactory. The hydrophilic nature of the polymer leads to low interfacial tension between the seed and continuous phase, therefore the driving force to merge multiple protrusions is small. Considering the desired surface properties of biocompatible particles, investigations on crosslinked hydrophilic polymers are meaningful. Comprehensive studies about the interplay of several parameters, such as the crosslinking density gradient in seeds, seed/monomer hydrophilicity, the effect of co-monomer/swelling solvent, surfactant type/concentration, and solvent, will provide an insightful

guidance for manipulating different particle systems and for expanding the operational window of seeded emulsion polymerization.

Another disadvantage of seeded emulsion polymerization is that it requires some degree of compatibility between the swelling monomer and seeds. We have proposed one way to partially solve this problem, which is to use an intermediate solvent, such as toluene and TEOS. However, when the monomer is too hydrophilic, it is hardly incorporated in the second lobe. Other promising approaches, such as the seeded dispersion polymerization, deserve more experimental work, considering that diversified functionalities can be potentially achieved.

For the moment, reports adopting seeded emulsion polymerization are primarily interested in making dimers. If particles with a higher degree of geometric anisotropy are desired, we need to elaborately tune the crosslinking densities among different lobes. Although a few groups managed to make trimers,[4,5] no formation of tetramers is reported via this method. We believe that both particle monodispersity and the amount of labor limits the extension of this method for making colloidal molecules with larger number of constituting units. One possible route is to adjust the wetting property CPS precisely. In the polyNiPAM system, when particles are hydrophilic enough, multiple protrusions can emerge and they do not coalesce. It is possible to find a subregime in the potential parameter space to control the number of the protrusions precisely. Another possible route is adding multiple monomers into second swelling stage and promoting phase separation later. The most feasible way might be to programmably link the particles together. Considering our recent success in linking spherical particles into colloidal chains by combining optical trap with magnetic fields, we believe similar approaches can be employed for colloidal dimers or a mixture of spheres and dimers to generate hierarchical colloidal molecules.

6.2.2 Applications of anisotropic particles

Colloidal molecules are promising building blocks for developing microrobots that can simultaneously perform multi-tasks, such as sensing, imaging, transportation, delivery, etc. With this in mind, the incorporation of smart materials in colloidal molecules is important for future investigations, although we have presented some preliminary results for pH-responsive colloidal dimers. It has wide applicability for stimuli-sensitive emulsifiers and targeted propulsion. For example, one can combine two types of functionalities to achieve that. In fact, the approaches for coating platinum nanoparticles and iron oxide nanoparticles are the same, both utilizing the amine groups on the CPS surface. Hence, we can coat these two particles on dimers together so that they exhibit bubble-induced propulsion and directional motion with applied magnetic field. Another system that we have not fully studied yet is the particles with magnetic anisotropy. It is particularly appealing to our group not only because the applications of magnetic materials in biomedical area, but also the ability of extension to magnetic-field assembly. When further combined with electric fields it can ultimately offer a versatile platform for directed-assembly of anisotropic particles.

The progress of developing biocompatible micro/nano-motors is slow. We have found that bubbles can grow even on concave micron-particle surface, if it has high reactivity and rough surface. Therefore, we can replace platinum with enzymes and switching the fuel from hydrogen peroxide to more biocompatible chemicals, such as glucose, as long as the high catalytic activity of the enzyme is retained during the coating process. The bubble propulsion is a more desirable swimming mechanism in biological fluids, since it is less sensitive to high salt concentration.

For the propulsion of anisotropic particles under perpendicularly applied electric fields, more theoretical work is needed. When probing the dominant propulsion mechanism, we have also noted that methods for directly probing the forces acting on colloids, especially the one with

anisotropic surface properties, are scarce. Even the pure surface properties of anisotropic particles are difficult to characterize. For example, when the surface charges are unevenly distributed on particles, there is no quantitative way to characterize the anisotropy in surface charges on particles. Currently, we are limited to use oppositely charged dyes to obtain qualitative results. By normalizing the setting of the imaging capture software and calibrating the fluorescence intensity, we can possibly estimate the charge densities on particle surfaces. However, due to particle size effect or coating variation between batches, the accuracy of analyses is still questionable.

We believe the next stage for the study of self-propelling motors is the collective behavior of an ensemble of particles. Certainly, the understanding and prediction of such systems would be much more complex since various types of particle-particle interactions are involved. However, research on collective behavior could not only deepen our understanding in real complex systems such as colonies of bacteria cells and flocks of birds but also help develop transforming technologies such as active drug delivery vehicles and mini-surgeons.

As one of the most well-studied applications, colloidal surfactants made of anisotropic particles have been proven to have more advantages compared with isotropic particles. However, the behavior and structures of the particles formed at the interfaces are still in mystery. In order to obtain a deeper understanding of the impacts of geometry and surface amphiphilicity, experimentalists and theoreticians need to collaborate with each other. Emulsions with more complex structures, such as double and triple emulsions, are of major interests for encapsulation of precious materials, such as drugs and cosmetics. In principle, the more stable Pickering emulsions can prolong the release of the precious agents or protect highly reactive products when colloidal surfactants can form intact shells at the emulsion interface.

In addition to the previously mentioned fabrication of stimuli-responsive colloidal surfactants, another interesting research area is utilizing a mixture of particles as colloidal emulsifiers. Current research always involves one particular type of particles. Inspired by the co-surfactant concept in molecular world, a mixture of colloids should be also worthwhile to study. It can not only simplify the procedure of integrating multiple functionalities into the emulsions, but also help to study the potentially synergic interactions of different particles at interfaces, which could also lead to the formation of hierarchical structures and advance the field of interfacial assembly. In addition, co-colloidal surfactants may also improve the stability and monodispersity of the emulsion droplets as co-surfactants do.[6,7]

References

(1) Tang, C.; Zhang, C.; Liu, J.; Qu, X.; Li, J.; Yang, Z. Large Scale Synthesis of Janus Submicrometer Sized Colloids by Seeded Emulsion Polymerization. *Macromolecules* **2010**, *43*, 5114–5120.

(2) Peng, B.; Vutukuri, H. R.; van Blaaderen, A.; Imhof, A. Synthesis of Fluorescent Monodisperse Non-Spherical Dumbbell-like Model Colloids. *Journal of Materials Chemistry*, **2012**, *22*, 21893–21900.

(3) Kraft, D. J.; Hilhorst, J.; Heinen, M. a P.; Hoogenraad, M. J.; Luigjes, B.; Kegel, W. K. Patchy Polymer Colloids with Tunable Anisotropy Dimensions. *J. Phys. Chem. B* **2011**, *115*, 7175–7181.

(4) Kim, J.-W.; Larsen, R. J.; Weitz, D. a. Uniform Nonspherical Colloidal Particles with Tunable Shapes. *Adv. Mater.* **2007**, *19*, 2005–2009.

(5) Park, J.-G.; Forster, J. D.; Dufresne, E. R. Synthesis of Colloidal Particles with the Symmetry of Water Molecules. *Langmuir* **2009**, *25*, 8903–8906.

(6) Li, G.-Z.; Friberg, S. E. Surfactant/cosurfactant Association and Emulsion Stability. *J. Am. Oil Chem. Soc.* **1982**, *59*, 569–572.

(7) Williams, J. M. High Internal Phase Water-in-Oil Emulsions: Influence of Surfactants and Cosurfactants on Emulsion Stability and Foam Quality. *Langmuir* **1991**, *7*, 1370–1377.